MICROCOPY RESOLUTION TEST CHART

NATIONAL BUREAU OF STANDARDS-1963-A

AD A133 969

REPORT DOCUMENTATION PAGE		READ INSTRUCTIONS BEFORE COMPLETING FORM
1. REPORT NUMBER AFOSR-TR- 83-0868	2. GOVT ACCESSION NO.	3. RECIPIENT'S CATALOG NUMBER
4. TITLE (and Subtitle) MODELLING PARTICLE - PARTICLE INTERACTION AT THE MICRO SCALE		5. TYPE OF REPORT & PERIOD COVERED FINAL 1 Nov 77 - 30 Sep 81
		6. PERFORMING ORG. REPORT NUMBER Report SM 83-2A
7. AUTHOR(s) J.L. Swedlow		8. CONTRACT OR GRANT NUMBER(s) AFOSR-78-3533
9. PERFORMING ORGANIZATION NAME AND ADDRESS DEPARTMENT OF MECHANICAL ENGINEERING CARNEGIE-MELLON UNIVERSITY PITTSBURGH, PA 15213		10. PROGRAM ELEMENT, PROJECT, TASK AREA & WORK UNIT NUMBERS 61102F 2307/B2
11. CONTROLLING OFFICE NAME AND ADDRESS AIR FORCE OFFICE OF SCIENTIFIC RESEARCH/NA BOLLING AFB, DC 20332		12. REPORT DATE 15 Mar 83
		13. NUMBER OF PAGES
14. MONITORING AGENCY NAME & ADDRESS(if different from Controlling Office)		15. SECURITY CLASS. (of this report) UNCLASSIFIED
		15a. DECLASSIFICATION/DOWNGRADING SCHEDULE

16. DISTRIBUTION STATEMENT (of this Report)

Approved for Public Release; Distribution Unlimited.

17. DISTRIBUTION STATEMENT (of the abstract entered in Block 20, if different from Report)

18. SUPPLEMENTARY NOTES

19. KEY WORDS (Continue on reverse side if necessary and identify by block number)

20. ABSTRACT (Continue on reverse side if necessary and identify by block number)

In high-strength alloys, microstructure can influence toughness in a manner not yet fully quantified. Computational mechanics offers a tool whereby the events leading to fracture may be simulated, but the success of such an enterprise depends heavily upon the quality of the model employed. This report outlines a sequence of events thought to precede ductile fracture and presents a finite element model designed to capture the main events. The model is considered to be an improvement over an earlier one, and data are presented to support this conclusion. ——(over)

DD FORM 1473 EDITION OF 1 NOV 69 IS OBSOLETE

DTIC FILE COPY

Work of this type requires a fine degree of resolution which normally will entail very large, detailed finite element maps. Such map sizes could easily exceed the capacity of research computers, and a substructuring technique is essential to pursue research of this sort. Such a technique has been developed for use without modification to an existing code, i.e., it may be implemented on a standard finite element program directly.

MODELLING PARTICLE - PARTICLE INTERACTION AT

THE MICRO SCALE - FINAL REPORT ON AFOSR 78-3533

J.L. Swedlow

March 1983

Report SM 83-2A

Department of Mechanical Engineering
Carnegie-Mellon University
Pittsburgh, Pennsylvania

83 10 10 017

This is a final report on AFOSR-78-3533 and includes three attachments: Report SM 80-14, "An Improved Model for Second Phase Particle Interaction Analysis," by R.R. Batarags; Report SM 81-1, "A Simple yet Effective Substructuring Procedure for Finite Element Analysis," by M. Kondo and G.B. Sinclair; and an abstract of the paper, "Computation of Slow, Stable Crack Growth in a Fracture Test Specimen using the J-Integral," by J.L. Swedlow, F.B. Prinz, Z.-C. Lai, and C.W. Cho.

The Research Grant covered the period 1 November 1977 to 31 October 1981 and was entitled, "Analysis of Critical Microscopic Flow Behavior." The research objectives, in general terms, were to simulate events preceding fracture in selected alloy systems via computational plasticity; the aim was to quantify these events beyond what is possible using standard metallurgical tools (e.g., microscopy, optical and electronic). In particular, it was held that interactions between second phase particles would significantly alter the size scale of damage in high strength alloys. [A detailed recapitulation of this hypothesis appears on pp. 1-2 in the Batarags report.]

At the outset, analyses were performed to this end. While the results tended to confirm the hypothesis, subsequent review of the models used (i.e., the finite element maps) showed that the models themselves were deficient in that their design tended to force the desired result. [A critique of these early results, together with an extensive sampling of the corresponding data, appears on pp. 3-8 of the Batarags report.]

Next, Batarags designed and throughly tested a new model which met the criteria that we had begun to recognize were crucial for the successful resolution of this problem. It is believed that Batarags was successful in

this respect, and his report is concentrated on those findings. In that respect and in others referred to above, this report stands as the central technical document for this Research Grant.

At this stage the human element intrudes. Mr. Batarags finished his studies for the Master of Engineering degree and left the University. Also, the Principal Investigator, Professor Swedlow, had been found to have a brain tumor and was scheduled for appropriate surgery in the Spring of 1981. The upshot was that the personnel who had been engaged in the mainstream of work on this Research Grant were unable or unavailable to continue it. In effect, no reportable work on the matter of particle interaction was performed beyond the date of the Batarags report.

It happened, however, that a new student, Mr. Lai, became available late in the Spring of 1981, and the PI had recovered sufficiently to resume his duties. After a modest learning period during which the new student assimilated the prior work, an effort to continue was made. In the relatively short time then available prior to the end of the granting period, no further reportable work was concluded on this aspect of the research. Since that time, however, additional analyses were concluded and a report is now in draft form. Its abstract is attached.

However, another line of inquiry was in progress. Professor Sinclair, the Associate Investigator, had been examining the issue of debonding between a particle and the surrounding matrix material. Crucial to this work is the question of what condition governs the event. His approach was to hypothesize a local criterion and then to determine whether the results were in some sense acceptable. At the outset, for example, he tested the notion of using a local

critical stress. If, at some part of the boundary, debonding began, it became evident that the initial debond would form a crack; this configuration, however, is such that debonding must continue owing to the large local stresses induced at the crack's tip. Clearly this forces the debonding process to become unstable, and particle-particle interaction would be greatly enhanced. Since this sort of instability is not commonly observed, it was concluded that a local stress criterion for debonding is not wholly appropriate, and a local energy release rate G^Δ was put forward as the quantity governing debonding. This condition was not fully tested prior to the end of the granting period.

To follow his line of inquiry, Professor Sinclair concluded that a fine degree of resolution would be required. Normally, this would equate to very large, very detailed models. Such finite element maps are infeasible to work with on the University's computers, and he therefore developed a technique for substructuring described in the attached report. This is a useful and effective technique for the purpose intended but was not followed up with further studies of the debonding problem.

The status of the research performed under this grant, therefore, is that:

1. The research questions have been significantly sharpened;

2. the requisite (computational) tools have been developed and documented; and

3. there has been unsponsored follow-on work now in the process of documentation

It is regrettable that the research objectives have not been met during the granting period but, in retrospect, the research objectives are now seen as overly ambitious and will probably take a number of years further to achieve.

Owing to the status of this work, none of the documentation has so far been submitted for publication. The report in preparation, item 3 above, will in all likelihood be published.

In the same vein, there have been no coupling activities nor inventions on this Research Grant.

AN IMPROVED MODEL FOR SECOND PHASE

PARTICLE INTERACTION ANALYSIS

Roberts R. Batarags

Report SM80-14   November 1980

ACKNOWLEDGEMENTS

I. INTRODUCTION

The role of microstructure and how its behavior under loading influences the ductile fracture process are of significant interest to metallurgists as well as the mechanics community. We have addressed the issue, centering our efforts on computer simulation of microstructural events preceding fracture - primarily dealing with the effect of second phase particles. To date our efforts have met with limited success. However, we believe that the modeling of the microstructure under consideration which comprises the bulk of this report, has been improved and should allow for further work to proceed at a more rapid rate.

In order to provide a framework for our efforts, as well as to impart some sense to the sections to follow, a recapitulation of how we envisage the ductile fracture process to proceed is presented first.

1. A dispersion of second phase particles, whose material properties differ from the bulk of the material (here termed the matrix and which is considered both homogeneous and isotropic) will, under the action of low level loading, cause a local stress concentration to appear.

2. As the level of load increases and small scale (i.e. contained) plastic yielding occurs, the elastic stress concentration tends to be suppressed, whereas the local strains (measured in terms of e.g. the octatedral strain) will tend to increase.

2a. The foregoing sequence can be observed in the vicinity of a single second phase particle, since the events are local to the particle-matrix interface - not long range.

3. Depending on variables such as relative material properties, particle-particle spacing, load direction vis-a-vis the particle-particle axis and lateral constraint, a level of excitation will be attained at which the size of the plastic zones are no longer confined to and determined by an individual particle, but will rather connect with the plastic zones surrounding a neighbor particle. In other words, a change of size scale can occur such that the extent and shape of the plastic zone is no longer governed by a characteristic dimension of a single particle, but is instead governed by a dimension relating to the proximity of neighboring particles.

4. Once plastic zones from neighboring particles have interacted, further excitation will tend to concentrate within such highly strained regions. The interaction of second phase particles creates a pathway for macroscopic ductile fracture. Further material damage, such as the metallurgically observed void growth and coalescense phenomena, will occur in the most severely strained regions, leading to development of small fissures initially, and gross section fracture ultimately.

Our efforts have been concentrated on the effects of interacting second phase particles, and on the development and extent of strain localization We have attempted to demonstrate that the mere proximity of neighboring particles can lead to interaction between the attendant plastic zones, at quite low far field levels of excitation. Furthermore and most importantly, we have attempted to show that the presence of multiple second phase particles will accelerate the growth of regions of high strain.

Unfortunately, we have of late become sidetracked from the main issue due to modelling problems, which are discussed in the next section. Consequently,

the brunt of our latest endevour has been to eradicate the problems with our model of the microstructure. We believe that an adequate representation for the microstructure has been developed, so that progress can be made on the initial objective.

II. DISCUSSION AND EVALUATION OF PREVIOUS WORK

The work discussed in this section has been documented earlier [1,2]. The objective here is not to detail or reiterate the findings discussed previously, rather to highlight some of these findings for continuity. Additionally to be discussed are the problems with those findings and substantiating evidence.

The initial work [1] addressed the question of second phase particle interaction, under the assumption that the particle-matrix interface remained "coherent." An attempt to estimate the effect of particle destruction was made, by allowing one particle to open up at its center (the "burst" model), although such a procedure was acknowledged to be not entirely realistic. The latter work, [2], concerns itself with the issue of a matrix-particle decohesion, and the effect of such an event on the interaction of particles.

The particular two phase system chosen for these analyses is a Titanium alloy (Ti-6AL-4V), consisting of cylindrical second phase particles (α) in an otherwise homogeneous matrix (β) phase. Elastically the α phase is stiffer than the β, however, the α possesses a lower yield stress. Furthermore, the phase exhibits an extremely flat stress-strain curve plastically. That is, α work hardens to a much lesser extent than the β phase. The stress-strain curves for both the α and β phase are presented in Figs. 1 and 2, respectively.

The fact that the second phase particles are regarded as cylindrical allows one conceptually to section the material in such a fashion as to achieve a two dimensional problem containing circular second phase particles. Since interaction is the issue, a minimum of two particles is necessary. In these studies, the center to center distance was held fixed at 11 1/2 diameters. Because this alloy system, heat-treated differently, can produce a wide variation in particle spacing, 11 1/2 diameters is very conservative.

Both analyses utilized the identical finite element model for the microstructure, which is presented in Figures 3-5. Figure 3 depicts the complete model allowing for two second phase particles and three of the five distinct orientations of the particle-particle axis with respect to the loading axis, assumed vertical. Figure 4 indicates the regions encompassing both second phase particles, and their connectivity. An enlargement of one particle, and its immediate surroundings is seen in Figure 5.

Excitation of the model (Figure 3) is effected by displacement boundary conditions - tensile in the vertical direction. Loading in the lateral direction is not as easily resolved. At least three distinct lateral loading conditions (constraints) can be envisaged:

1) no motion normal to the direction of tensile loading permitted (Full Constraint)

2) no lateral constraint whatsoever (Nil Constraint)

3) lateral motion associated with Poisson contraction (Poisson Constraint)

A fuller discussion can be found in SM77-7, pages 7-9 (ref. 1).

See also the generalized discussion by Swedlow and Smelser (ref. 3).

DISCUSSION OF SM77-7

This analysis attempted to establish the phenomena of second phase particle interaction computationally, at far field strain levels smaller than those typically viewed by metallurgists studying the identical problem. The intent was to demonstrate that the presence of neighboring particles would alter the strain fields, even at such low levels of straining. If this were the case then the existence of second phase particles provides a precursor to large scale material damage. In effect - from the relative material properties of matrix and particles and their separation - the load under which the material will fail ductidely could be inferred.

Representative results are given by Figures 6-9. The first two figures (numbers 6 and 7) show octahedral strain values around one particle. The data are normalized with respect to octahedral strain at the proportional limit, a value of 0.012257. The radial location is in the matrix material, very close to the particle-matrix interface. The four curves indicate varying far-field levels of strain, with the lowest curve being an elastic result. Figures 8 and 9 depict the regions in which the local octahedral strains exceed far field values by 5%, (i.e. 1.05 times far field strain).

At the time the results were obtained, they were viewed as disappointing, although not inaccurate. The elastic curves on Figures 6 and 7 indicate no interaction, as should be expected at such a large particle spacing. Furthermore, the curves are smooth and reminiscent of elastic results for say a hole in a plate. From Figures 8 and 9, which represent the least and the most interaction seen, respectively, again benign conclusions were drawn. Consequently, work proceeded with an attempt to deal with matrix-particle decohesion, as detailed in the next section.

DISCUSSION OF SM79-8

Using the identical finite element model, an attempt was made to evaluate the effects of a local matrix-particle decohesion on the ability of second phase particles to interact. The so-called burst model indicated that the regions of high strain would exhibit a propensity to join at much lower levels of far field loading. Consequently, the assumption was that a decohesion would also accelerate the interactive effects; but would the level of load at which such a decohesion occurs be a major variable?

Representative results are given by Figures 10-16. Figures 10 and 11 show the variation, with angular position around the particle at which the decohesion was enforced, of ϵ_R Figures 12 and 13 – the variation of the normalized octahedral shear stress, both sets for two orientations. Figures 14-16 indicate regions exhibiting a high level of octahedral strain in relation to the far field values.

A few words of explanation are in order at this point: Since we were and still are lacking a criterion for decohesion, the decohesion was enforced at different levels of far field strain. "Coherent" model implies no decohesion; "initial debond" implies particle-matrix surface is separated but not opened prior to application of any load; "debond on 10" - small local plastic yielding present prior to debonding; "debond on 20" - plastic flow throughout the model prior to debonding; "debond on 15" - intermediate load level to "debond on 10 and 20." Additionally, the extent of the debond is approximately 1/12 of the circumference of the second phase particle.

The conclusions drawn from the analysis were that the orientation of the particle-particle axis with respect to the load axis was a very important

variable, lateral constraint less so. Futhermore, the more plastic flow present at the time of debond, the more pronounced the tendency for the regions of high octahedral strain to propogate. Finally, that the level of interaction seen for any analysis with a decohesion introduced was substantially greater than the level of interaction seen in either the corresponding "cohesive" or "burst" model case.

DISCUSSION OF THE MODEL AND ITS LIMITATIONS

The finite element model discussed so far, shown in Figures 3-5, has severe limitations for the purposes intended, although this is not obvious from the results presented and discussed previously. Elastic analyses, such as can be inferred from the lowest curves on Figures 6 and 7 are not indicative of the quality of results obtainable from the model for a plastic analysis. That, however, is essentially due to the nature of plastic flow itself. Once a region has yielded, further straining tends to accrue there, as opposed to necessarily yielding the surrounding regions. In a finite element sense, an element is considered as yielded if the yield criterion is exceeded at the centroid of a constant strain triangle i.e. a binary decision. Consequently, if a large element extends into regions of both high and low stress, a good possibility exists of its not yielding even if nearly 50% of the region is experiencing stress levels high enough to initiate plastic flow. Such a result may appear in Figures 8 and 9 since there is no apparent reason for the particular distribution of elements not exhibiting extensive strains, save for their having yielded later than their neighboring smaller elements.

The bipolar coordinate scheme used to facilitate the modeling introduces several other geometric flaws. The element size gradations that exist are

prejudicial since along the particle-particle axis the elements remain rather small between the particles, but not as much in other directions emanating from the particles. In effect, the plastic flow has been forced to occur between the particles. Similarly, there is also an angular bias built in around each particle - that being that the smallest elements around the particle occur directly on the particle-particle axis closest to the neighbor particle. In short, the region most likely to yield first occurs between both particles, and the path of least resistance to plastic flow lies directly towards the neighbor particle.

The existence of element size gradations in the direction of the neighbor particle is obvious from Figure 4, as is the angular size distribution. Whether such gradations are fatal to the analyses performed is definitively answered by Figures 17-19. These three figures are directly analogous to Figures 14-16 with the exception that the results shown in Figures 17-19 are taken from analyses where matrix material properties were substituted in the region normally associated with the neighbor particle. That is, Figures 17-19 are for a one-particle model. It should be mentioned that even though these results show regions over which the normalized octahedral shear strain exceeds far field values by 5% (Figures 14, 15, 17, and 18) and 10% (Figures 16 and 19) the entire region has yielded. Quite clearly then, if Figures 14 and 17, 15 and 18, 16 and 19 are viewed as pairs, the findings - with some small local perturbations - are identical! Consequently, the conclusion must necessarily be that the analyses have not been overly sensitive to the presence of a second, second-phase particle with second phase material properties, but rather the results appear dependent and quite sensitive to the finite element model itself. Hence the model must be rejected!

NEW MODEL AND INDICATIVE RESULTS

Having shown the bipolar modeling to be unacceptable in the previous section, we embarked on devising a new model. A number of considerations serve both as guides and constraints. The requirements and limitations we must address are:

1) A clearly defined 1:1 check case comparing single particle results to multiple particle results must be available

   a) in a model sense this is easily conceivable and must be easily obtainable

   b) on an exitation level the question that arises and still needs a definite answer is - is the comparison made on equal stress levels or equal far field strain levels?

2) Minimization, if not elimination of element size gradations. There are two distinct gradations, i.e., angular and radial, both of which need to be kept in mind.

3) The ability to vary orientation of the particle-particle connection axis vis-a-vis the load axis must exist.

4) The ability to vary L/D (distance between particles to diameter ratio) must be easily attainable.

5) Points 1-4 to be met without excessive computational cost.

The scheme settled upon attempts to consider all of the requirements established, and has done so with some level of success.

In order to keep the model size within limits and preserve the ability to vary L/D, a simple coarse to fine substructure technique is employed. The coarse or matrix model is shown in Figure 20, where the cell along which displacements are carried over to the fine or particle model is indicated by the heavy point. Figures 21 and 22 indicate how the L/D ratio can be varied from two to four approximately. The L/D is approximate as each particle is modeled as a square, whose area is then converted into a circle of equivalent area yielding a diameter (D). L is measured from center to center.

A single particle problem is analyzed by substituting second phase material properties into only the center square region darkened in Figure 22. The single particle case is the reference case, to which all further multiple particles cases must be compared. The comparison is imperative since the question being asked is: to what extent are the high strain regions altered due to the presence of neighboring particles?

The particle model is presented in Figures 23 and 24 in its actual size and configuration, and an enlargement, respectively. The model as presented can easily offer two distinct length to diameter ratios i.e. L/D = 2 and L/D = 4. Furthermore, larger length to diameter ratios can be designed by simply decreasing the size of the particle itself on the matrix model. This does, however, actually create new finite element models, which we have chosen not to depict at this time. In fact, we have dealt solely with the L/D = 2 model, trying to ensure that it performs sufficiently well for our needs. The close spacing is a result of a change of perspective. Since the previous analyses dealt with L/D~11 1/2, and were somewhat unsuccessful, it was decided that a more reasonable approach, especially considering the difficulties encountered with the model itself, is to analyze a situation where heavy interaction is certain to occur. Hence the close spacing.

From Figure 24, it is obvious that angular size gradations do not exist. However, modest radial size gradients are present. Essentially this is due to computer limitations. We recognize and acknowledge that the model is a compromise. However, we also believe it to be vastly superior to the previous model.

Variations of the particle-particle axis with respect to the load axis has been approached from a slightly different viewpoint than previously. The now discarded model actually consisted of five different models, three of which are

given by Figure 3. We have chosen to effect the rotation of load axis with respect to particle-particle axis through the input boundary conditions. That is, instead of imposing uniaxial tension on the model shown in Figure 20 vertically, we can impose boundary conditions to be those of say 45° off vertical on the model. Through transformation equations any off angle (from vertical) boundary conditions can be calculated.

The microstructure we are modeling contains cylindrical second phase particles, which should be modeled as circles in two dimensions. Since the matrix model, Figure 20, models the second phase particles as squares, some justification is in order. During the attempts to create a new model, we had designed a very similar model to that presented here, although containing somewhat less detail. Using that model we analyzed the problem of a hole in an elastic plate in tension. The problem was solved in two distinct ways that are:

1) direct loading of the fine model, and

2) loading of the matrix model, and subsequent substructure loading, i.e., of the fine model.

The importance is two-fold. First we can compare results to well-known analytic solutions and secondly loading of the matrix model and subsequent loading of the particle model informs us of the quality of results we can obtain by an extremely crude modeling of a circular particle by a square.* Both analyses showed excellent agreement with theory. Since the material properties of the second phase are not

---

*When the boundary conditions are input on the matrix model, a square region similar to that seen on the center of Figure 20 possesses essentially nil elastic properties. The displacements are then carried onto the particle model where a circular hole is vastly better modelled.

nearly as dissimilar form the matrix as compared to nil elastic properties, we expect two material problems to show the same kind of agreement. In short, we feel justified in our approximation of a circular region, on the matrix model, to be a square.

DISCUSSION OF RESULTS - Testing of the Element Model

We have run a rather extensive list of elastic check cases which essentially are an attempt to insure that:

1) we have no built-in bias

2) we have sufficient detail on the particle model

3) we are justified and introduce no difficulties by rotating our input to simulate rotation of the particle-particle axis WRT the load axis.

We also have preliminary plastic results available which will be presented as well.

Although, from our experience, elastic results are not necessarily conclusive indicators of the quality of plastic results, it is nevertheless important to examine elastic results in some detail. Furthermore, with the present model, we can obtain a sense of the quality of our model, since we can compare single to multiple particle results. Additionally, we expect to see differences in the elastic results since $L/D = 2$. Therefore, a comprehensive set of elastic results are presented in Figures 25 and 26. The angular variation of σ_r/σ for various locations are given by Figures 25-32, of $\sigma_{\theta\theta}/\sigma$ by Figures 33-40, of $\tau_{r\theta}/\sigma$ by Figures 41-48. Normalized octahedral shear stress angular variations are depicted by Figures 49-56. The radial location measured from the center of the particle starts at the closest element ring in the matrix material and progresses outwards for each of the sets of data presented.

The results presented substantiate our belief that the present model is a vast improvement over the previous model. The darkened symbols indicate single particle results for various angles of far field tension with respect to particle-particle axis. Since these points fall essentially onto one single curve, we can safely conclude that our method of simulating differing particle-particle axis orientations WRT the loading axis through input boundary conditions introduces no discernable errors.

Since these analyses were performed for a particle spacing given by L/D=2, we expect to see differences in the stress components once we analyze the multiple particle cases. These differences do appear as well. In general, from Figures 49-56 we can say that the stress level is somewhat higher i.e., clearly distinguishable from the single particle results. The scatter of the data is somewhat greater for the multiple particle results, than the single, but not objectionably so.

A rather interesting event is noticeable on Figures 49-56 for the multiple particle data. The nominal average value for T_{oct}/T_{lim} is on the order of .28, maximum ~.32. Now as we proceed radially outwards from the particle, the trend that appears is for the peak values of T_{oct}/T_{lim} to remain roughly constant, while the minimum values tend to increase. Certainly the fact that the curves tend to flatten out is not surprising - in fact for single particle results at a large enough distance we expect the T_{oct}/T_{lim} curve to be flat. Nevertheless, why do the 'valleys' get deeper in Figure 49, rather than the peaks becoming higher in comparison to Figure 56?

For our purposes the more important question is how does this particular model perform when plastic yielding occurs? Preliminary results have been obtained and are presented in Figures 57-62. These figures graphically depict regions

of high strain (measured by the octahedral shear strain) for both single particle and multiple particle analyses. The figures represent data obtained for an analysis where the far field loading is presumed tension at 22.5° from vertical on the matrix model, at an accumulated strain level of ~4%. There are very distinct differences between single and multiple particle results. On Figures 57 and 58 the elements exceeding far field strain levels by 5% are darkened and a shift is apparent from extensive yield in the load line direction (Figure 57) to preferred yield towards the neighbor particle (Figure 58). In fact on the basis of the 105% characterization, the particles have already connected. As we use a stricter characterization - 107% for Figures 59 and 60, and 110% for Figures 61 and 62, of course the high strain regions become progressively smaller. However, in all cases the effect of multiple particles is clearly visible.

One note of caution should be mentioned concerning the results given on Figures 57-62. The results are not precisely symetrical as we have depicted the data. The principal reason is since the tension axis is at 22.5° there is no precise symetry of element distributions. For example, had we chosen to have the tension axis at a multiple of 30°, the elements would be distributed precisely symetrically about the tension axis. Clearly, a polygonal representation for a circle has a finite number of such symetry lines. Nevertheless, had the load been applied in such a symetrical direction, we would expect symetrical results. In addition, the use of a 5% exceedance of the strain criteria is rather arbitrary and does not account for the minor numerical variations which occur in any analysis of the type presented.

An interesting observation can be made by viewing Figures 62, 60 and 58, in that order. Although, we are then viewing a progression of less severe criteria for the determination of high strain regions, the following extension also applies. Since the exceedance is highest on Figure 62 it can be assumed that these regions necessarily yielded first. The new regions darkened on Figure 60 yielded intermediately, and the regions darkened only on Figure 58 yielded last. The point is that the second phase particles which appear to have connected on Figure 58, have done so by 'growing' high strain regions from the neighbor particle, not radially out from the particle represented by the center of the particle model. Simply stated, information at the boundaries of the particle model is propogated inwards even though it is harder to do, than propogate plastic zones out from the particle, since those elements tend to be much smaller. It is to be noted, that this observation per se, does not indicate any problem - it is, however, interesting.

In conclusion, we believe the model presented here, substantiated by the results obtained and presented here, is a tremendous improvement over the previous model. We have paid great attention to eradicating the flaws of the previous model, and have succeeded. We believe that the model will allow meaningful analyses to be performed that will readdress the issue of interaction of second phase particles, and its importance.

REFERENCES

1. Swedlow, J. L. and G. B. Sinclair, "Two Cases of Inclusion - Inclusion Interaction in a Ti Alloy," Report SM77-7, Department of Mechanical Engineering, Carnegie-Mellon University (October 1977)

2. Batarags, R. R. and J. L. Swedlow, "The Effect of a Local Matrix-Inclusion Decohesion On The Interaction Between Inclusions In A Ti Alloy," Report SM79-8, Department of Mechanical Engineering, Carnegie-Mellon University (April 1979)

3. Swedlow, J. L. and R. E. Smelser, Materials and Science Engineering, 40 (1979) 139-140.

Figure 1. Presumed stress-strain curve for α phase.
$E = 17.5 \times 10^6$ lb/in^2 and $\sigma_{lim} = 115 \times 10^3$ lb/in^2

Assumed stress-strain curve for α-phase in terms of effective stress and effective strain, normalized on proportional limit.

Effective stress/proportional limit
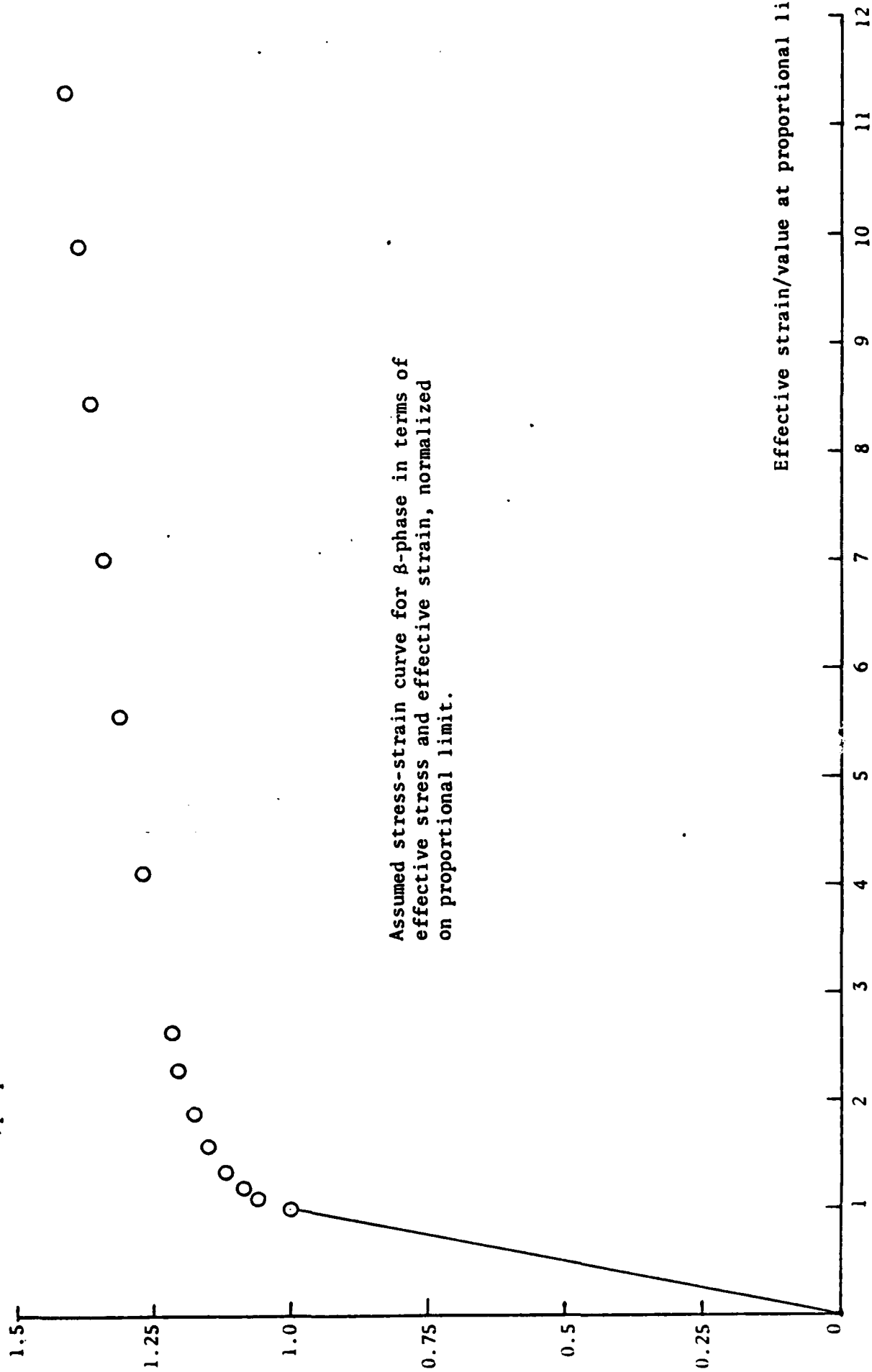
Effective strain/value at proportional limit

Figure 2. Presumed stress-strain curve for β phase.
$E = 13.0 \times 10^6$ lb/in^2 and $\sigma_{lim} = 130 \times 10^3$ lb/in^2

Assumed stress-strain curve for β-phase in terms of effective stress and effective strain, normalized on proportional limit.
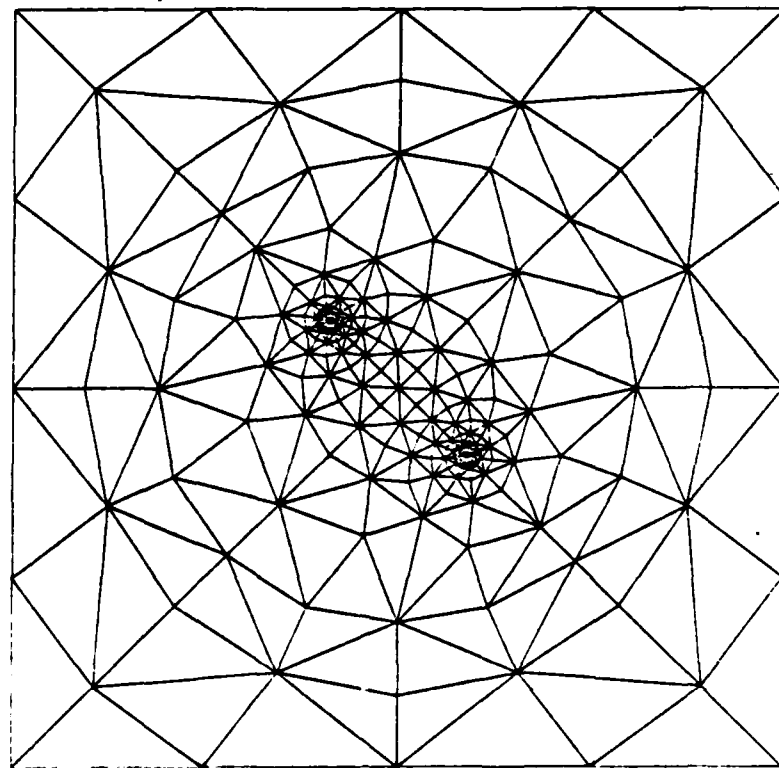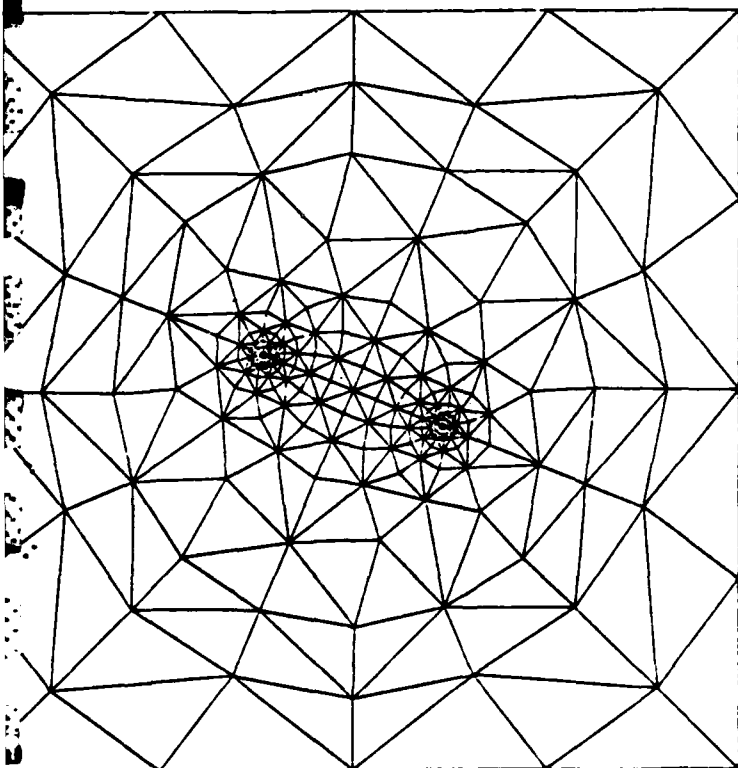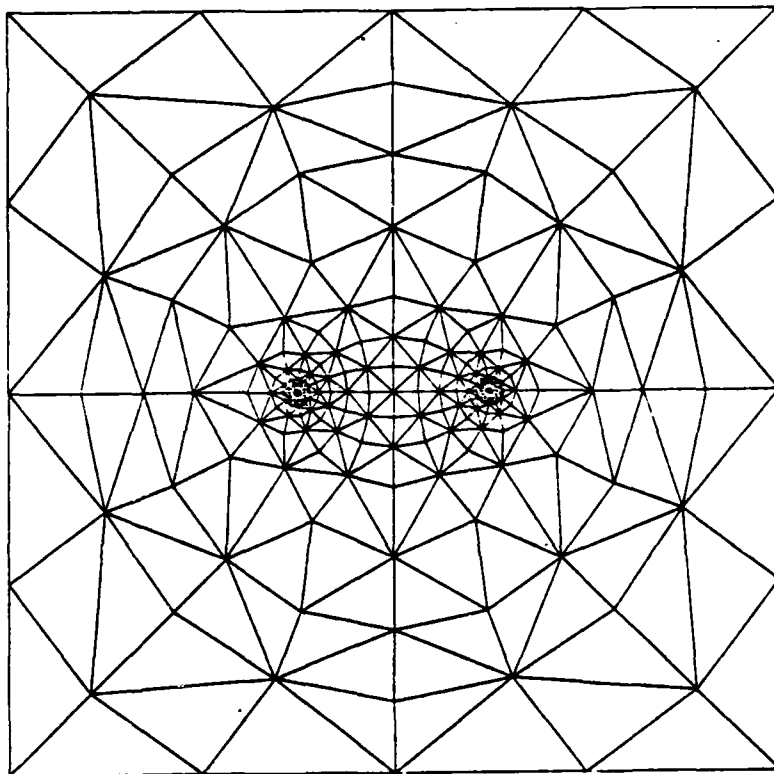
Figure 3. Bipolar element model, showing 3 of 5 available rotations
of particle-particle axis. Excitation is vertical, constraint
horizontal.
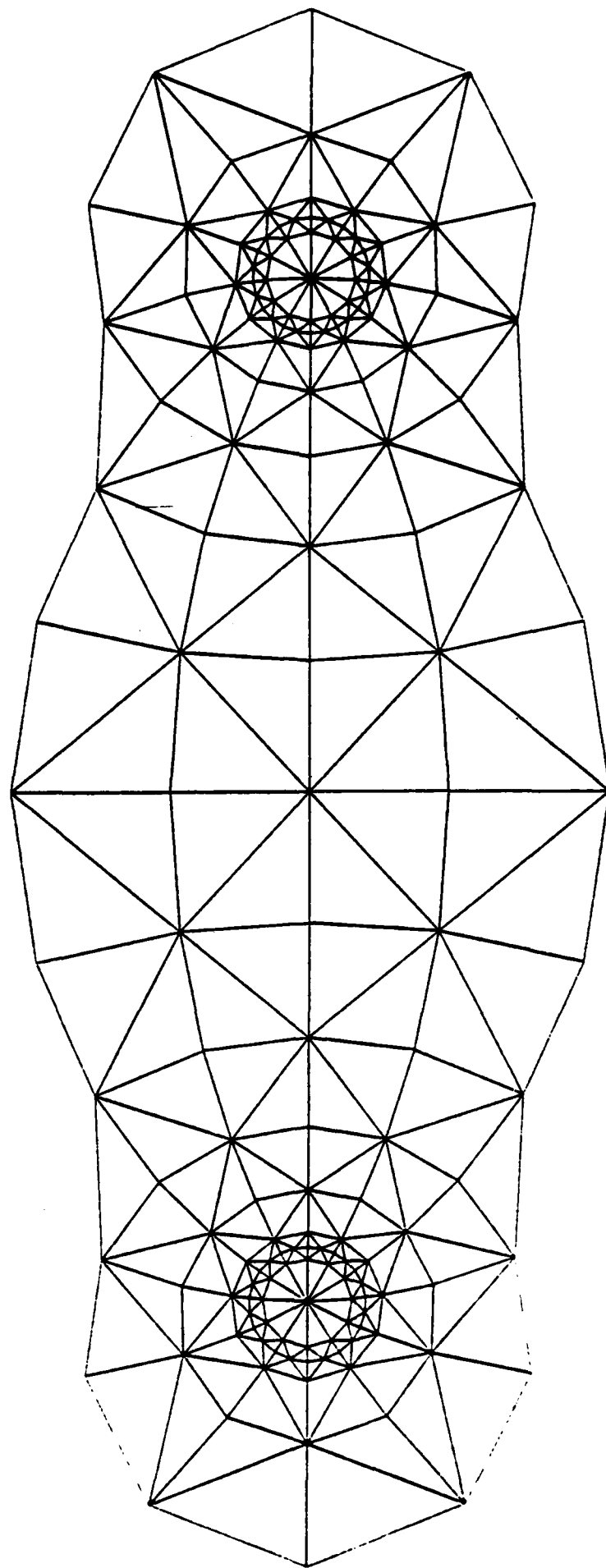
Figure 4. Enlargement of central region
of bipolar map.
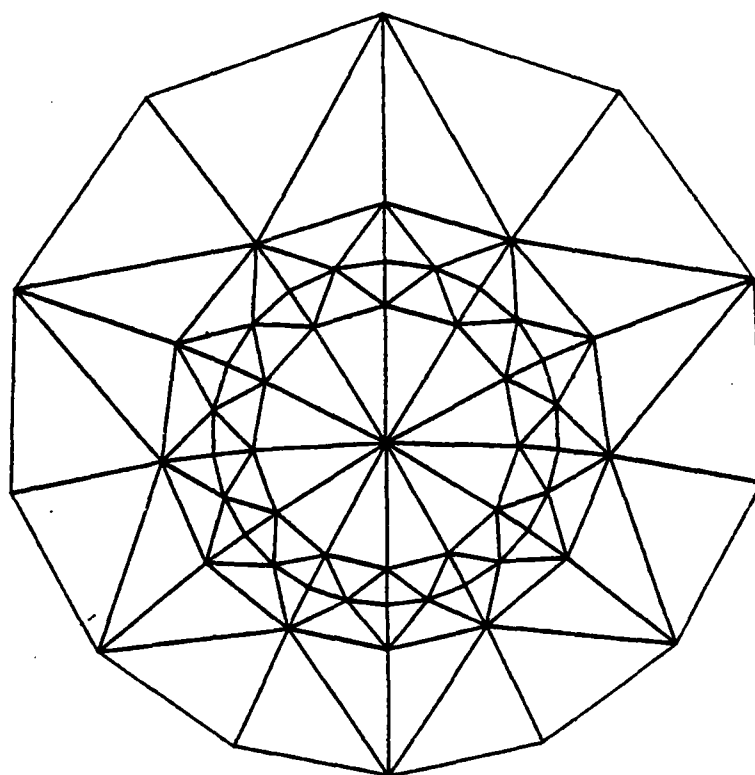
Figure 5.   Enlargement of single
            particle and region
            directly contiguous.

Figure 6. (for coherent model):
Octahedral strain at inclusion-matrix interface as a function of
angular position, four levels of excitation. Full constraint,
rotation is 0.0 deg.

position of tensile axis

far-field value

far-field value

far field value

far field value

Octahedral strain at interface/octahedral strain at proportional limit

approximate angular position, beginning at connection axis, clockwise for lower inclusion

Figure 7. (for coherent model):
Octahedral strain at inclusion-matrix interface as a function of
angular position, four levels of excitation. Full constraint,
rotation is 45.0 deg.

position of tensile axis

far-field value

far-field value

far-field value

far-field value

far-field value

approximate angular position, beginning at connection axis, clockwise for lower inclusion

Figure 8. Regions with greatest propensity for extensive strain, full constraint, rotation is 0.0 deg, coherent model
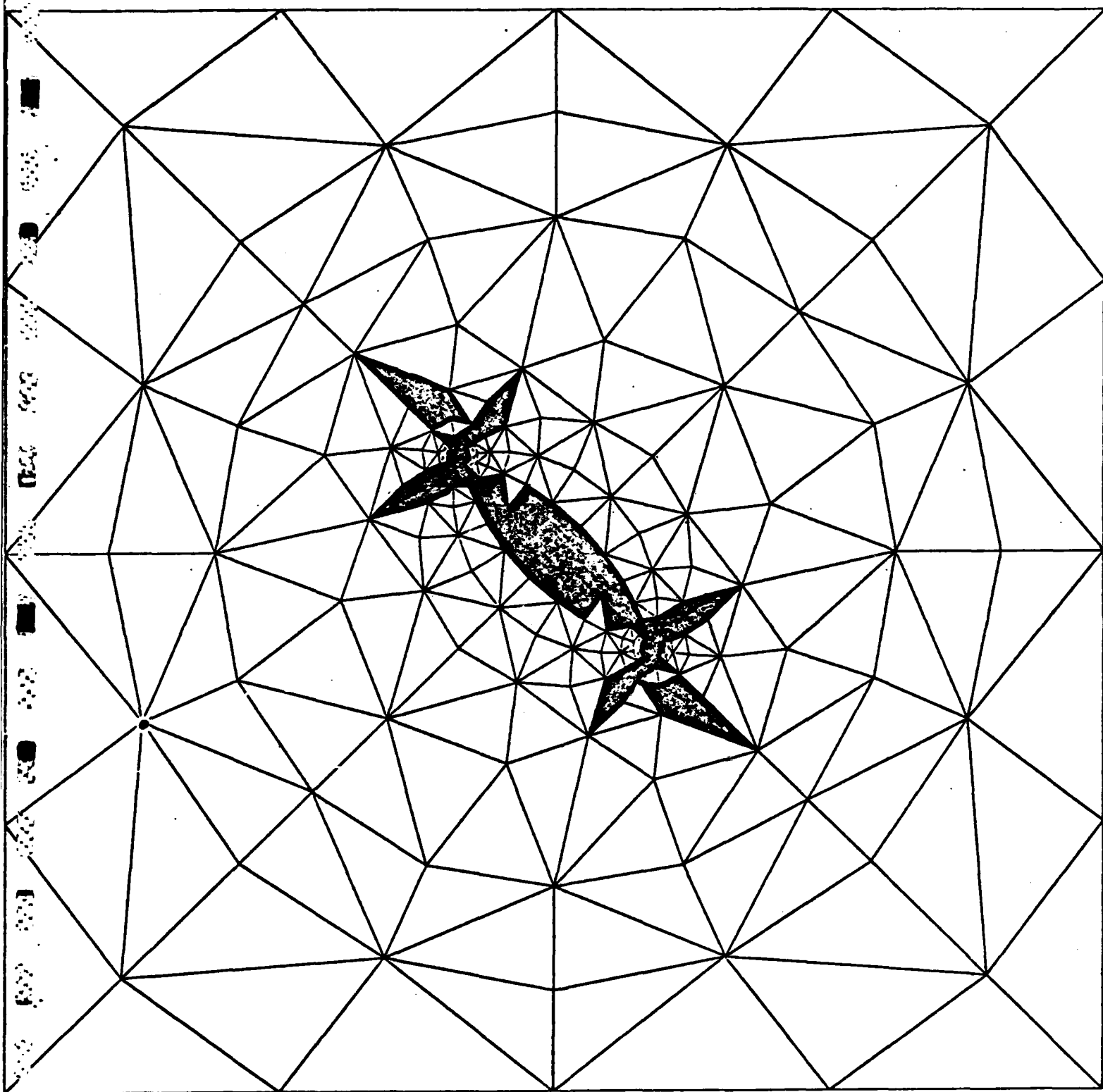
Figure 9. Regions with greatest propensity for extensive strain, full constraint, rotation is 45.0 deg, coherent model
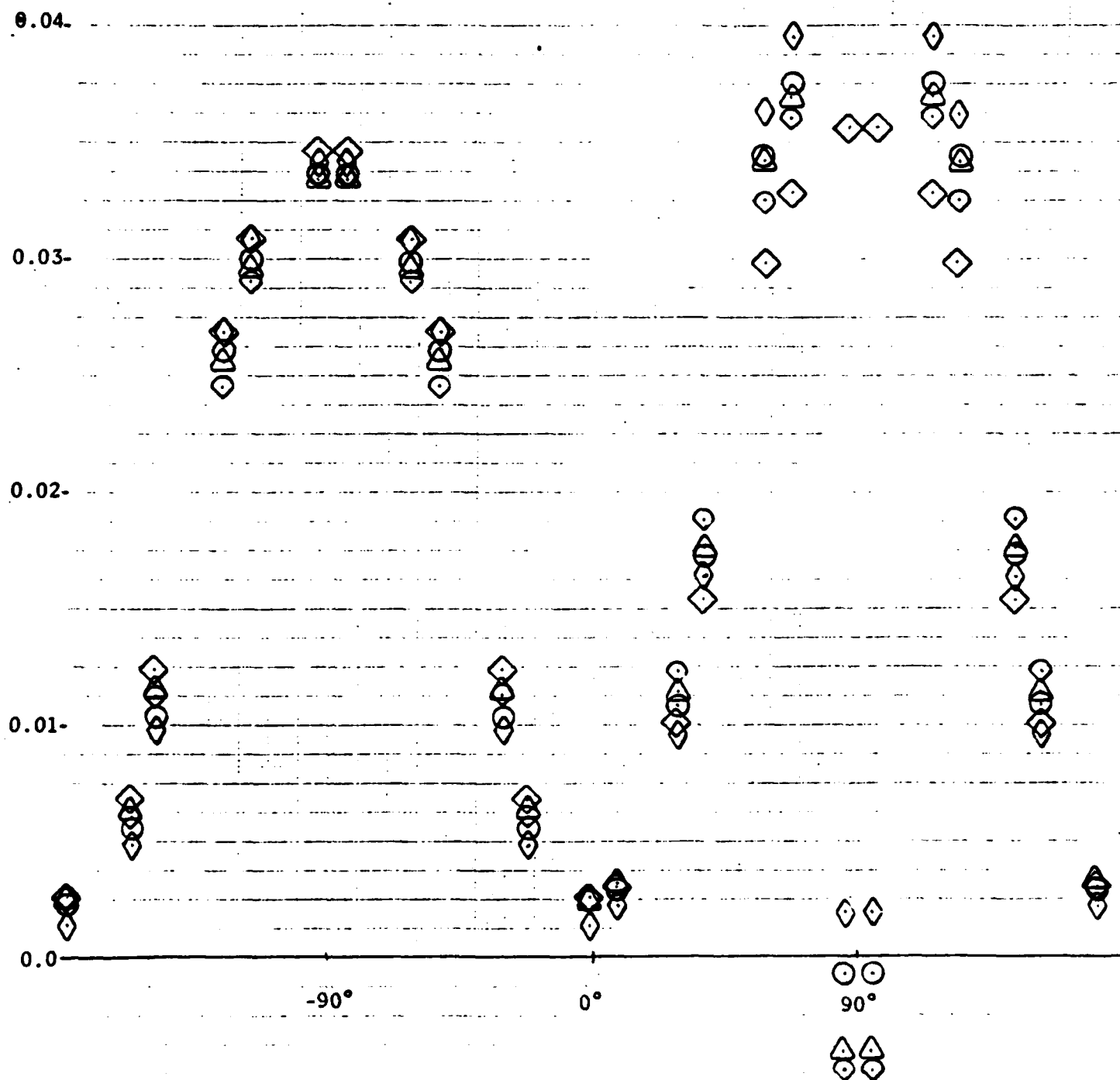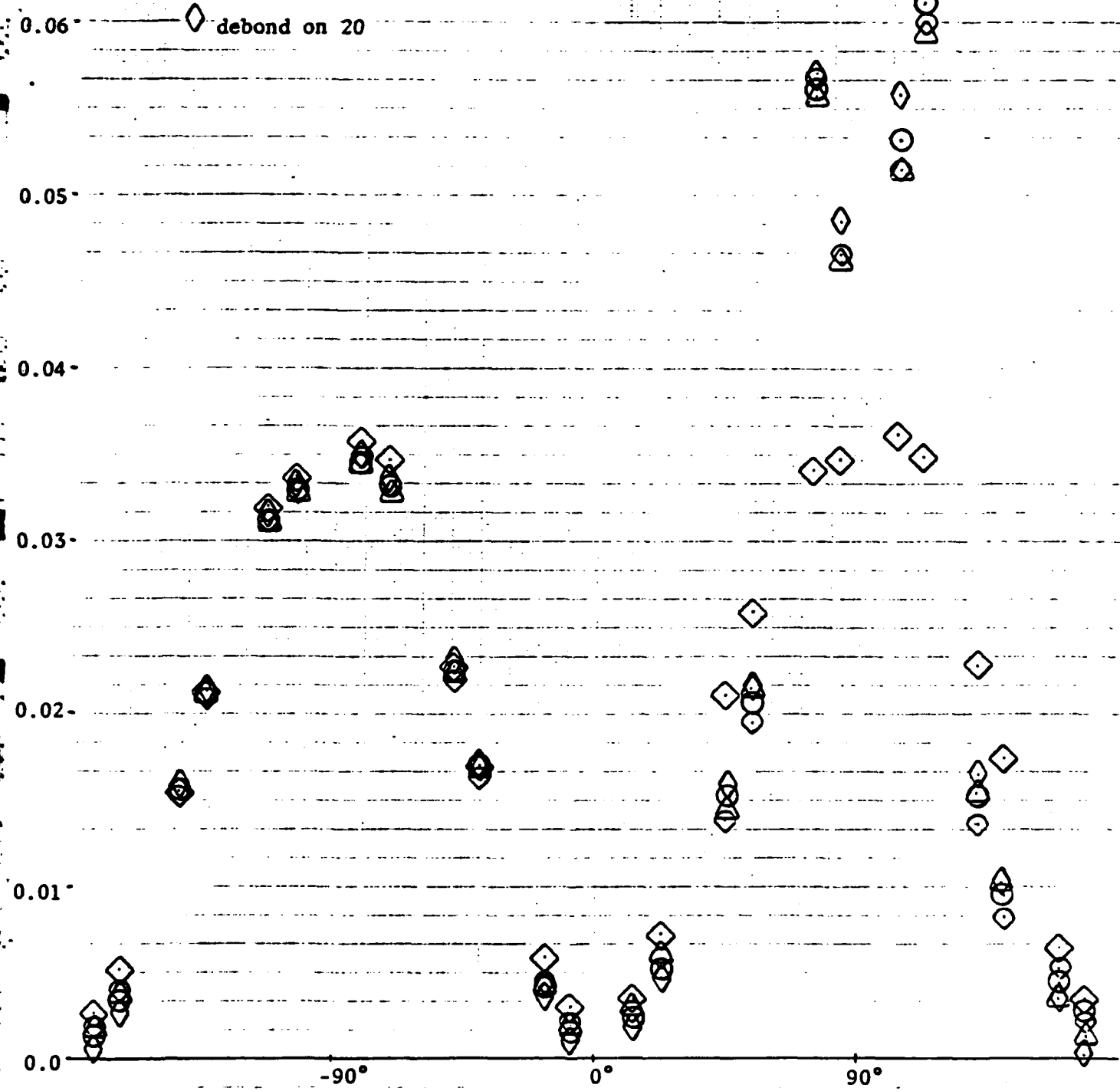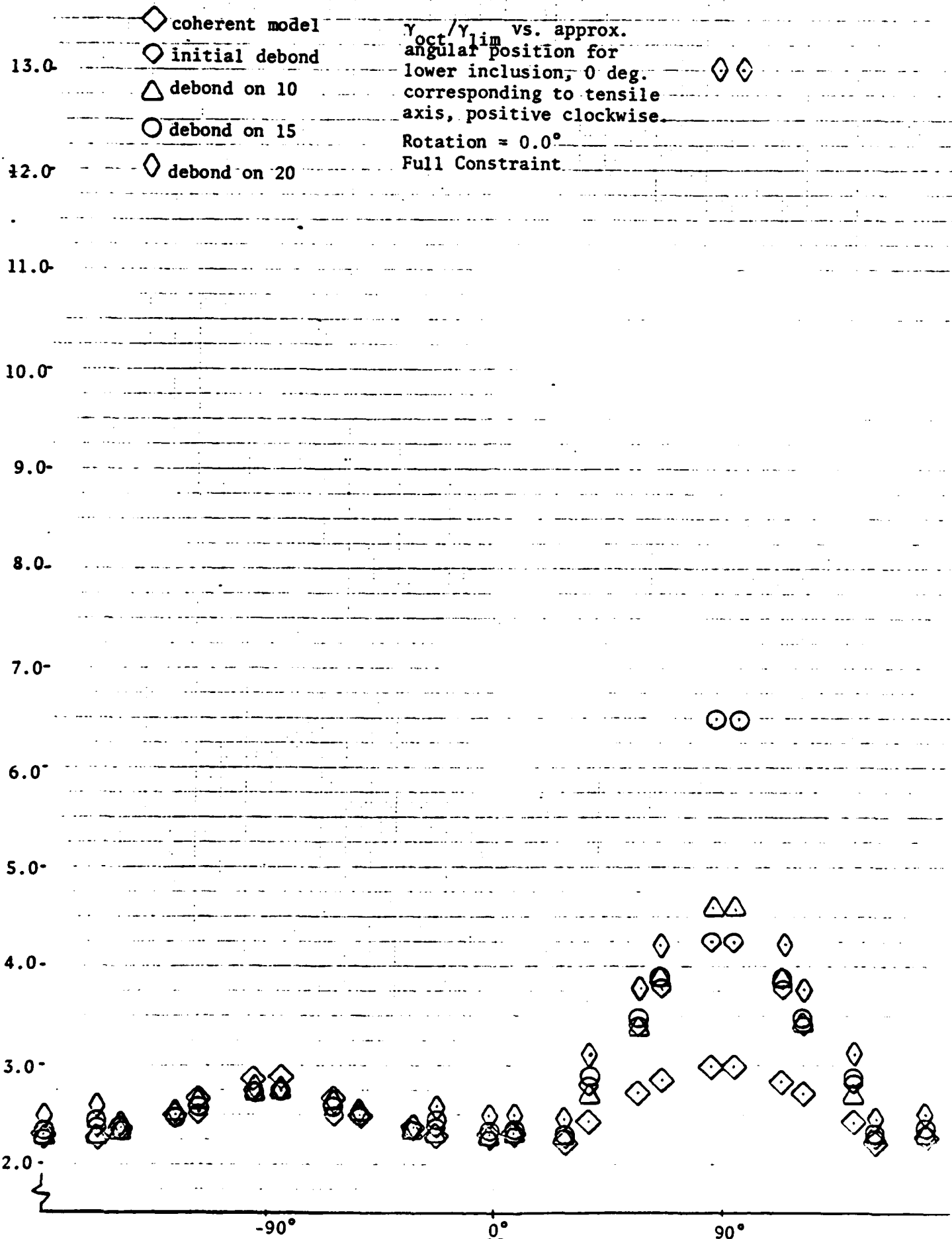
Figure 10.
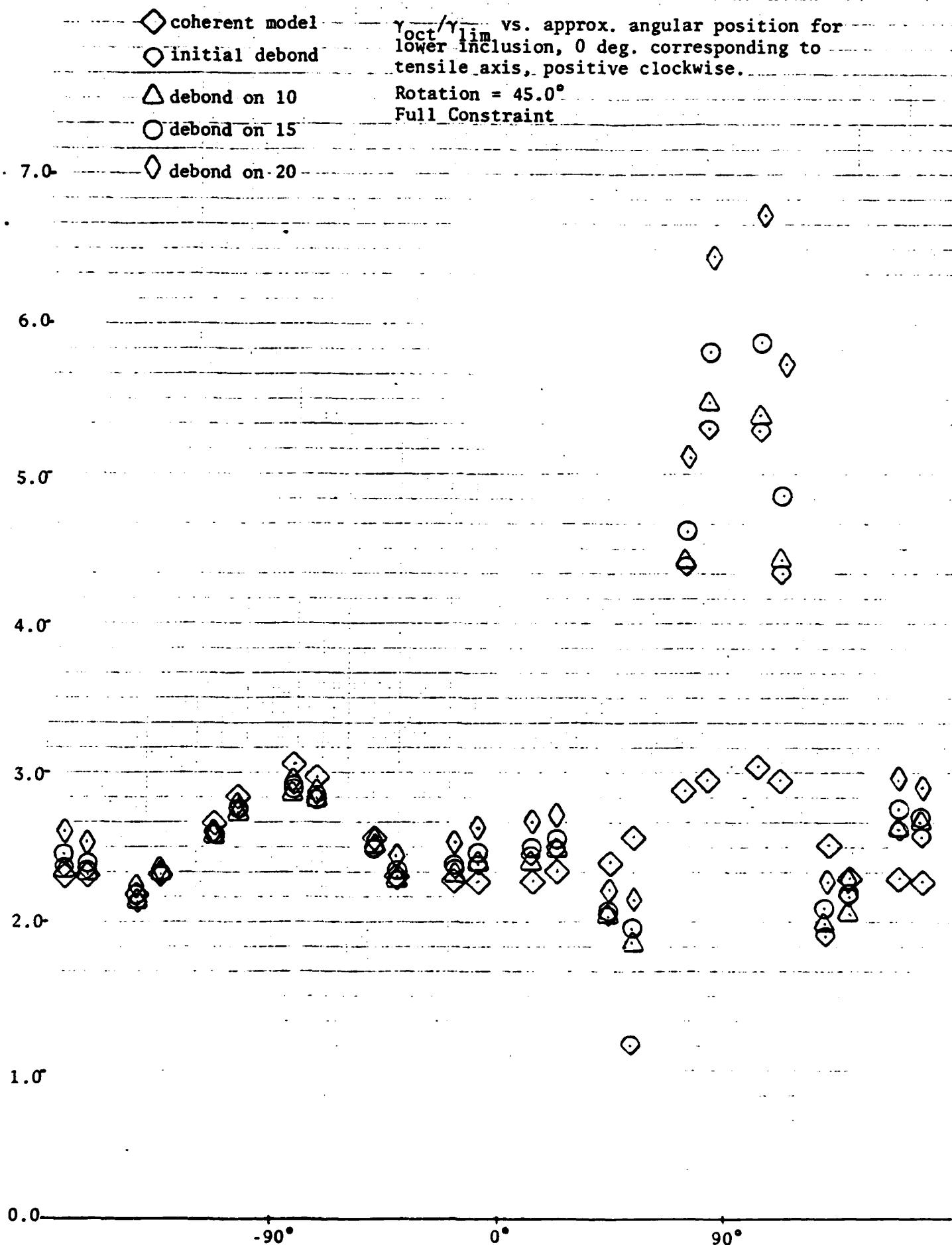
Figure 11

Figure 12.

Figure 13.
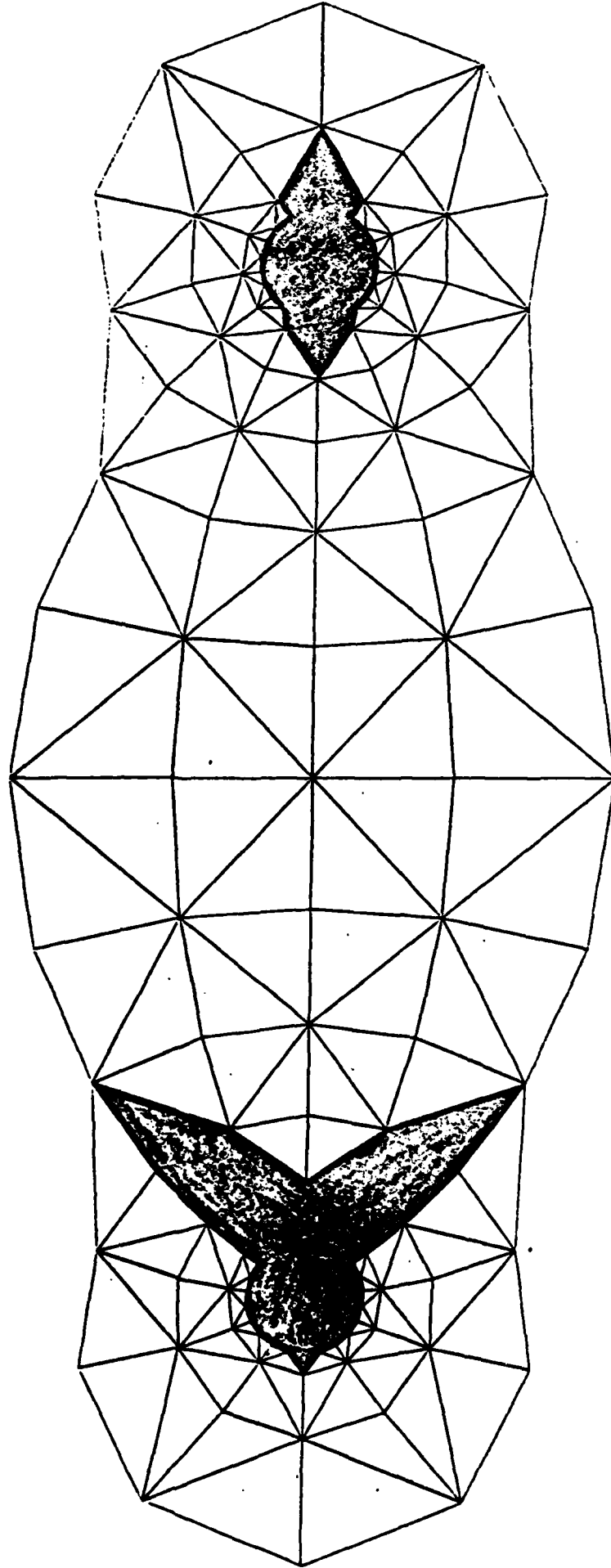
Darkened Regions Indicate

$$\frac{\gamma_{oct}}{\gamma_{lim}} > \left.\frac{\gamma_{oct}}{\gamma_{lim}}\right|_{far\ field} \times 1.05$$

Debond on 15, Rotation = 0°, Full Constraint

Figure 14.
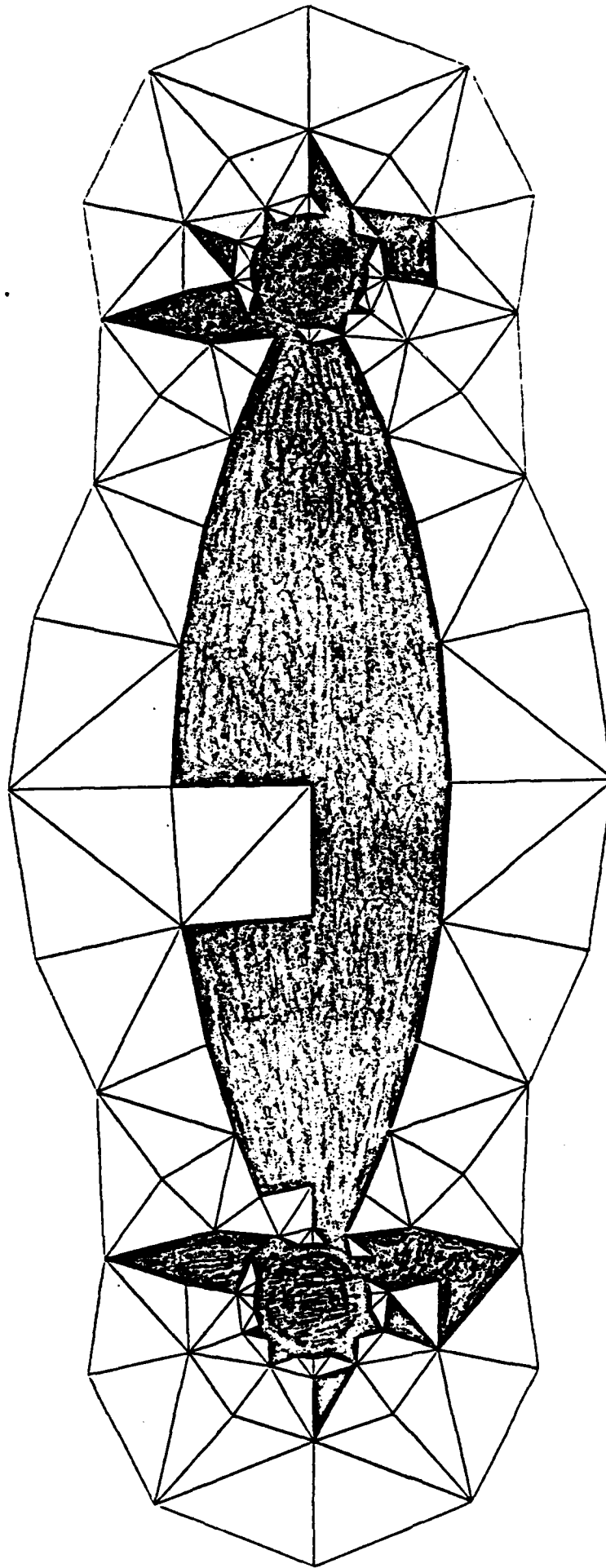
Darkened Regions Indicate

$$\frac{\gamma_{oct}}{\gamma_{lim}} > \left.\frac{\gamma_{oct}}{\gamma_{lim}}\right|_{far\ field} \times 1.05$$

Debond on 20, Rotation = 45°, Poisson Constraint

Figure 15

Darkened Regions Indicate

$$\frac{Y_{oct}}{Y_{lim}} > \left.\frac{Y_{oct}}{Y_{lim}}\right|_{far\ field} \times 1.10$$
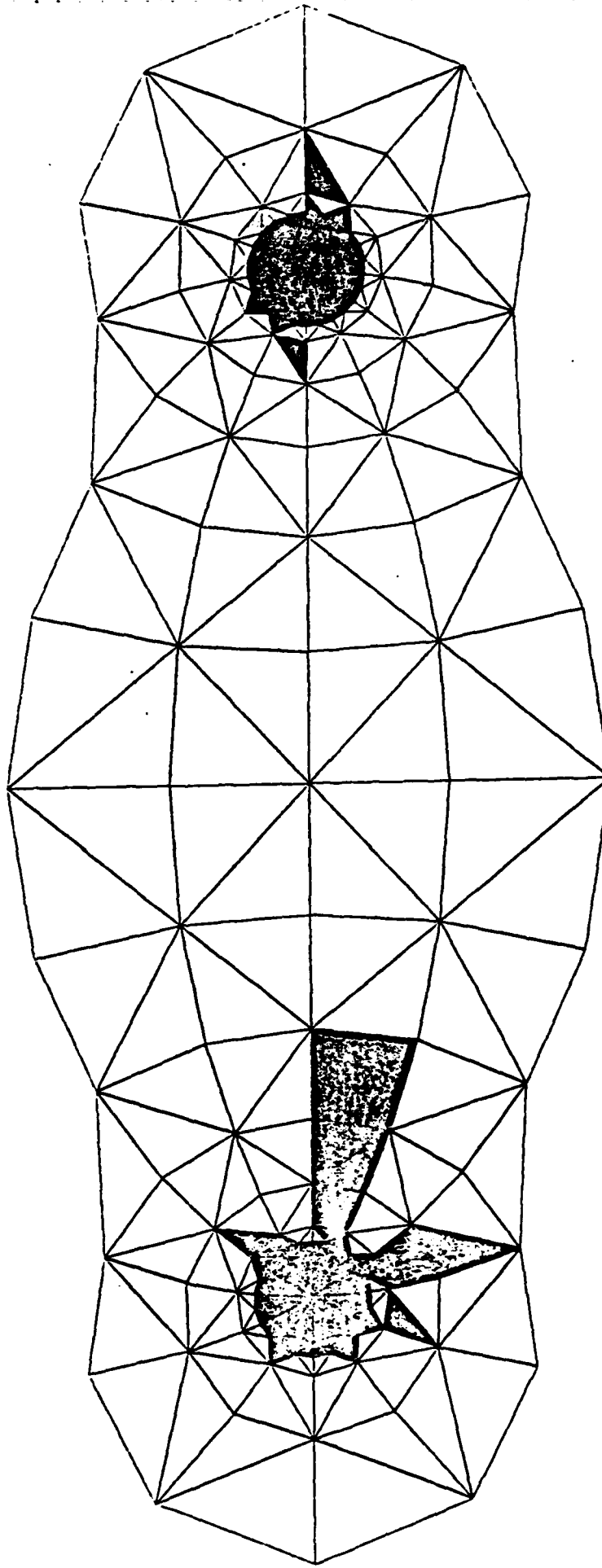
Debond on 20, Poisson Constraint

Figure 16.
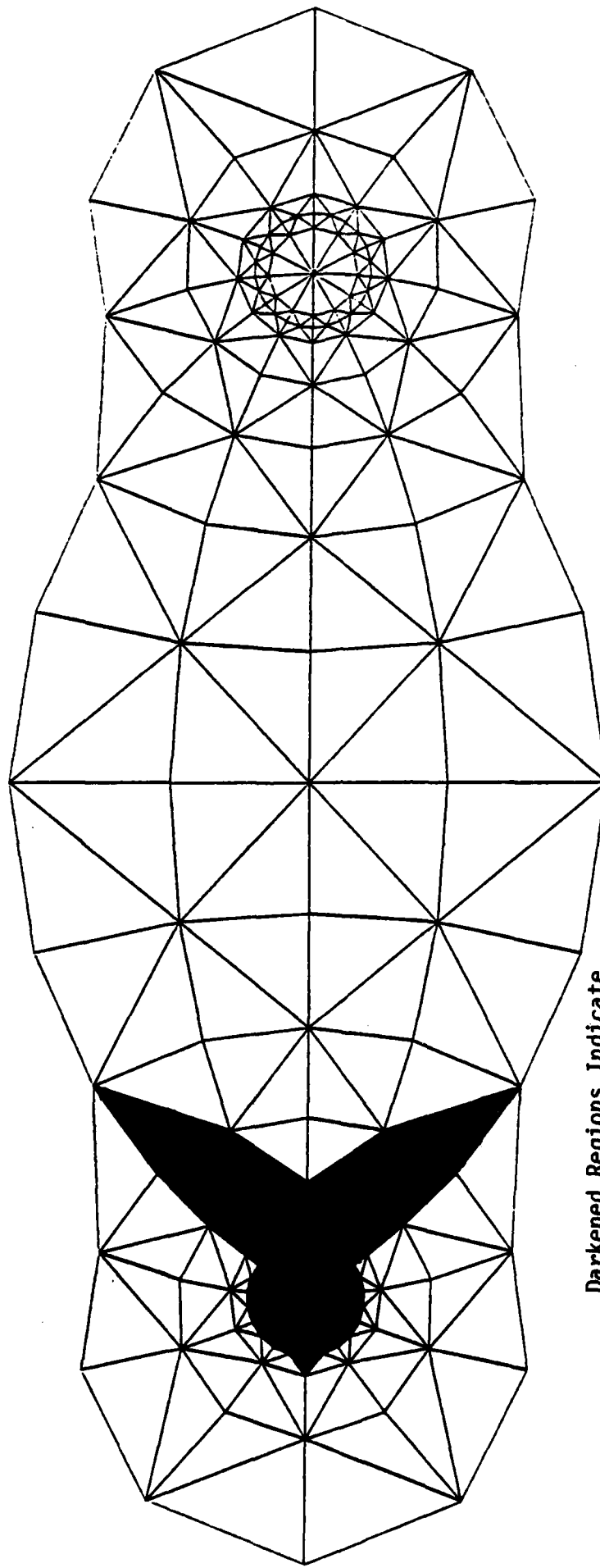
Darkened Regions Indicate

$$\left.\frac{\gamma_{oct}}{\gamma_{lim}} > \frac{\gamma_{oct}}{\gamma_{lim}}\right|_{far\ field} \times 1.05$$

Debond on 15, Rotation $\theta=0^\circ$, Full Constraint, Single Particle

Figure 17.
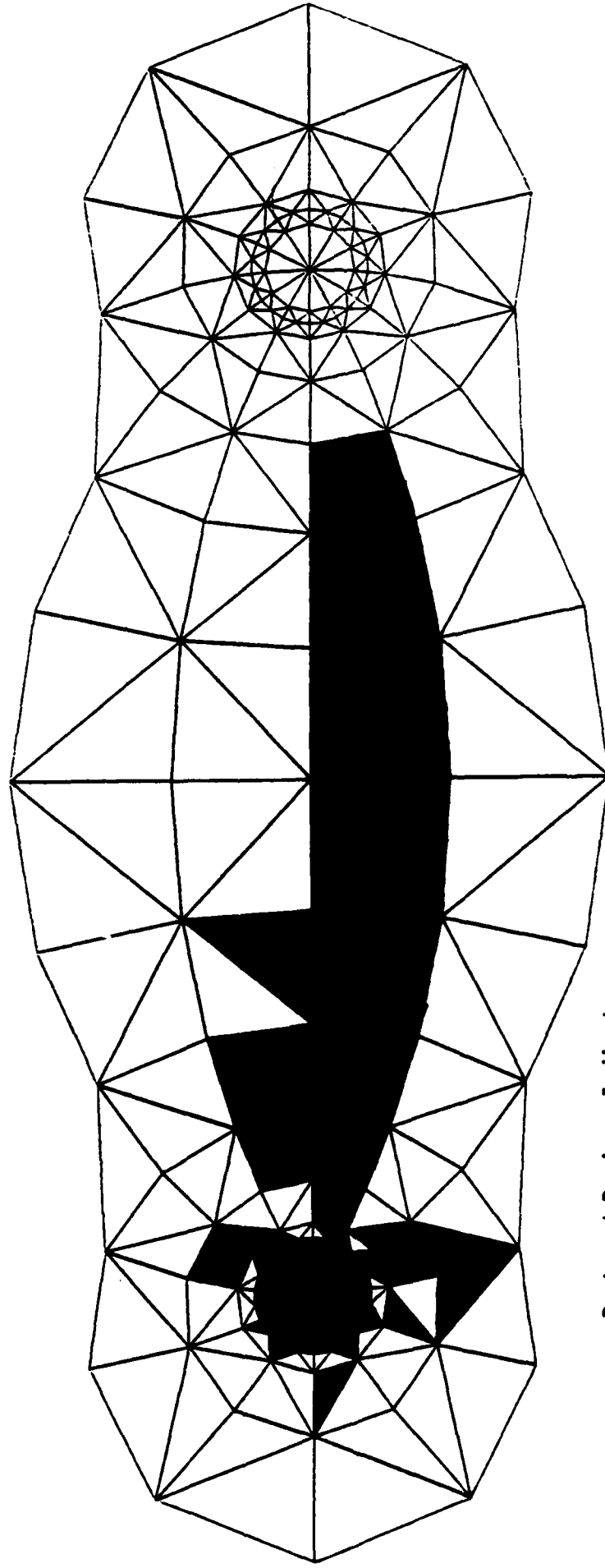
Darkened Regions Indicate

$$\left. \frac{Y_{oct}}{Y_{lim}} > \frac{Y_{oct}}{Y_{lim}} \right|_{far\ field} \times 1.05$$

Debond on 20, Rotation=45.0°, Poisson Constraint, Single Particle

Figure 18.
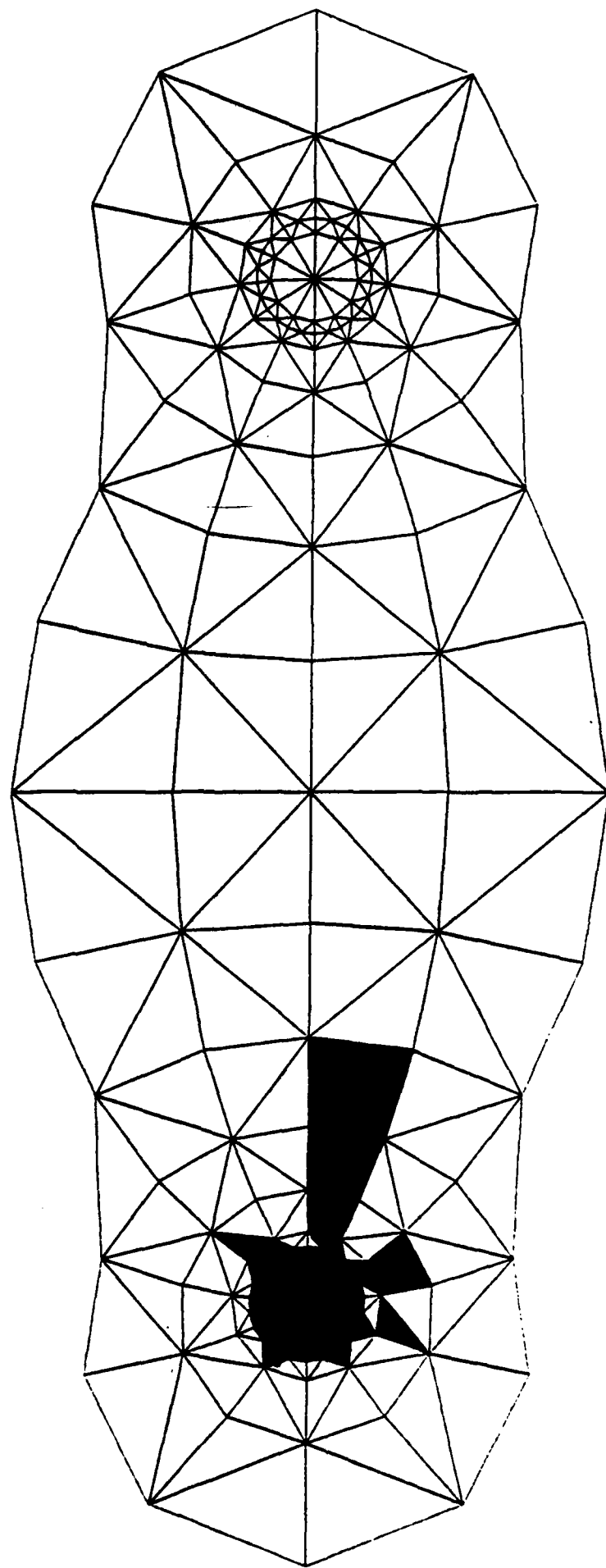
Darkened Regions Indicate

$$\frac{Y_{oct}}{Y_{lim}} > \frac{Y_{oct}}{Y_{lim}}_{far\ field} \times 1.10$$

Debond on 20, Rotation=45.0°, Poisson Constraint, Single Particle

Figure 19.
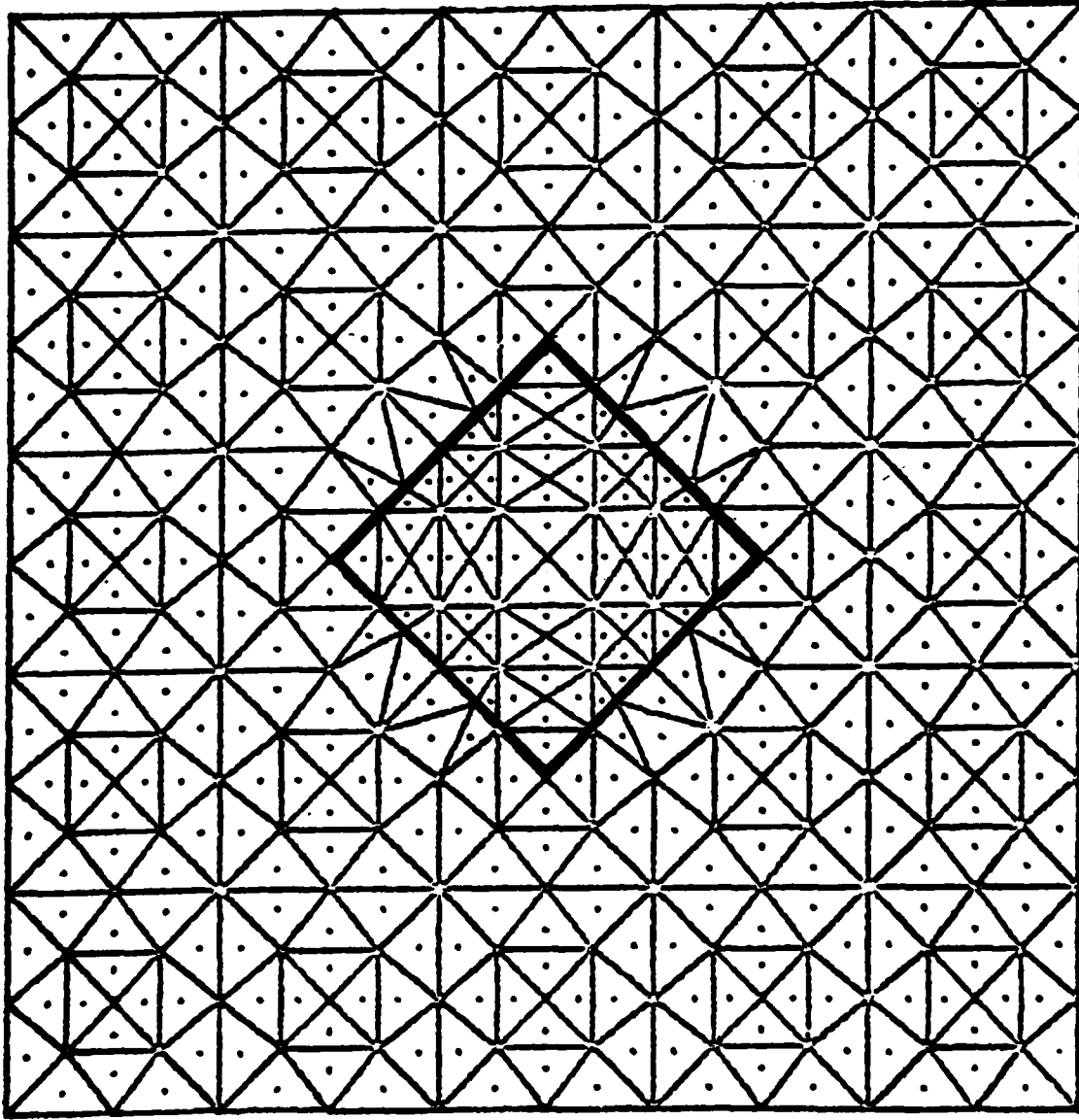
Matrix or Coarse Model. Substructuring
occurs over region encompassed by heavy
print.

Figure 20.
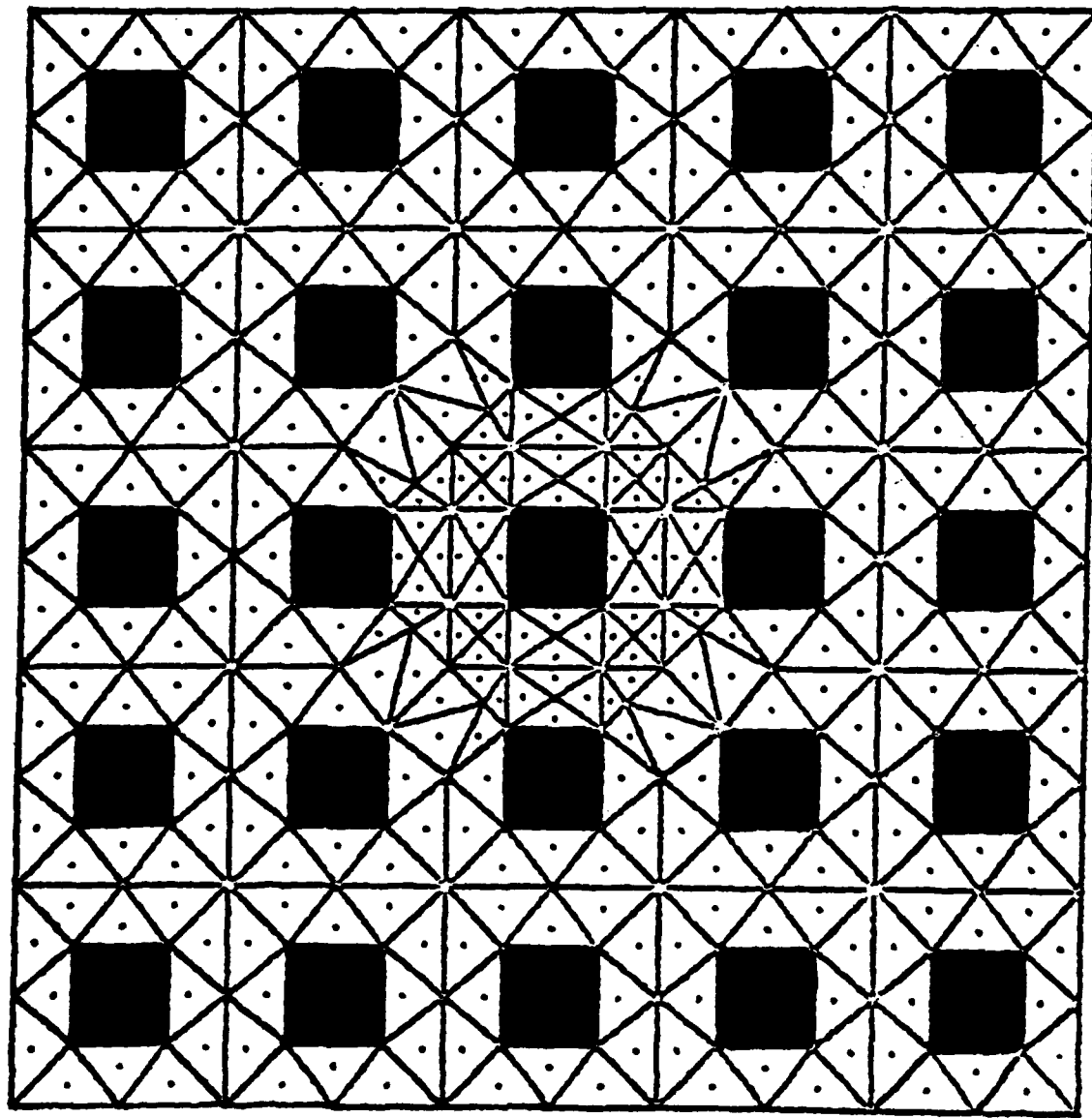
Matrix Model indicating L/D=2.

Figure 21.
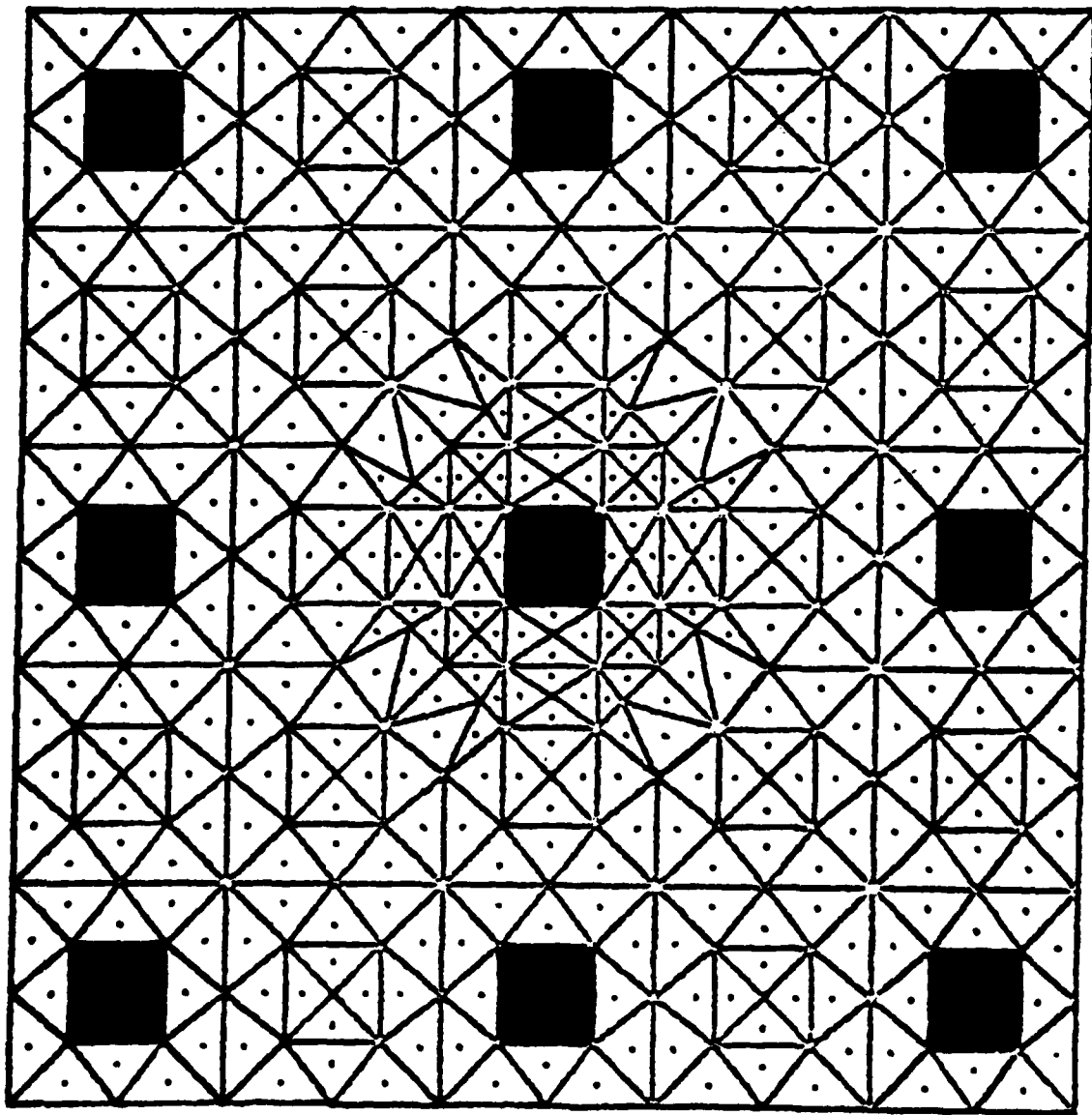
Matrix Model Indicating L/D=4.

Figure 22.
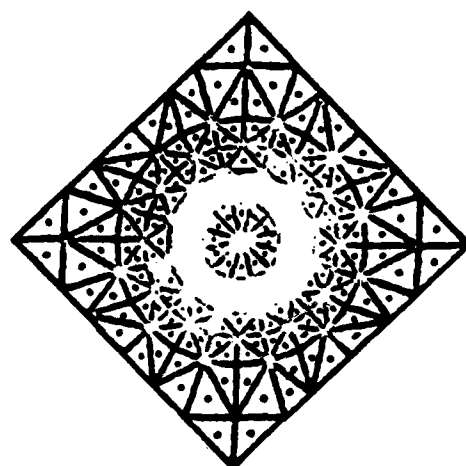
Particle or fine model presented in
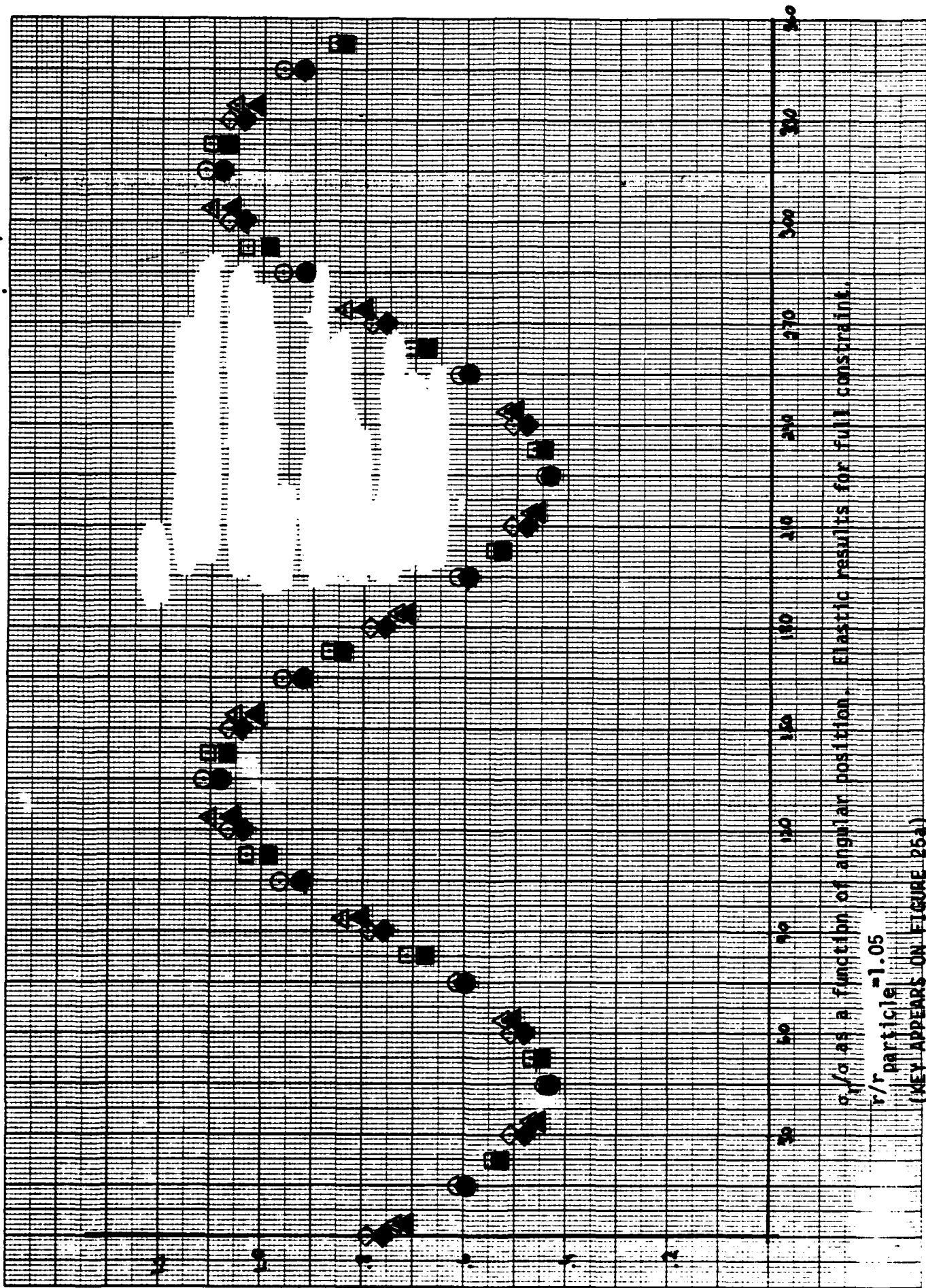actual size and configuration.

Figure 23.
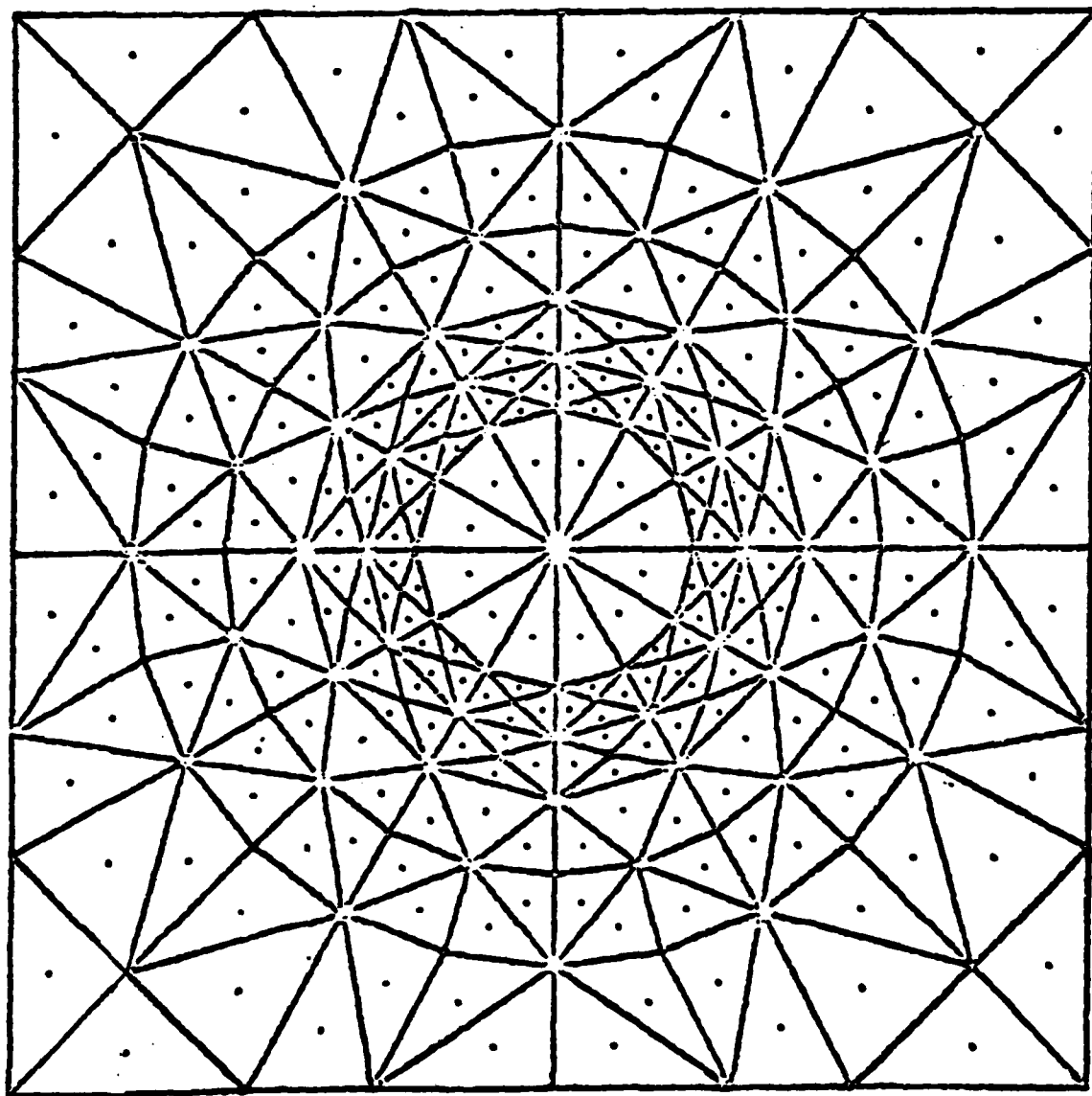
Enlargement of Particle Model and regions
directly contguous.

Figure 24.

<u>KEY:</u>

⊙   PARTICLE-PARTICLE AXIS COINCIDES WITH TENSILE AXIS.

△   PARTICLE-PARTICLE AXIS FORMS 11.25° ANGLE WITH TENSILE AXIS.

⊡   PARTICLE-PARTICLE AXIS FORMS 22.5° ANGLE WITH TENSILE AXIS.

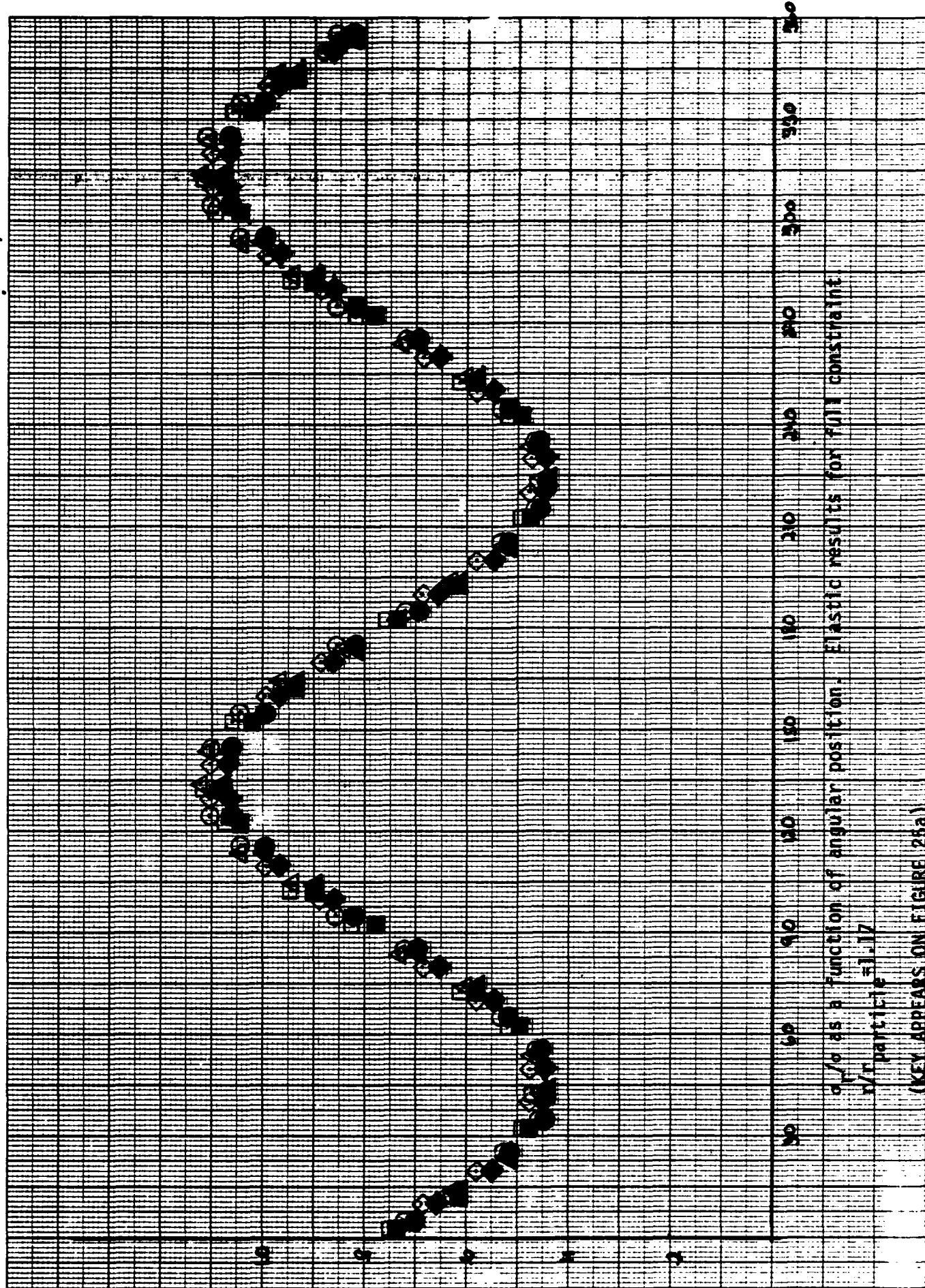◇   PARTICLE-PARTICLE AXIS FORMS 45.0° ANGLE WITH TENSILE AXIS.

● ▲ ■ ◆   ANALOGOUS EXCEPT SINGLE PARTICLE ANALYSIS.

Figure 25a.

σ_{rr}/σ as a function of angular position. Elastic results for full constraint.

$r/r_{particle} = 1.05$

(KEY APPEARS ON FIGURE 25a)

Figure 25b.

Figure 26.

q/q_o as a function of angular position. Elastic results for full constraint. $r/r_{particle} = 1.17$ (KEY APPEARS ON FIGURE 26a)
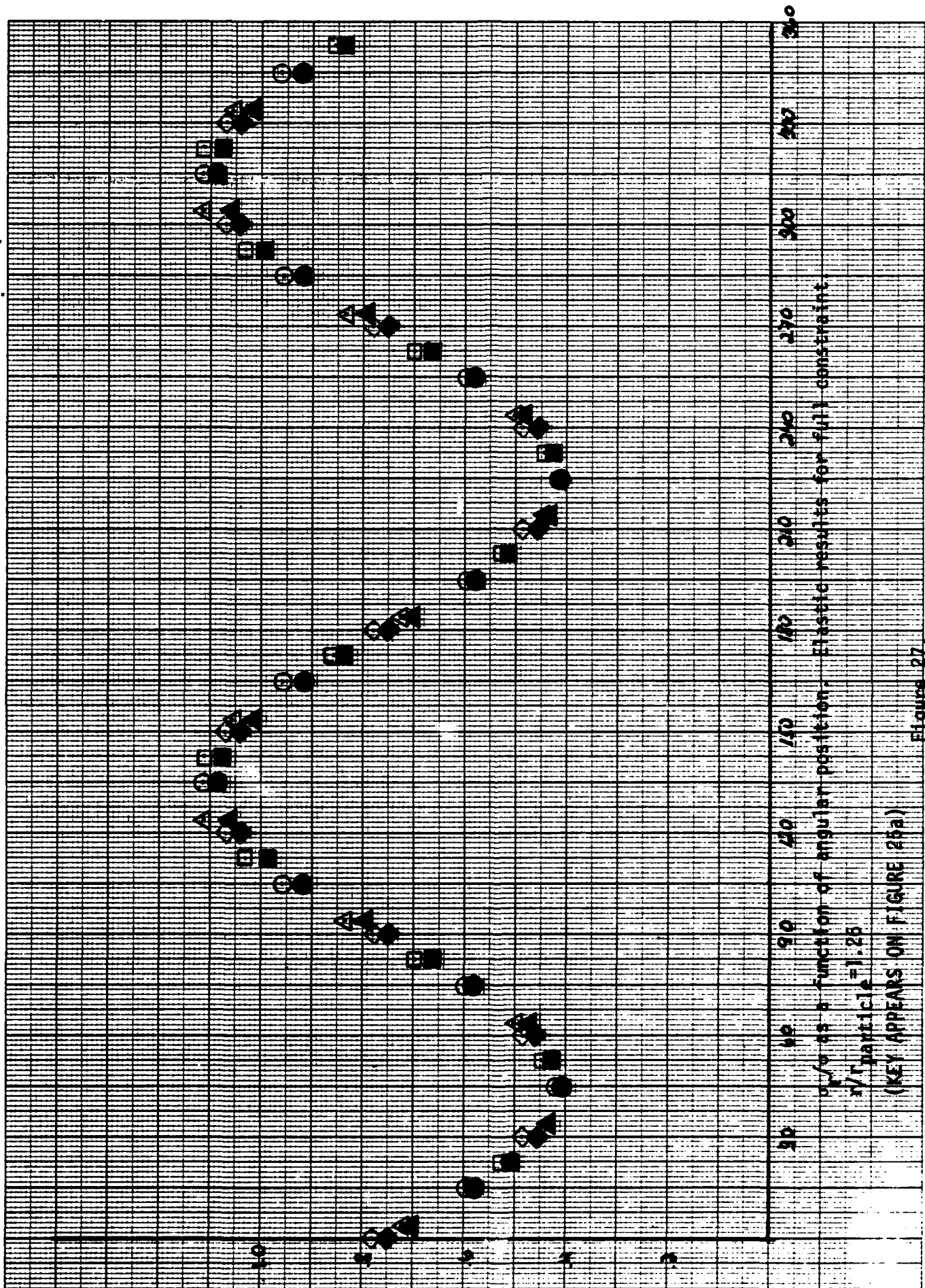
σ_r/σ as a function of angular position. Elastic results for full constraint.
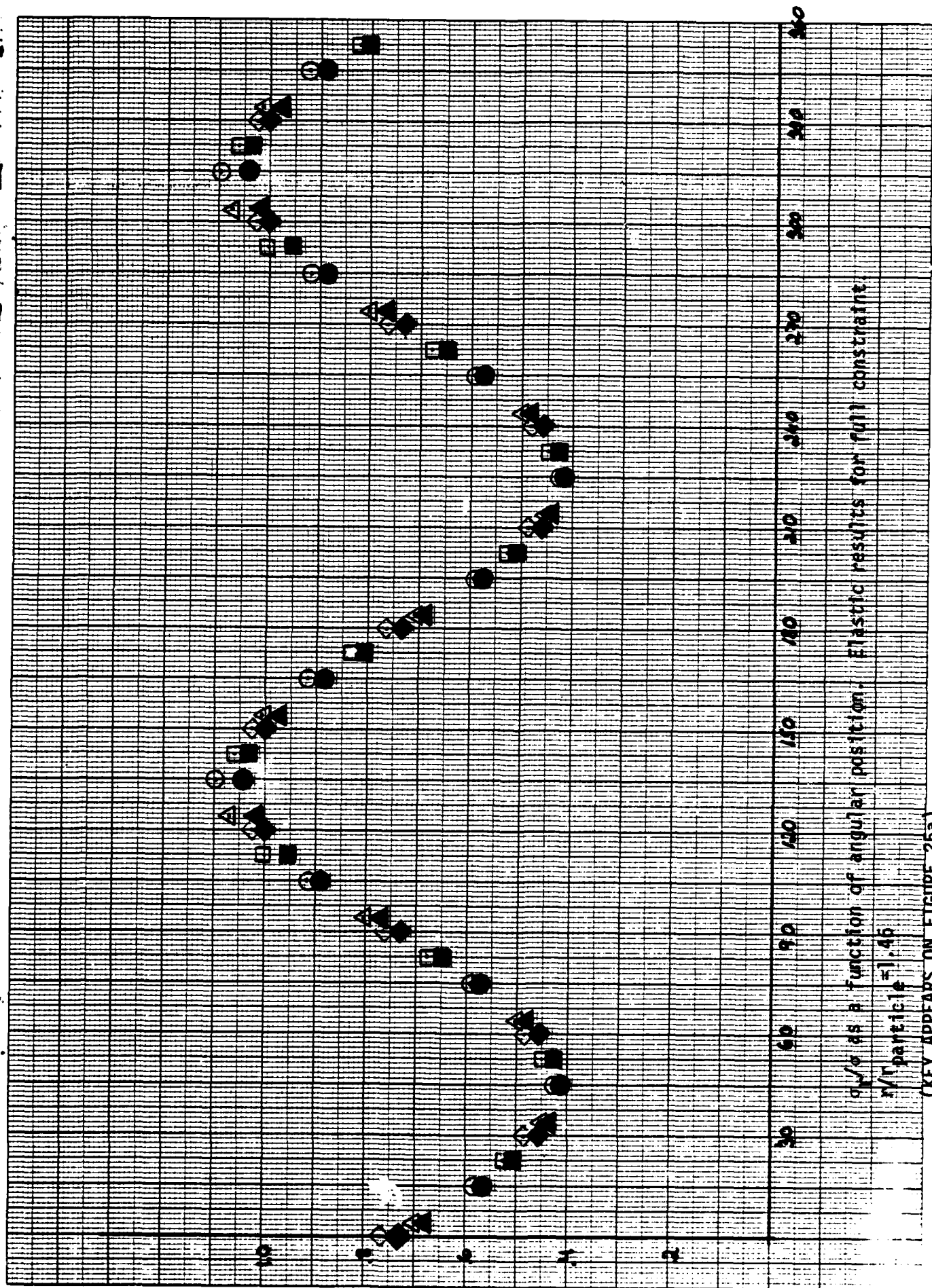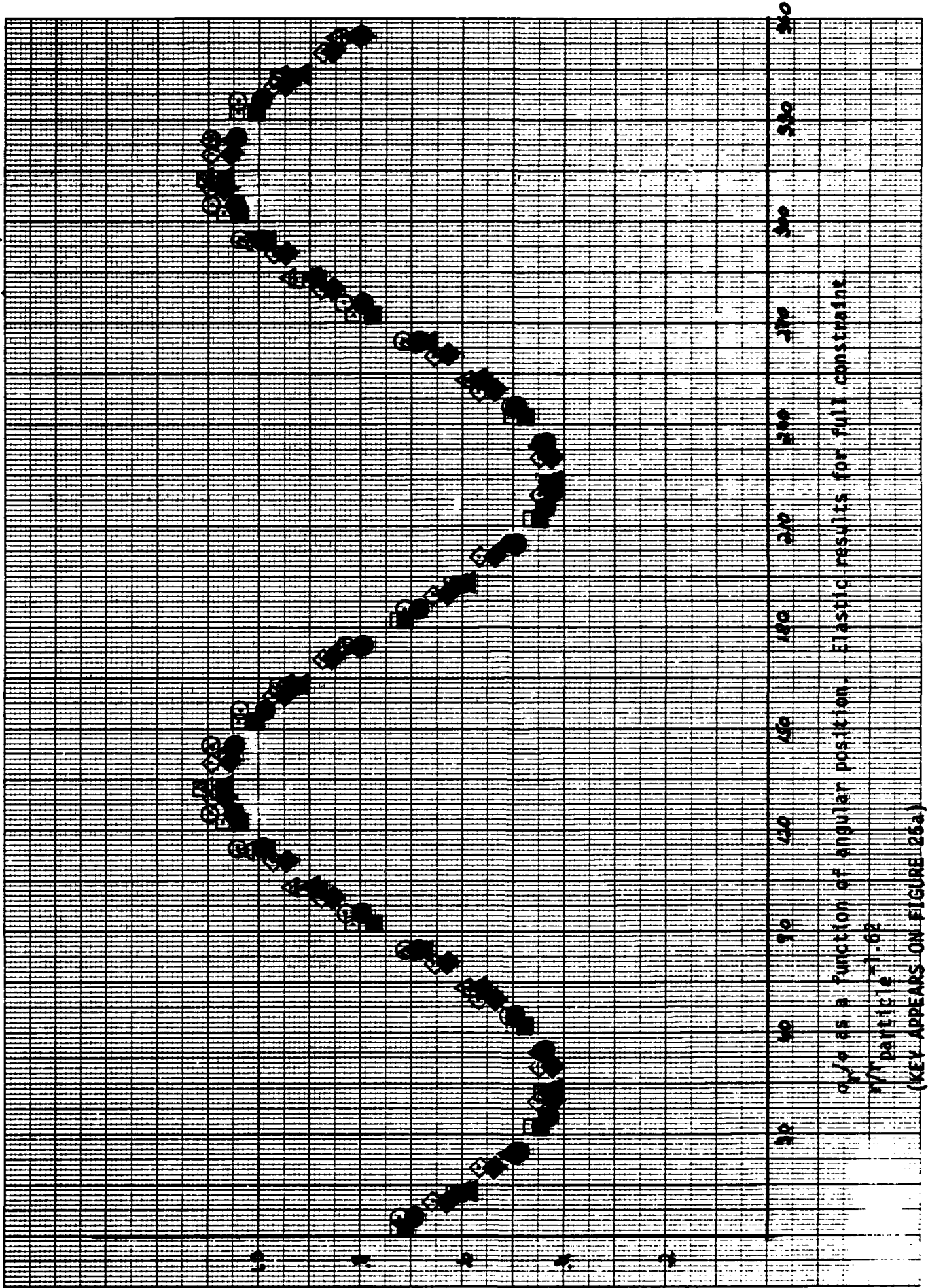
$x/r_{particle} = 1.25$

(KEY APPEARS ON FIGURE 25a)

Figure 27

Figure 28. q_w/q as a function of angular position. Elastic results for full constraint.
r/r particle = 1.46

(KEY APPEARS ON FIGURE 25a)

σ_ϕ/σ_o as a function of angular position. Elastic results for full constraint.

r/r particle = 1.62

(KEY APPEARS ON FIGURE 26a.)

Figure 29.

Figure 30.

σ_r/σ as a function of angular position. Elastic results for full constraint.
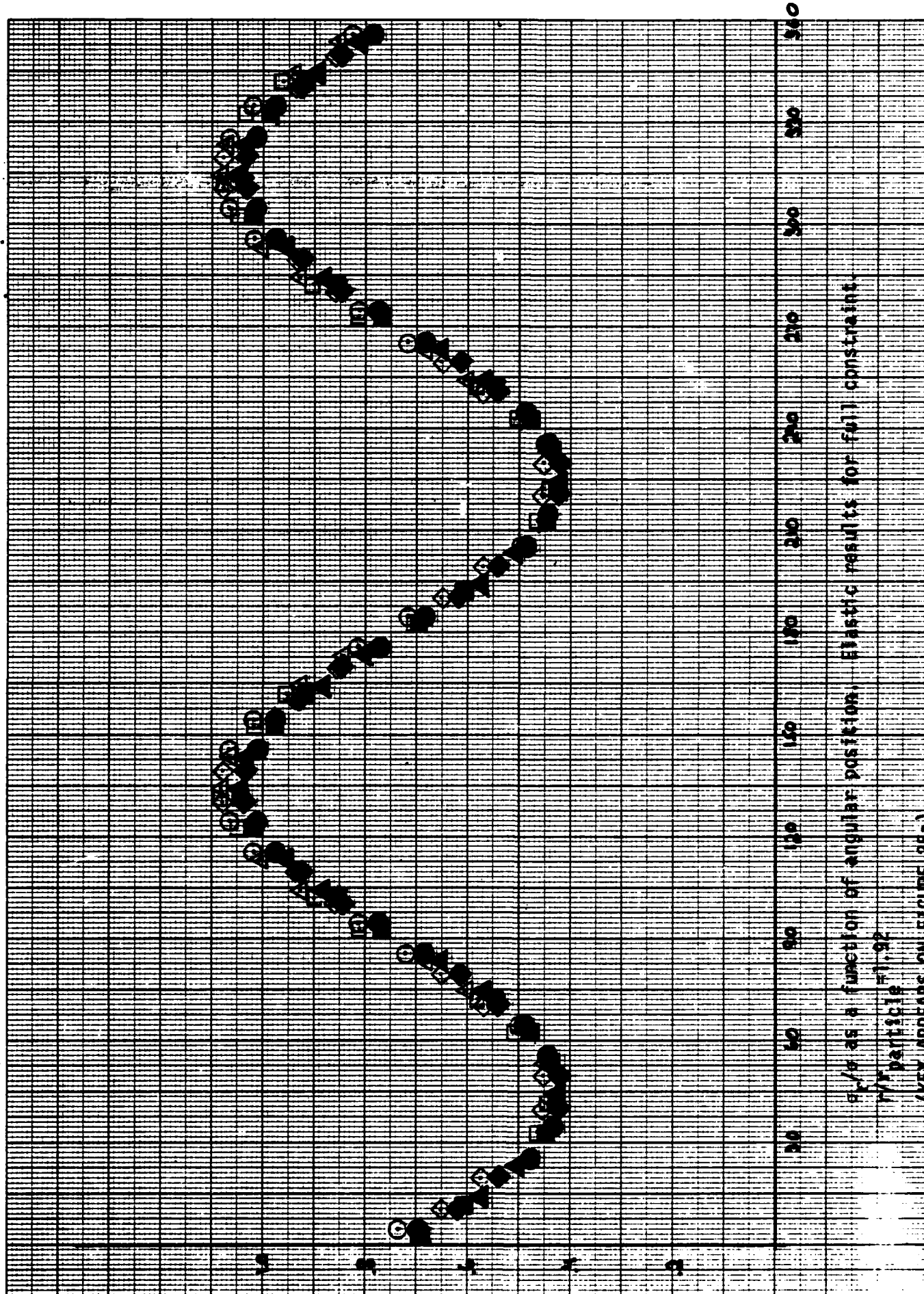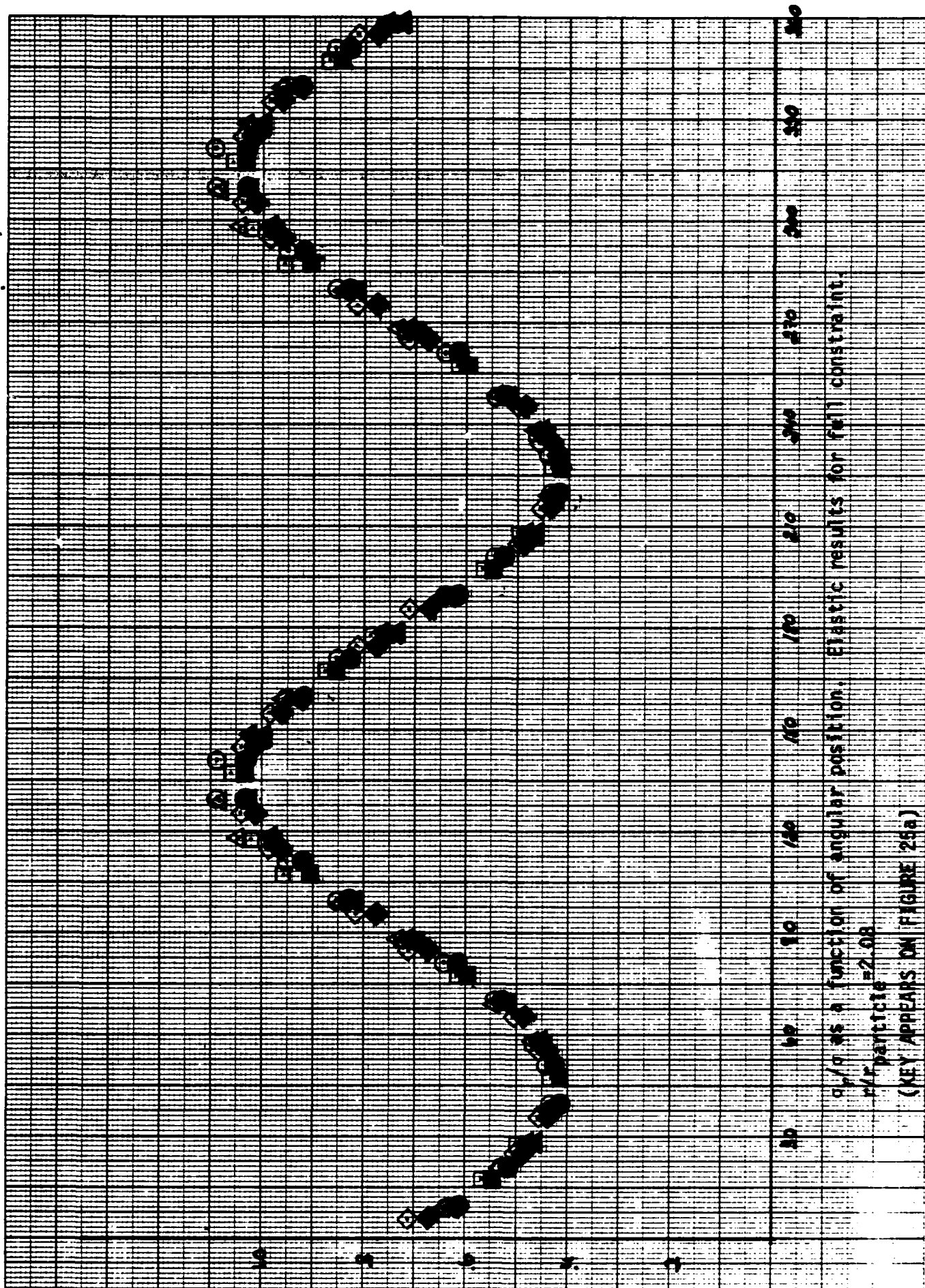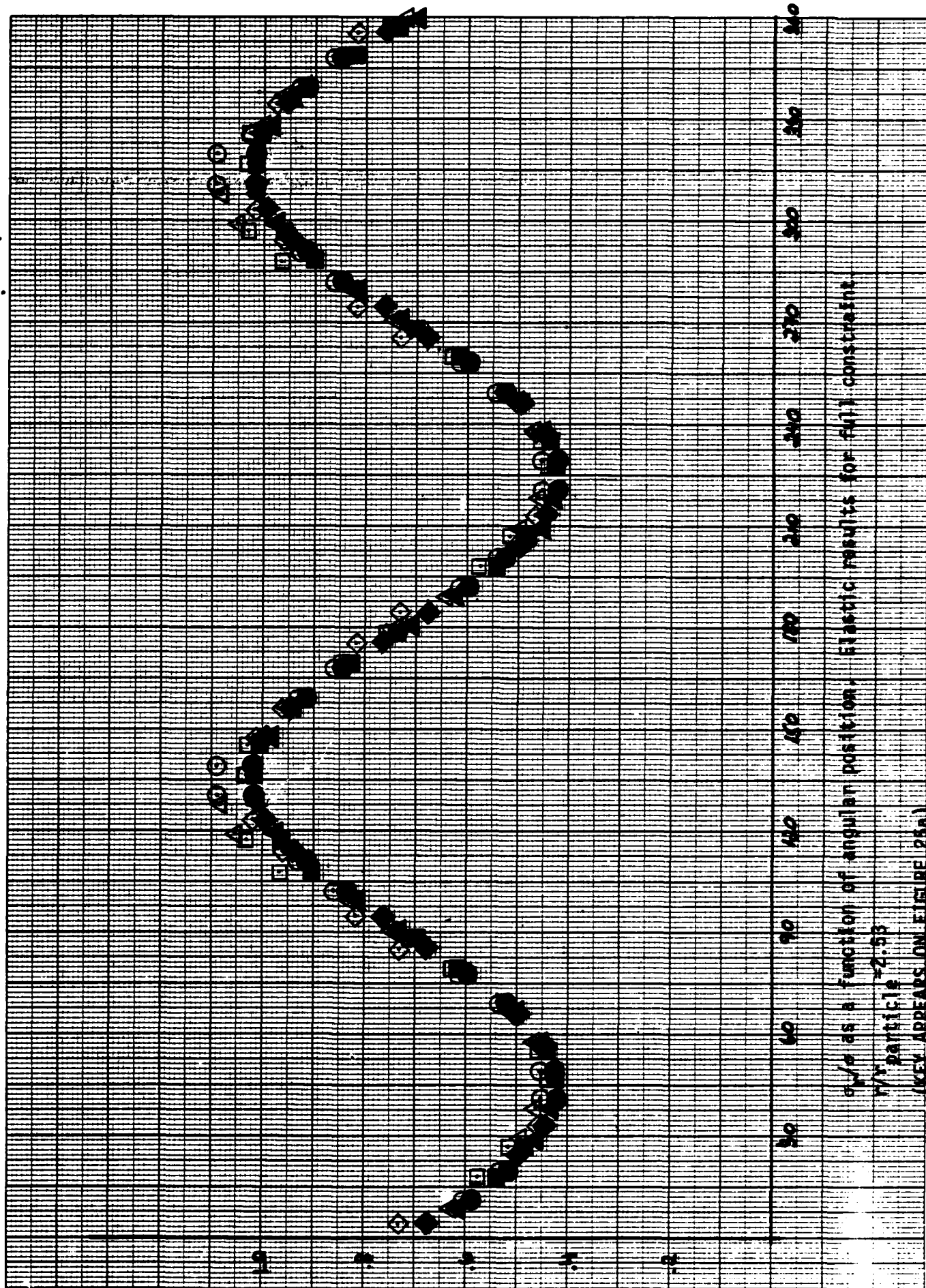
r/r particle = 1.92

(KEY APPEARS ON FIGURE 26a.)

Figure 31.

q_p/q as a function of angular position. Elastic results for full constraint.
r/r particle =2.08
(KEY APPEARS ON FIGURE 26a)

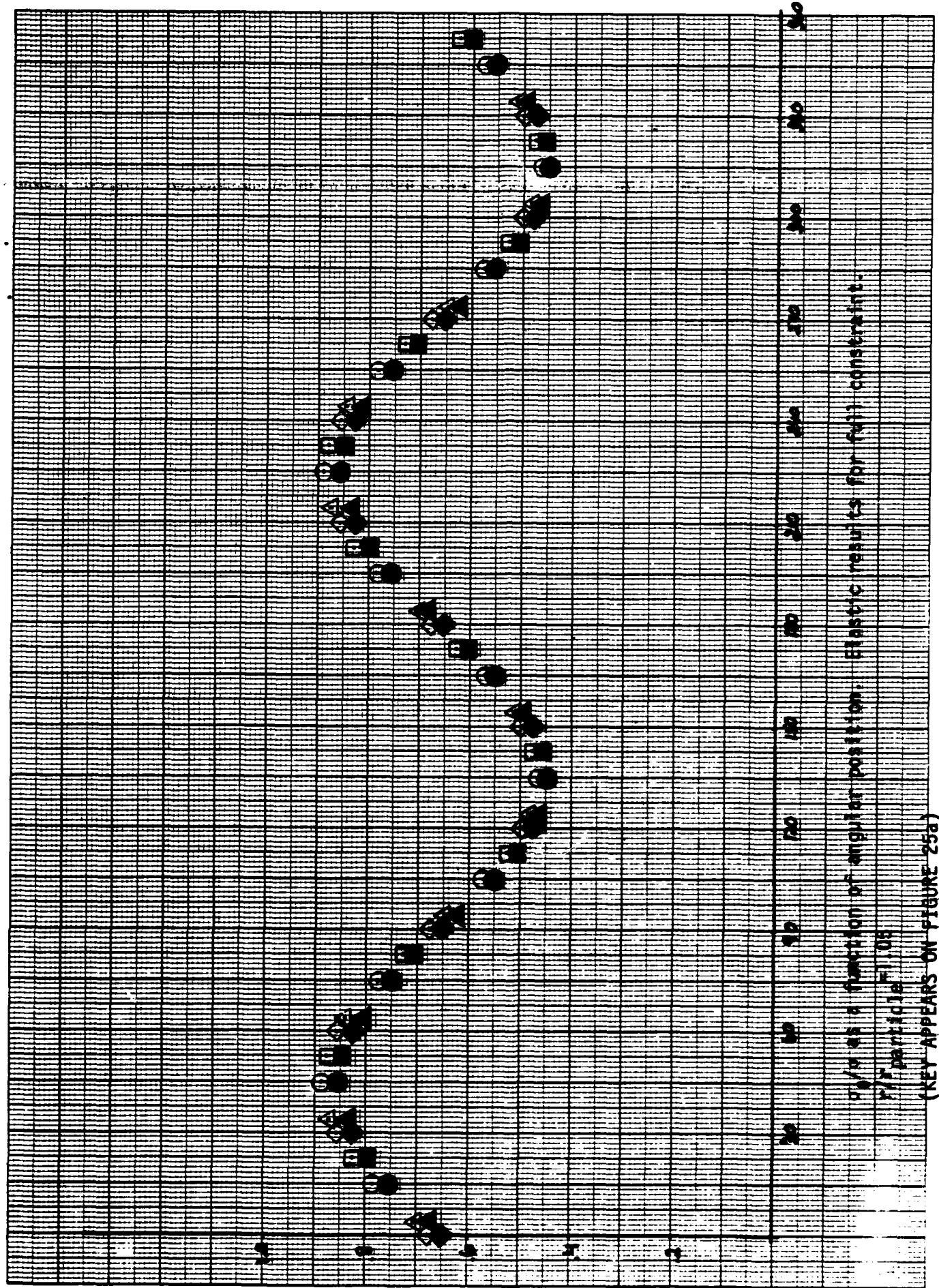σ_n/σ_o as a function of angular position. Elastic results for full constraint.

"N" particle

P/Po =2.55

(KEY APPEARS ON FIGURE 25a)

Figure 32.

Figure 33.

q/m as a function of angular position. Elastic results for full constraint.

T/F Particle F1.05

(KEY APPEARS ON FIGURE 25a)

σ_e/σ as a function of angular position. Elastic results for full constraint.

Figure 34.

Figure 35.

q_0/σ as a function of angular position. Elastic results for full constraint.
$+/-$ particle = -1.26

(KEY APPEARS ON FIGURE 25b)

VERNON McMILLAN, INC. ELIZABETH, N.J. 07208

No. 19-0610 (R-2470-10-C) 10 Millimeters to a Centimeter • Made in U.S.A

Figure 36. $d\sigma/d\Omega$ as a function of angular position. Elastic results for full constraint. Particle $\theta_0 = 1.46$. $r/r =$ (KEY APPEARS ON FIGURE 25a)

Figure 37.

σ_β/σ_r as a function of angular position. Elastic results for full constraint.

r/r particle =1.62

(KEY APPEARS ON FIGURE 25a)

Figure 38.

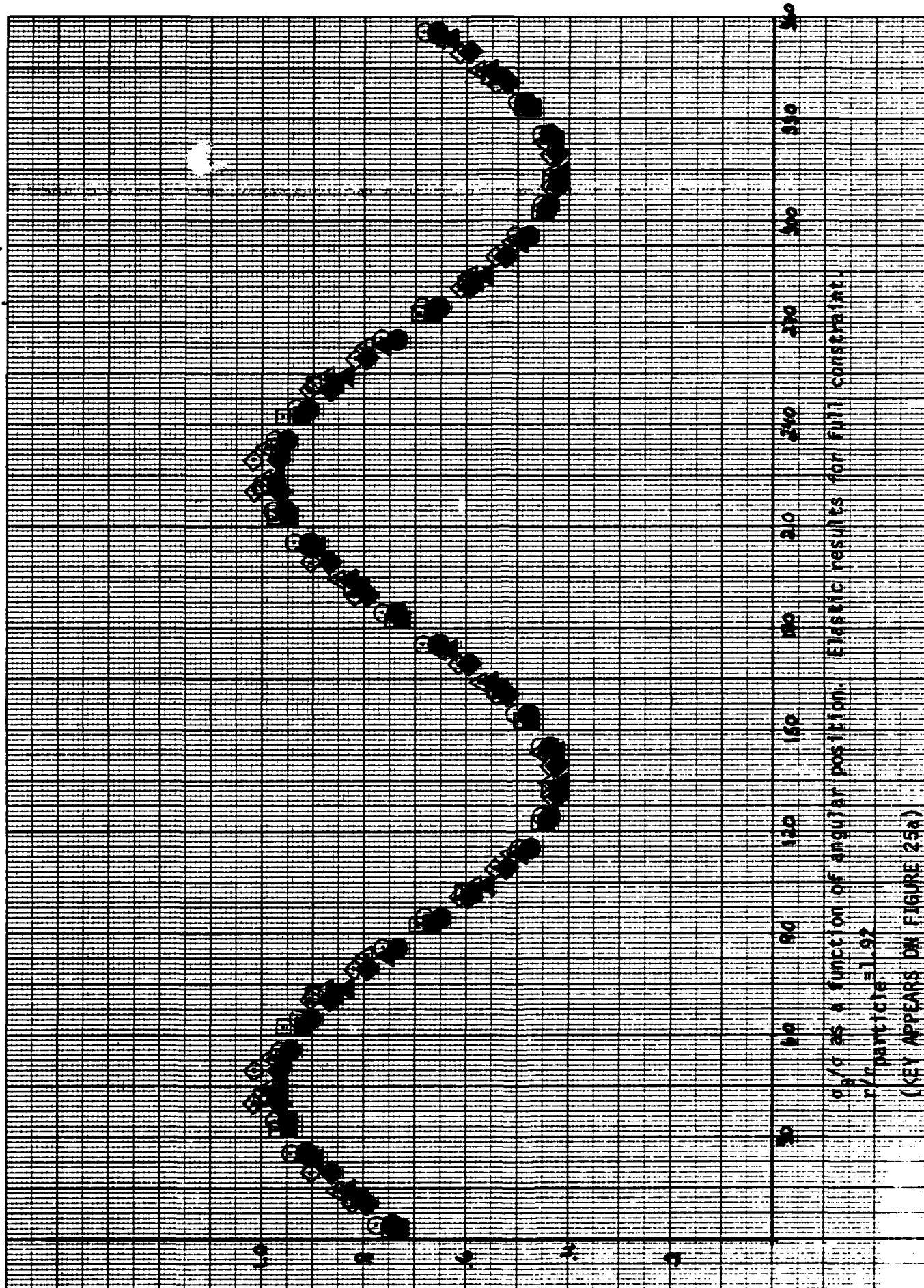q/q_0 as a function of angular position. Elastic results for full constraint. r/r_p particle $=1.92$ (KEY APPEARS ON FIGURE 25a)

Figure 39. σ_3/σ as a function of angular position. Elastic results for full constraint. $r/r_{particle} = 2.08$ (KEY APPEARS ON FIGURE 25a).

Figure 40.

$q/\bar{q}$ as a function of angular position. Elastic results for full constraint.
r/r part $1-1\xi$ $=2.53$
(KEY APPEARS ON FIGURE 25a)

Figure 41.

T_θ/σ as a function of angular position. Elastic results for full constraint.
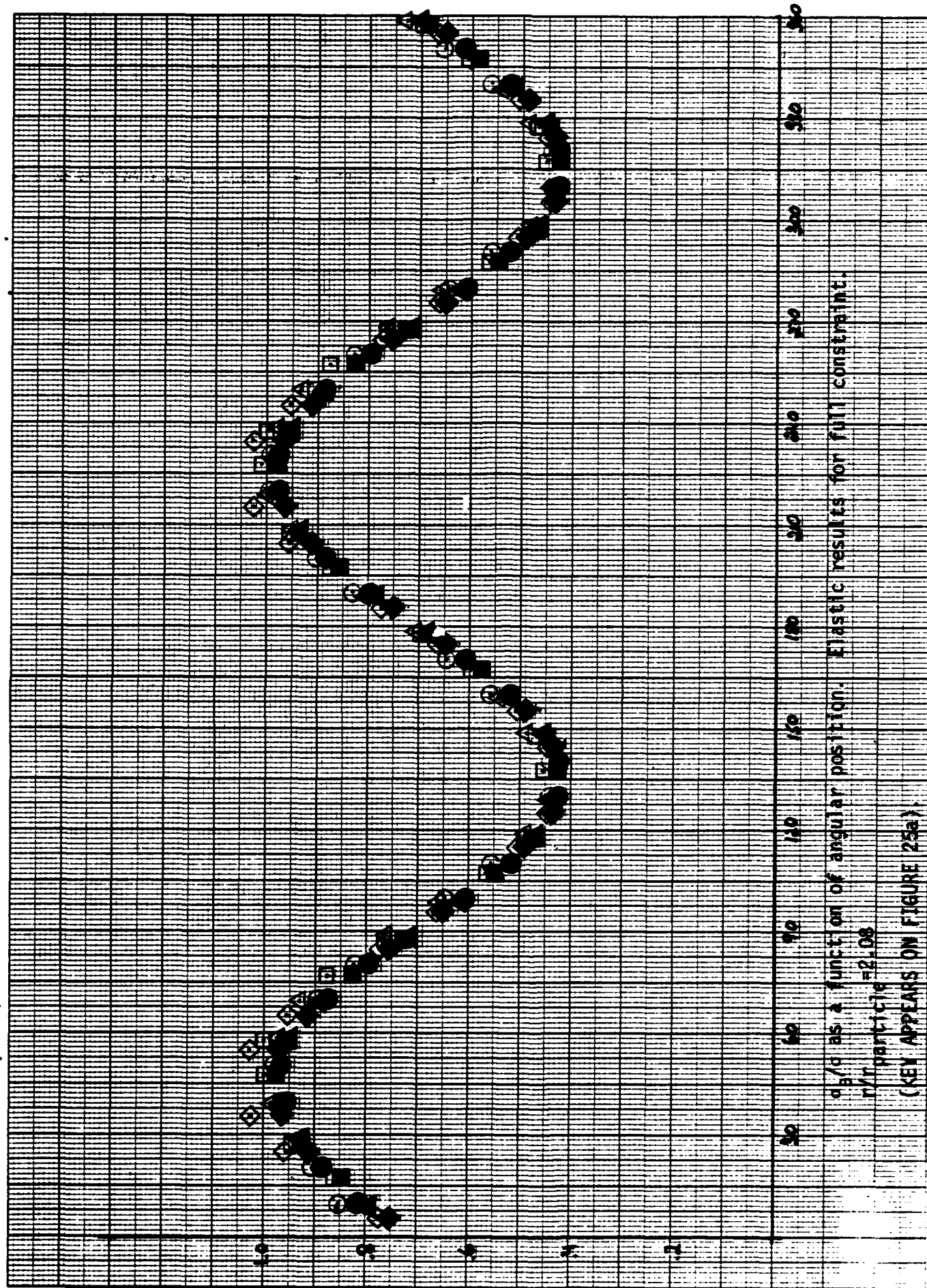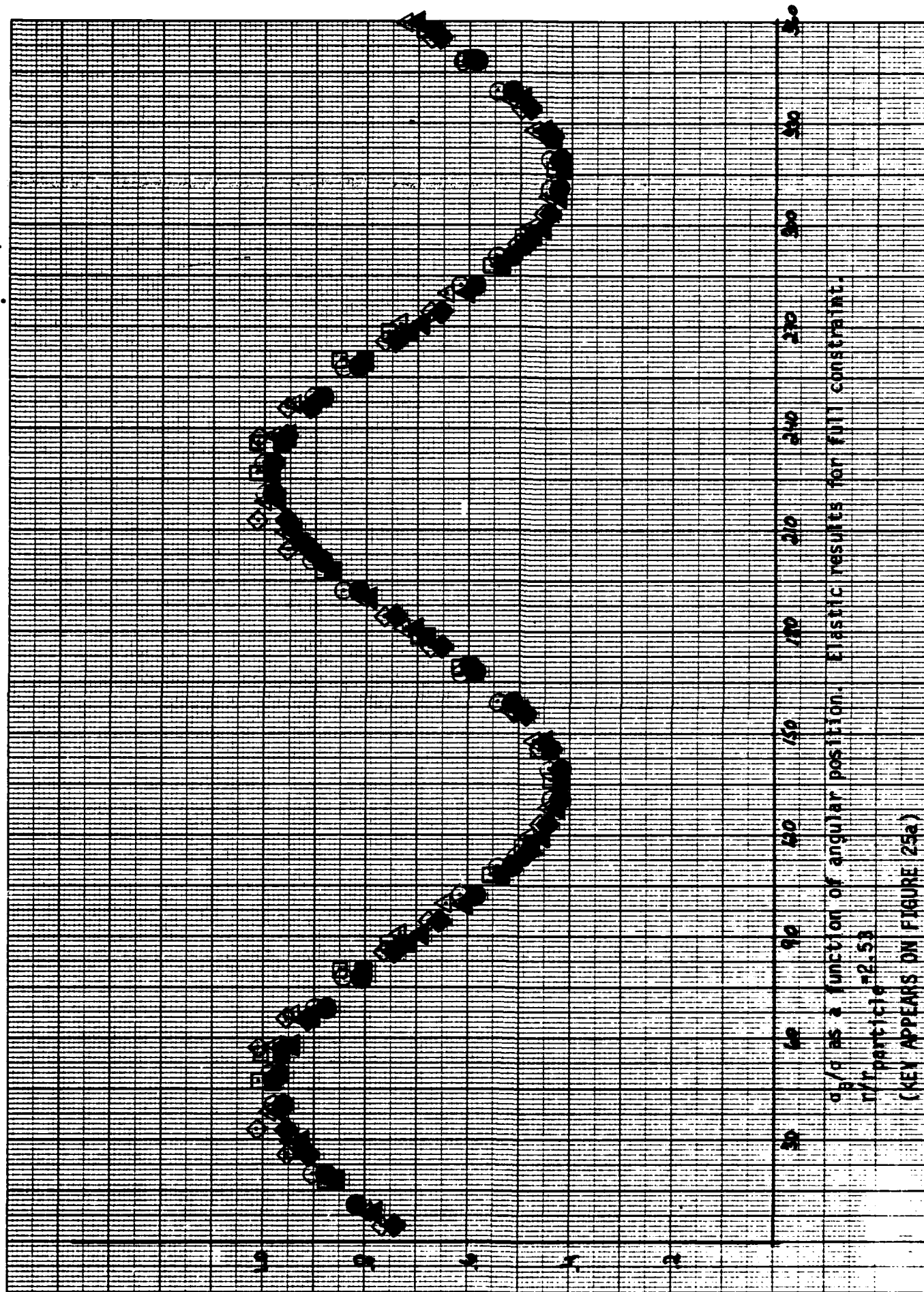$r/r_{particle} = 1.05$
(KEY APPEARS ON FIGURE 25a)

Figure 42. $\tau r_\theta / \sigma$ as a function of angular position. Elastic results for full constraint.
$r/r_{particle} = 1.17$
(KEY APPEARS ON FIGURE 25a)

Figure 43.

$\tau_{r\theta}/\sigma$ as a function of angular position. Elastic results for full constraint. $r/r_{particle} = 1.26$

(KEY APPEARS ON FIGURE 25a.)

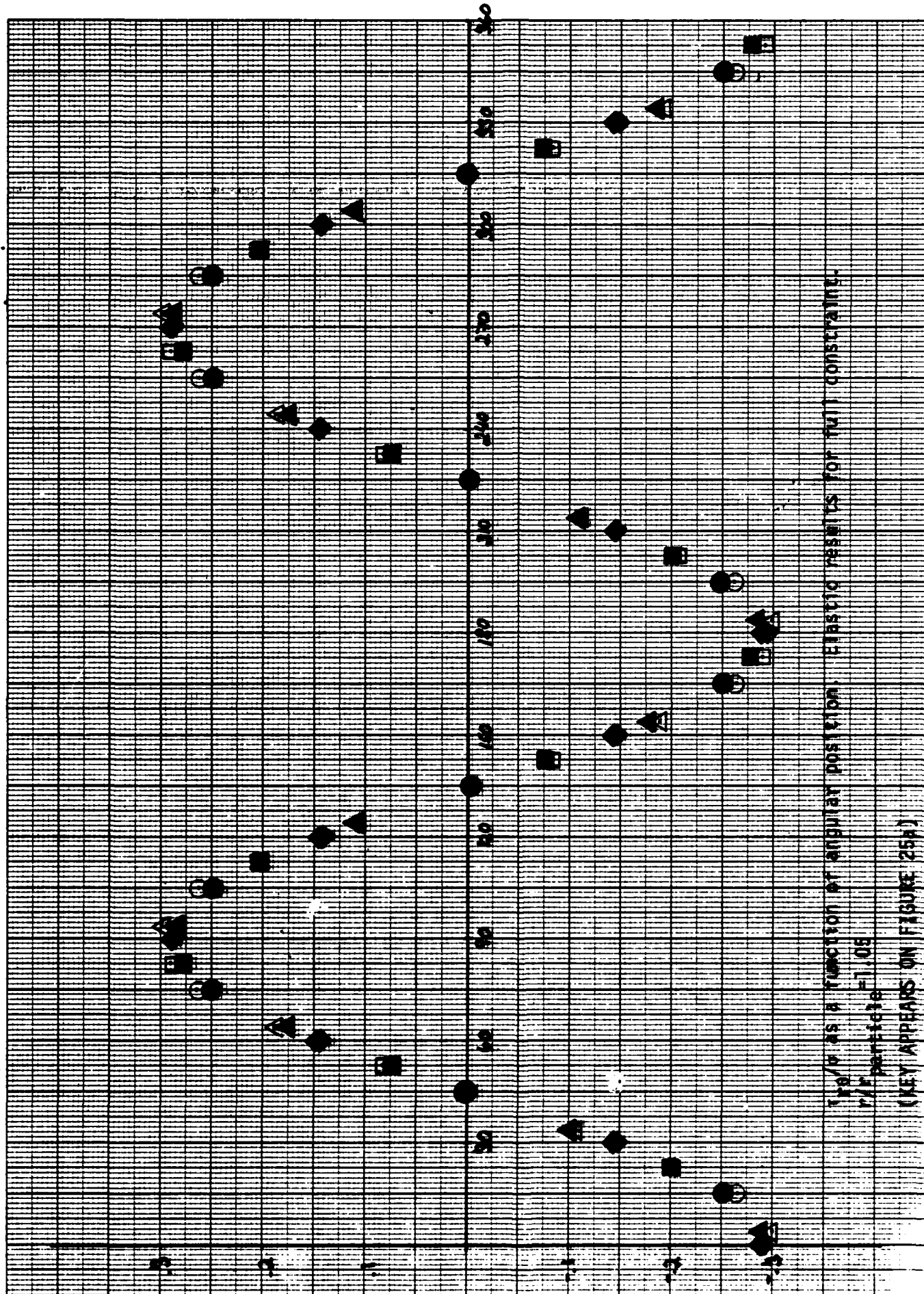Figure 44. $\tau_{r\theta}/\sigma$ as a function of angular position. Elastic results for full constraint. η/r particle #1.45

(KEY APPEARS ON FIGURE 23a)

$\sigma(\theta)/\sigma_R$ as a function of angular position. Elastic results for full constraint.

r/r particle = 1.62

(KEY APPEARS ON FIGURE 25a)

Figure 45.

Figure 46. Elastic result for angular position. Elastic result for angular position. Elastic result of angular position as a function of angular position. Elastic result for angular position.

r/r particle = 1.92

(KEY APPEARS ON FIGURE 25a)

Figure 47. $\tau_{r\phi}/\sigma$ as a function of angular position. Elastic results for full constraint.
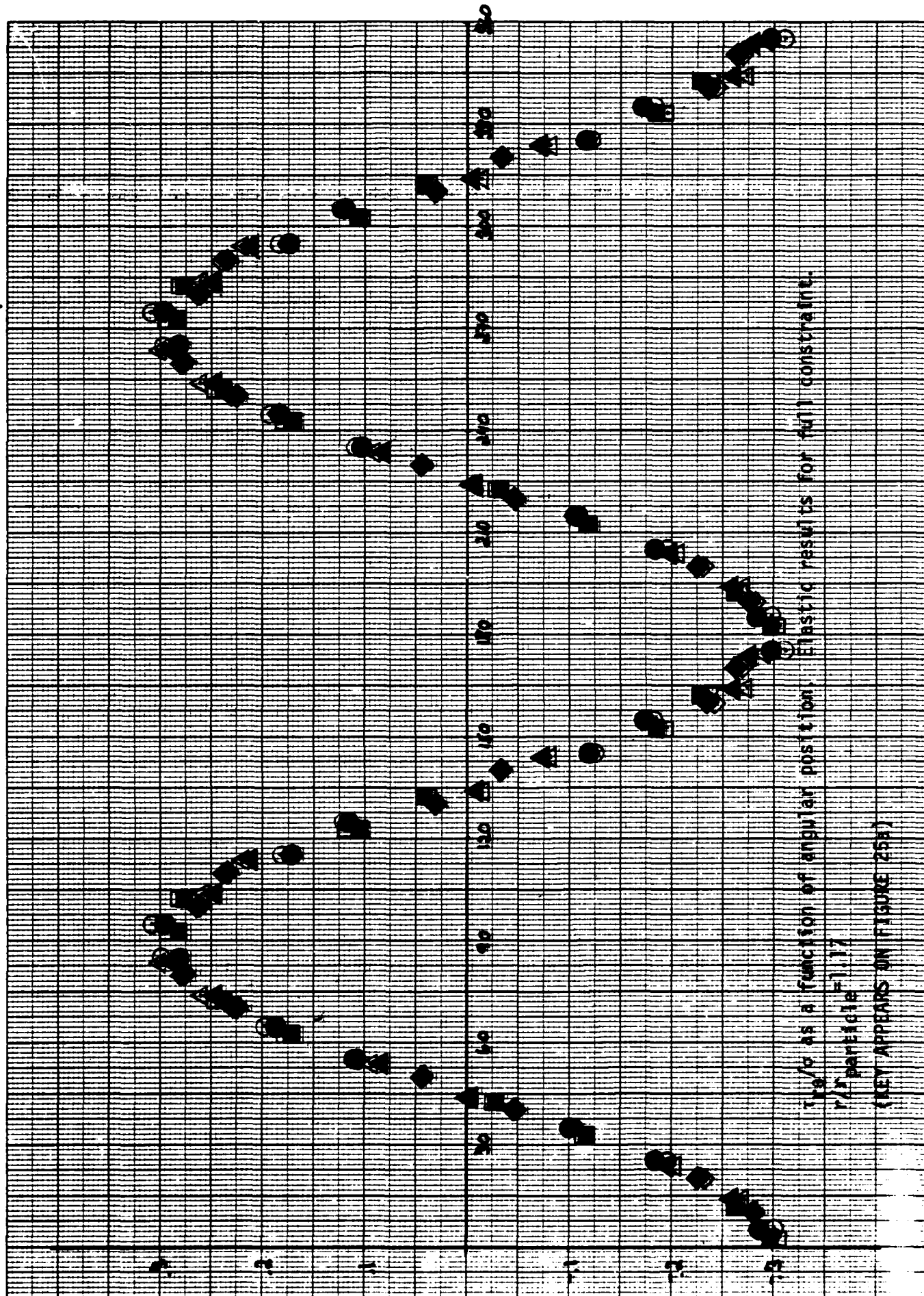
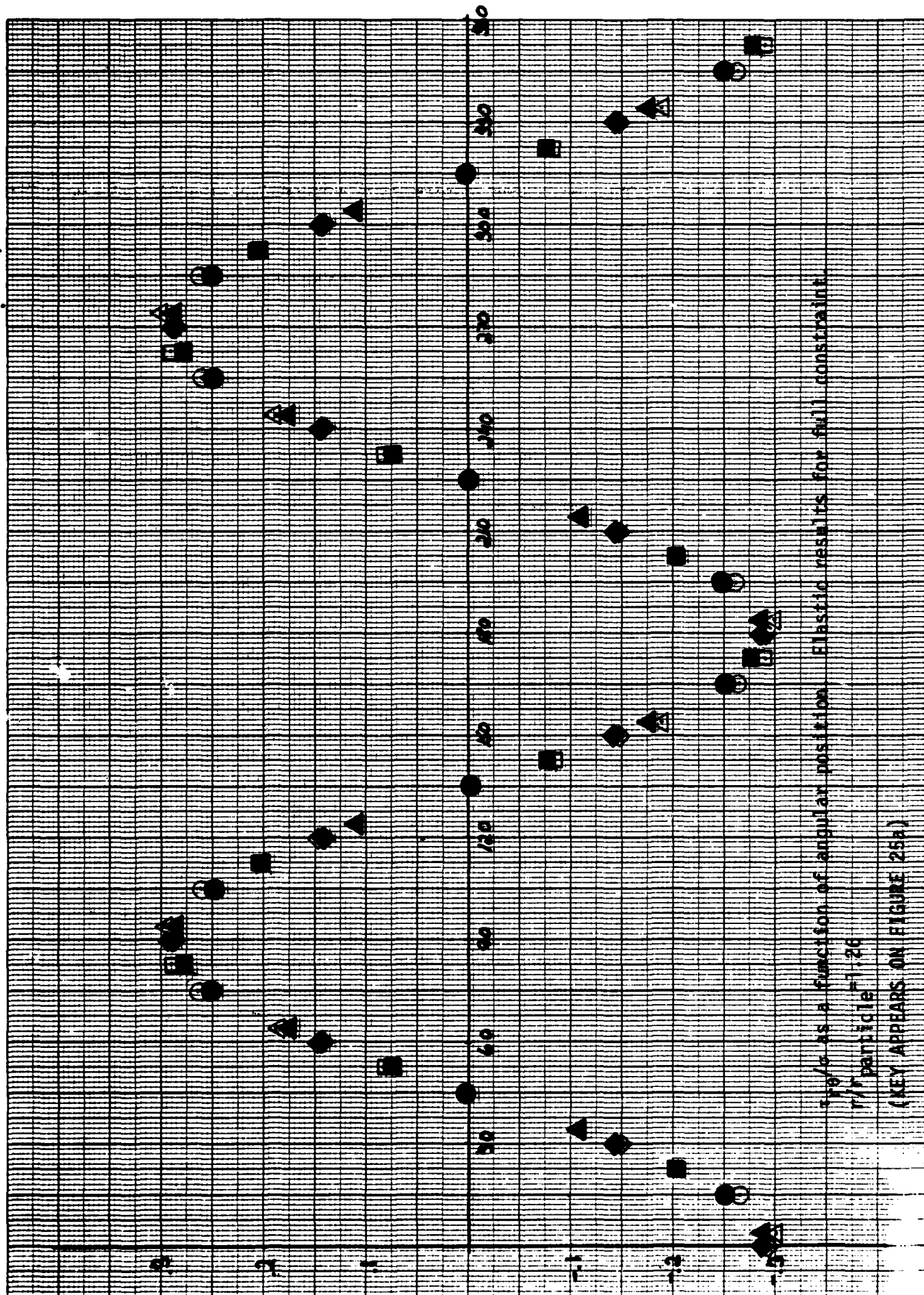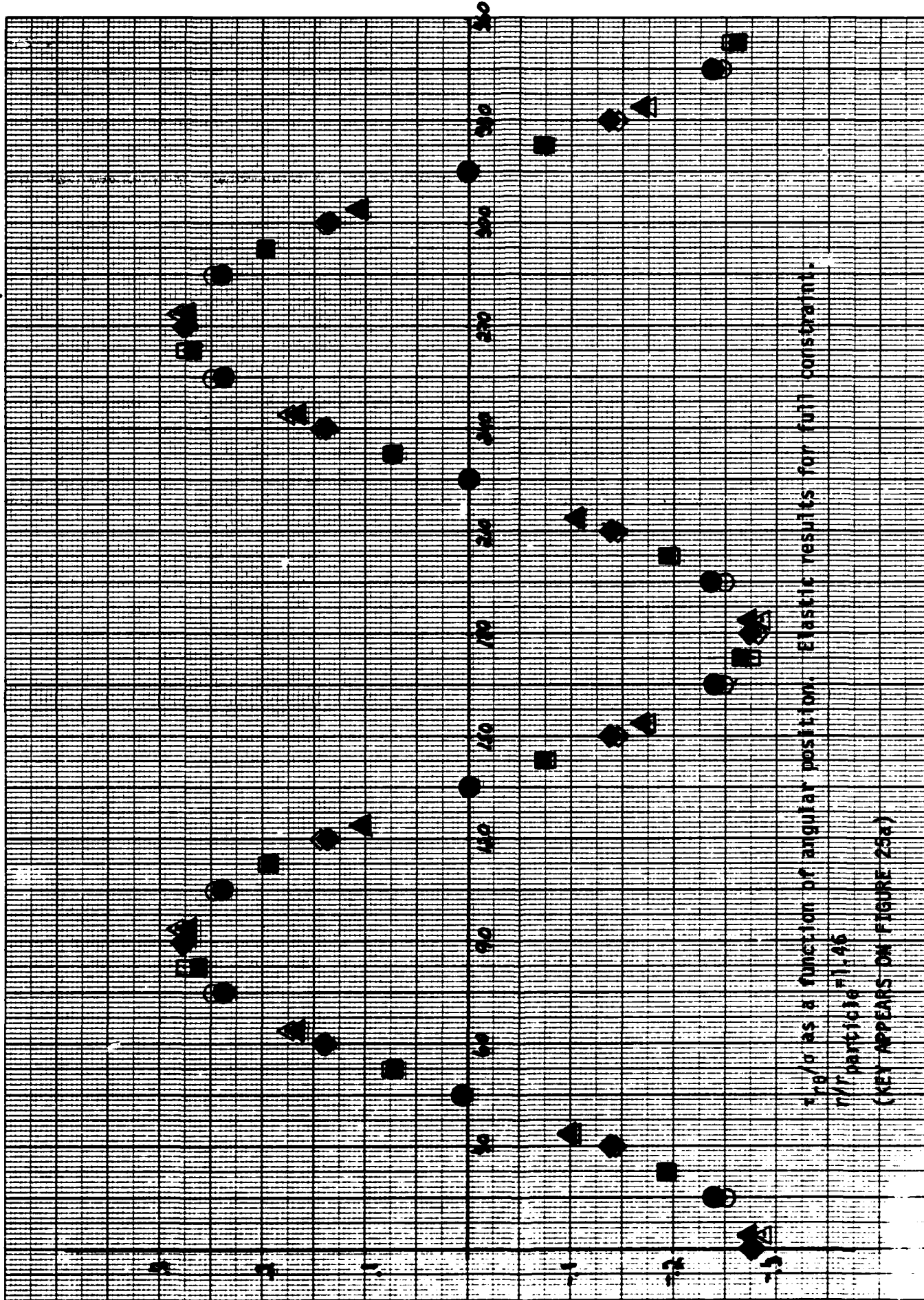r/r particle = 2.08

(KEY APPEARS ON FIGURE 25a)

Figure 48.

Toe/e as a function of angular position. Elastic results for full constraint.

r/T particle: =2.58

(KEY APPEARS ON FIGURE 29.)

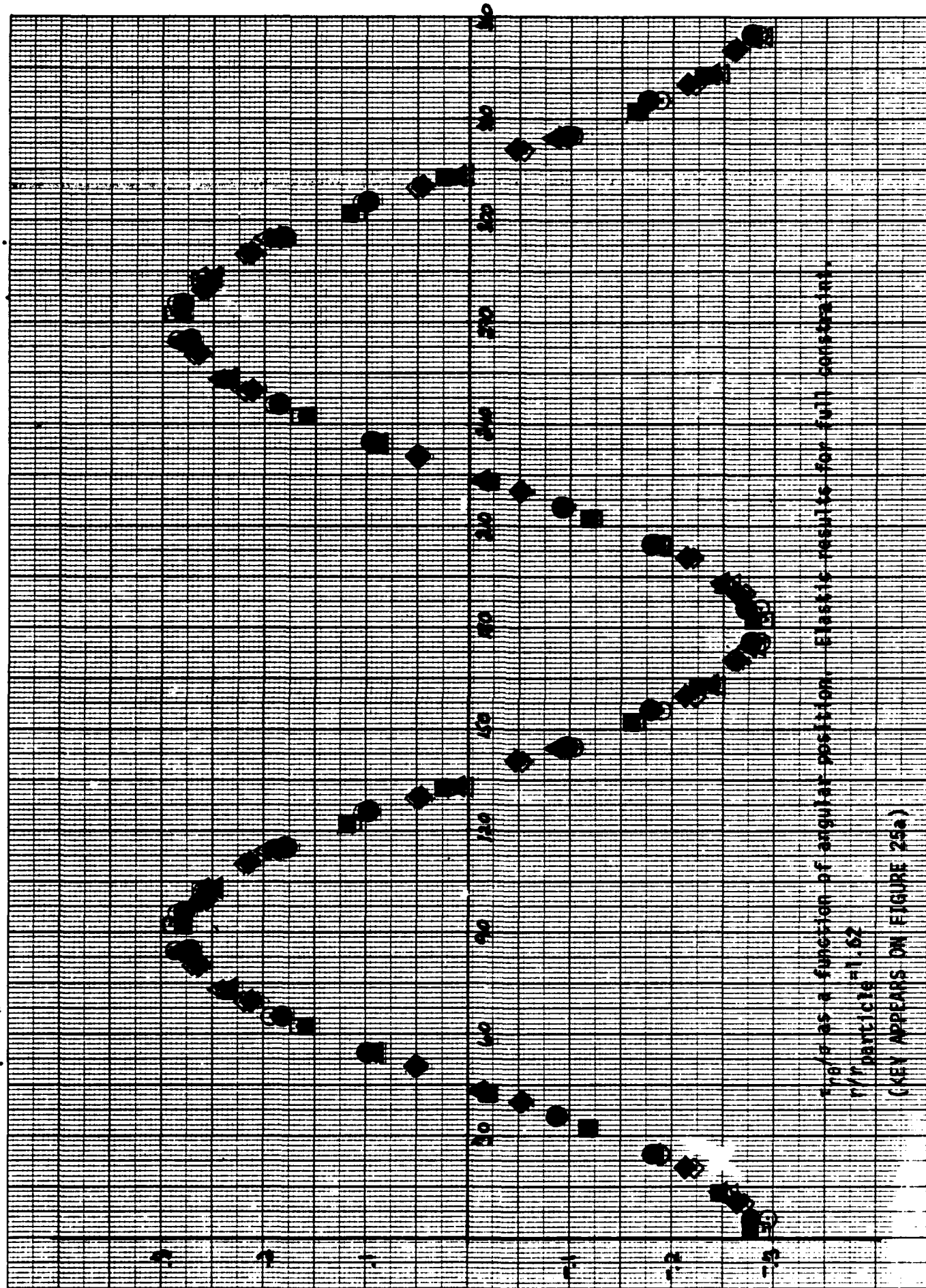Figure 49.

Tpct/Tlim as a function of angular position. Elastic results for full constraint.

P/Pparticle=1.05

(KEY APPEARS ON FIGURE 25a)

Figure 50.

$\sigma(\theta,\phi)/(\lambda/\pi)$ as a function of angular position. Elastic results for full constraint.

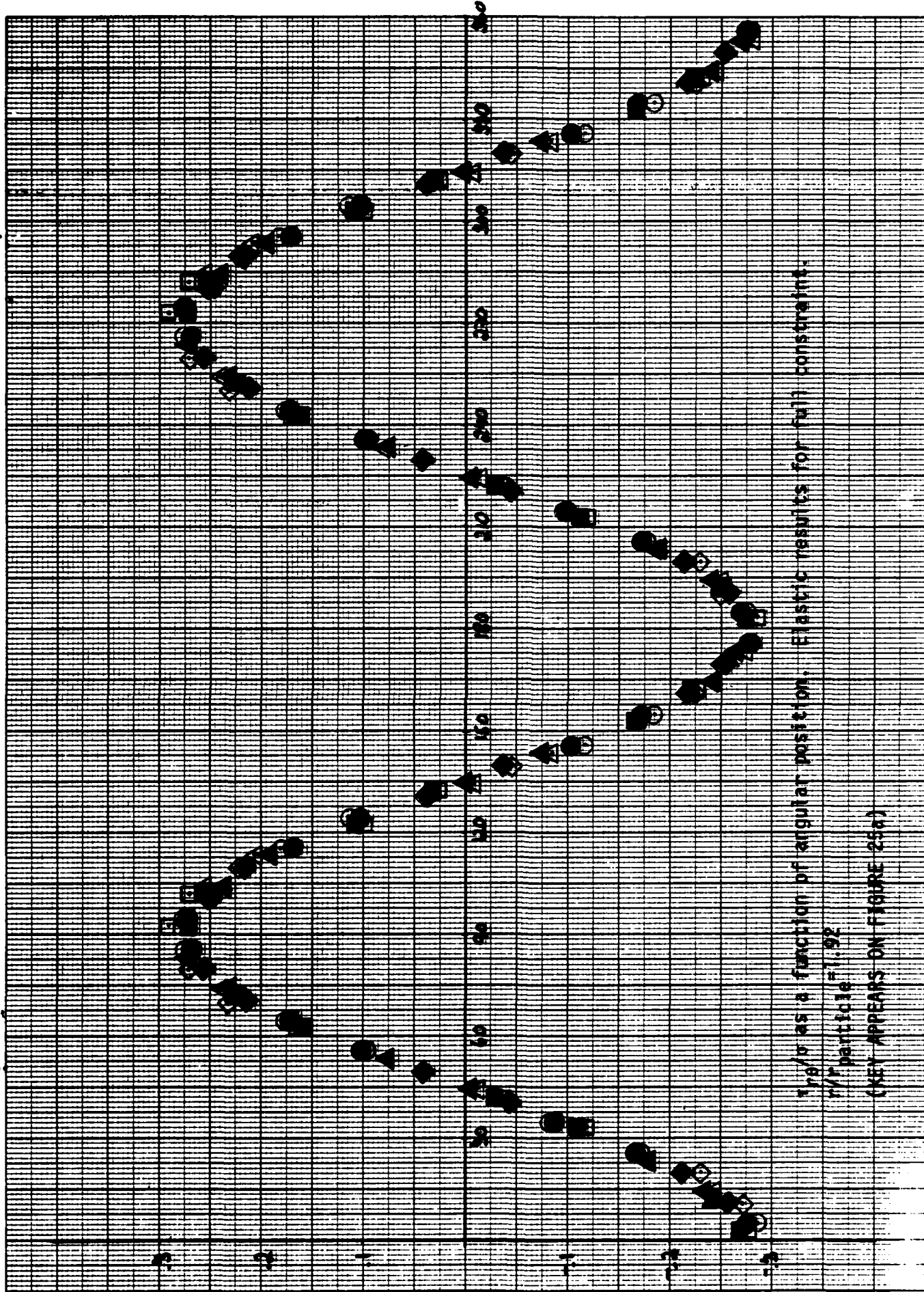γ/γ particle = 1.17

(KEY APPEARS ON FIGURE 25a)

Figure 51. Tpct/Tim as a function of angular position. Elastic results for full constraint.

r/r particle=1.26

(KEY APPEARS ON FIGURE 25a)

Figure 52.

T_{occ}/T_{ijn} as a function of angular position. Elastic results for full constraint.

x/t particle = 1.46

(KEY APPEARS ON FIGURE 25a)

Figure 53. σ_{cc}/σ_{jim} as a function of angular position. Elastic results for full constraint.
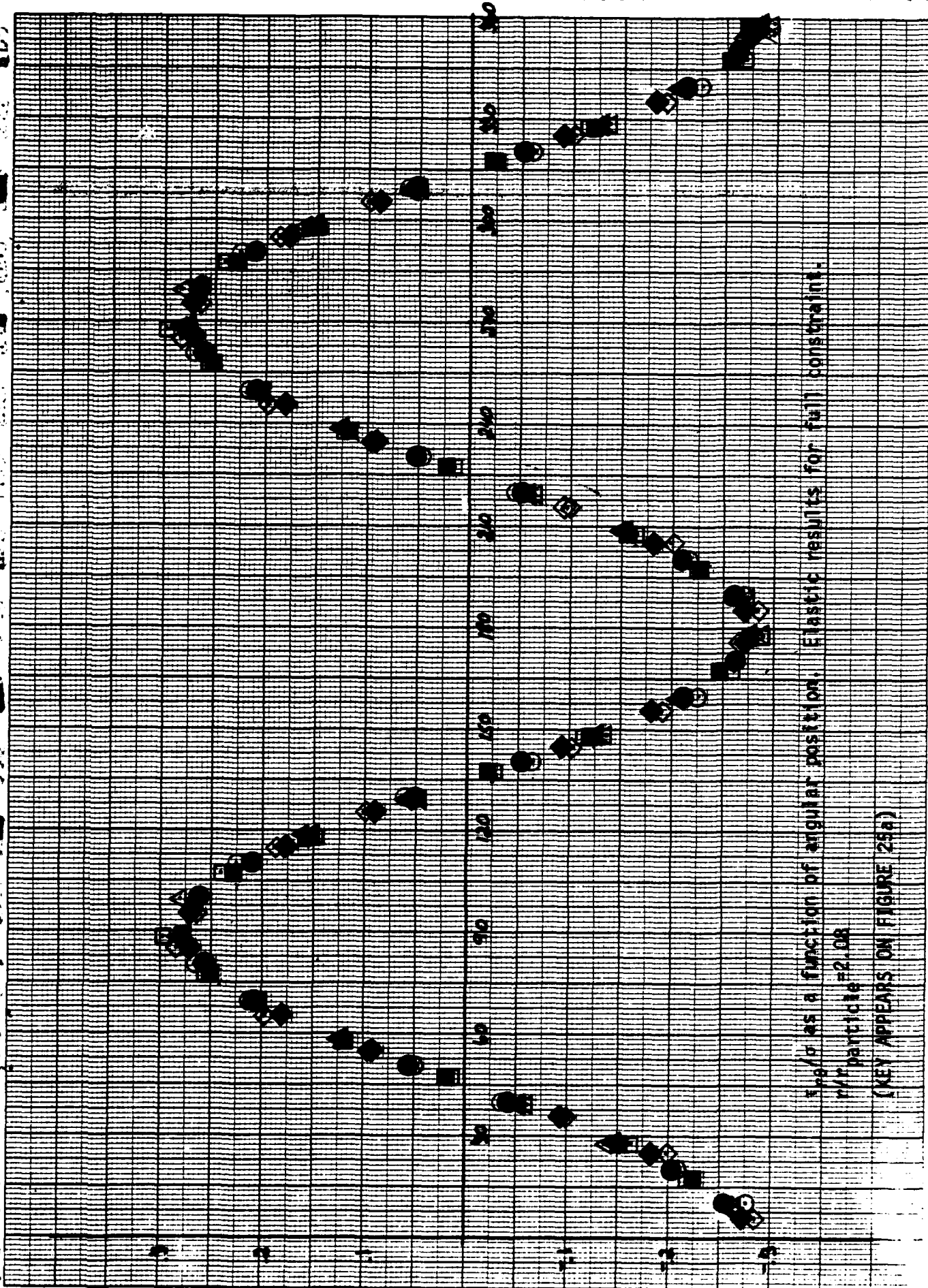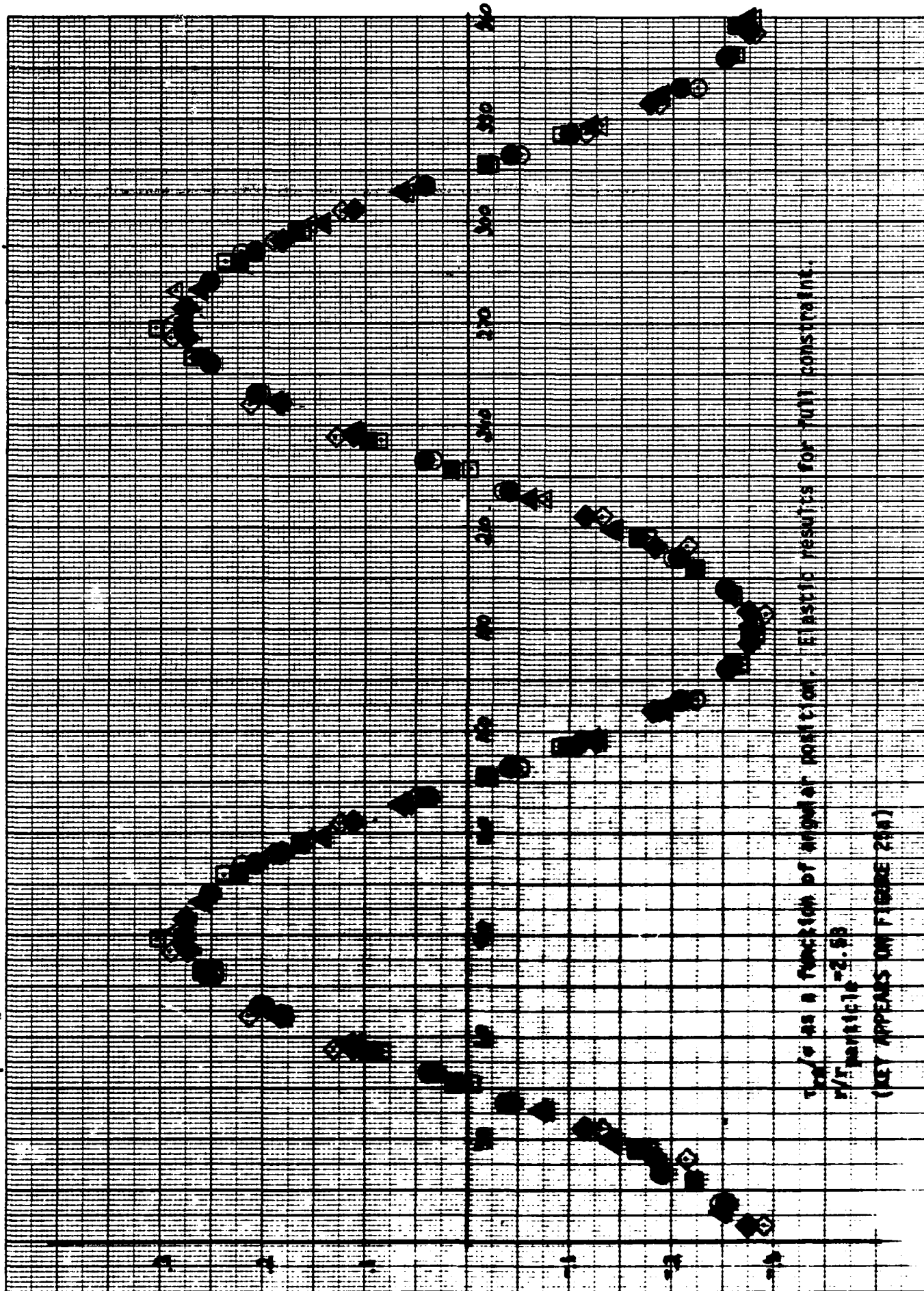s/r particle = 1.62
(KEY APPEARS ON FIGURE 25a).

Figure 54.

Toct/llim as a function of angular position. Elastic results for full constraint.

r/r particle = 1.92

(KEY APPEARS ON FIGURE 25a.)

No 19-0610 (R-2470-10-C), 10 Millimeters to a Centimeter • Made in U.S.A

VERNON McMILLAN, INC., ELIZABETH, N.J 07208

Figure 55

r_{bet}/r_{ilm} as a function of angular position. Elastic results for full constraint.

r/r particle #2.08

(KEY APPEARS ON FIGURE 25a)

Figure 56

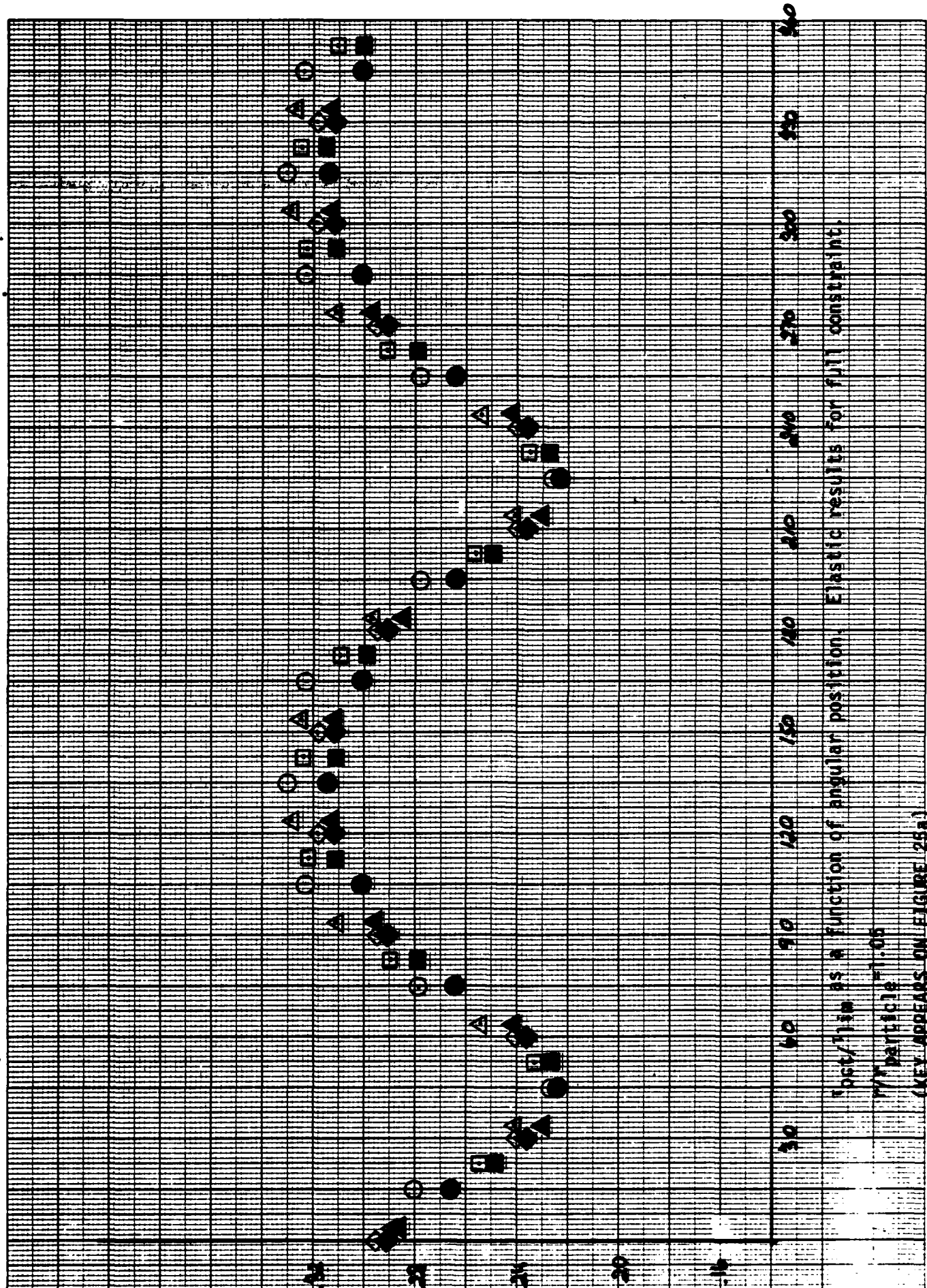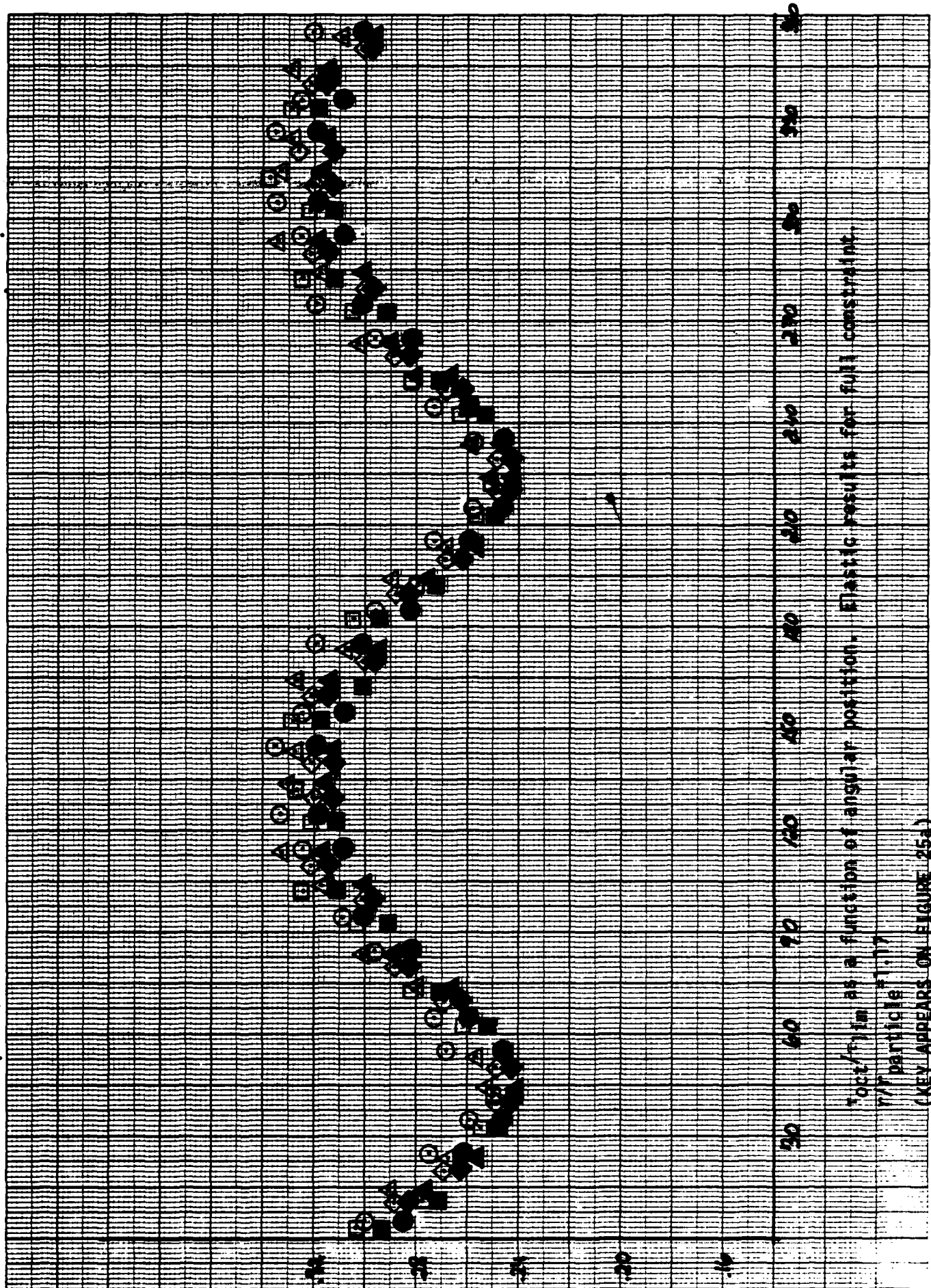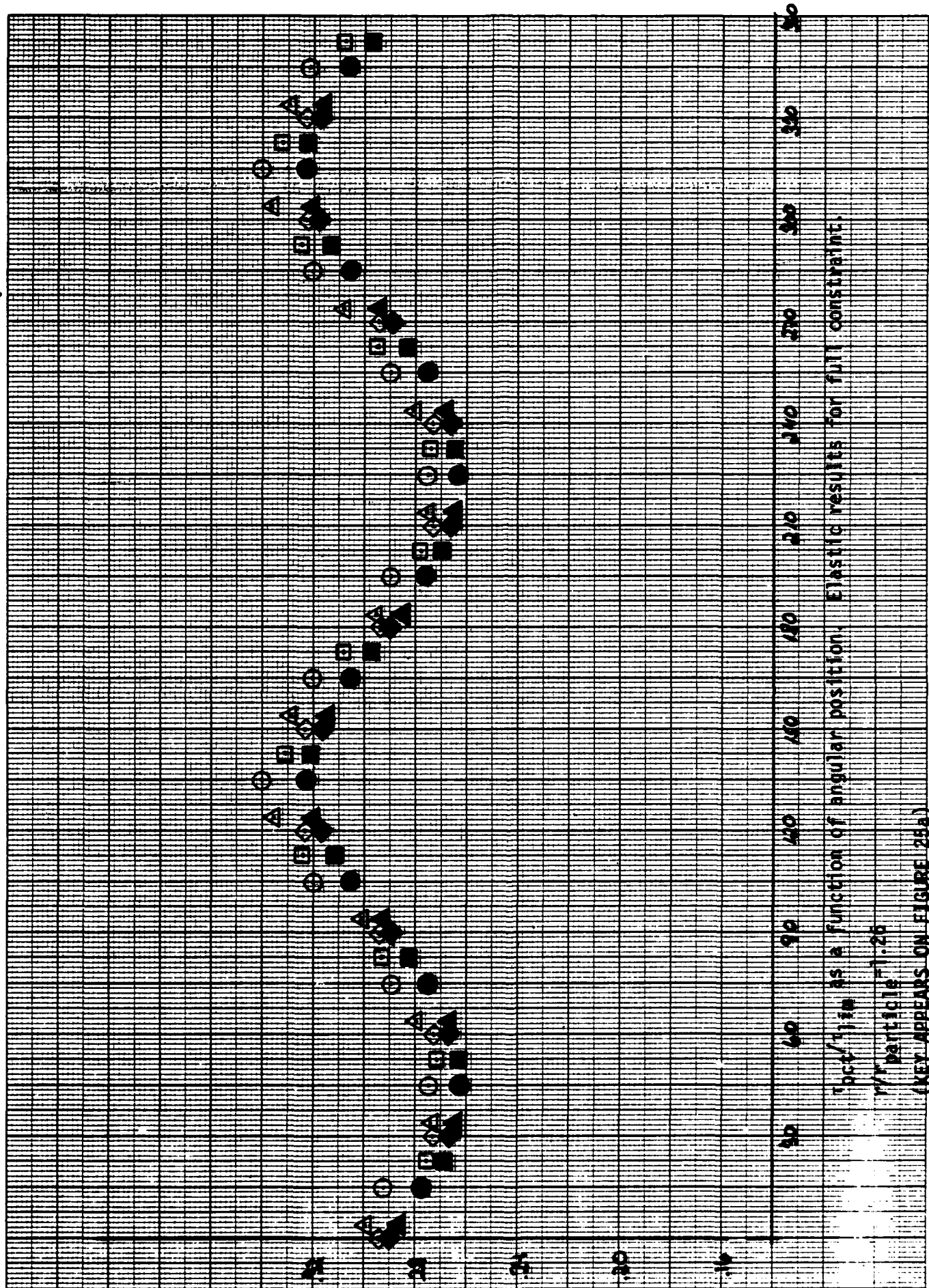No. 19-0610 (R-2470-10-C) 10 Millimeters to a Centimeter • Made in U.S.A

$T_{\text{oct}}/T_{\text{lim}}$ as a function of angular position. Elastic results for full constraint.

$r/r_{\text{particle}} = 2.53$

(KEY APPEARS ON FIGURE 26a)
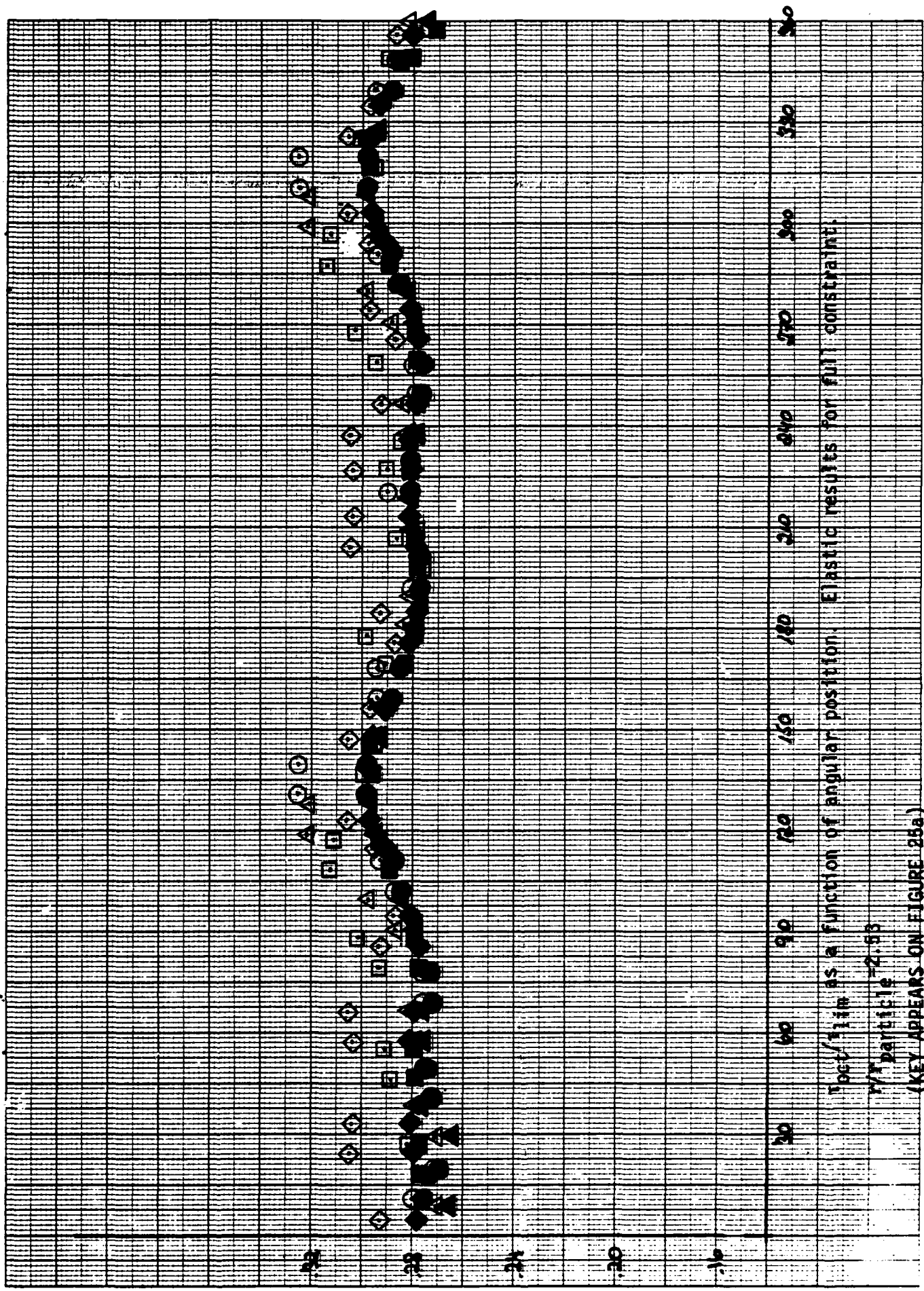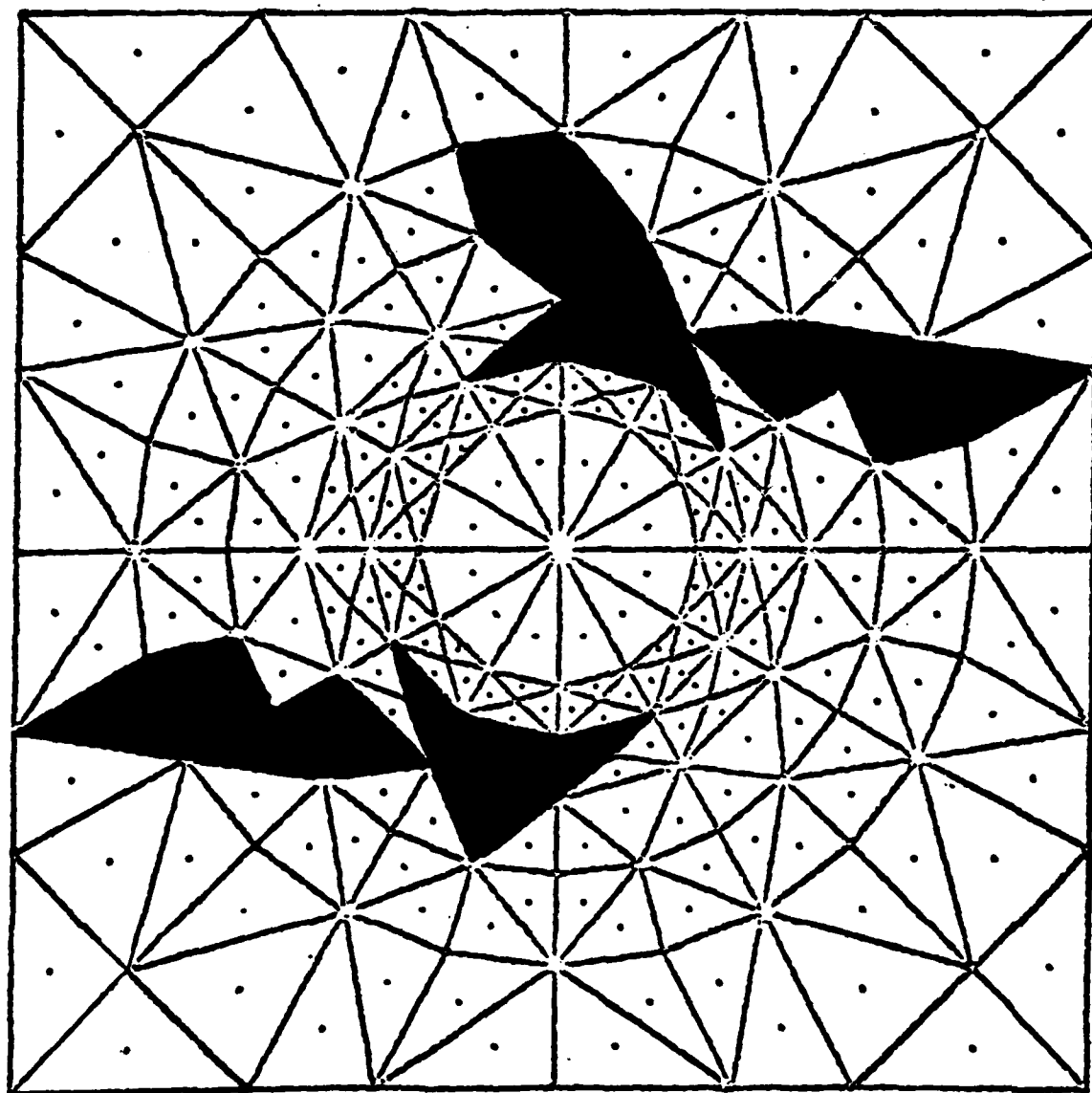
$$\frac{\gamma_{oct}}{\gamma_{lim}} > \left.\frac{\gamma_{oct}}{\gamma_{lim}}\right|_{far\ field} \times 1.05$$

Single particle

Figure 57.
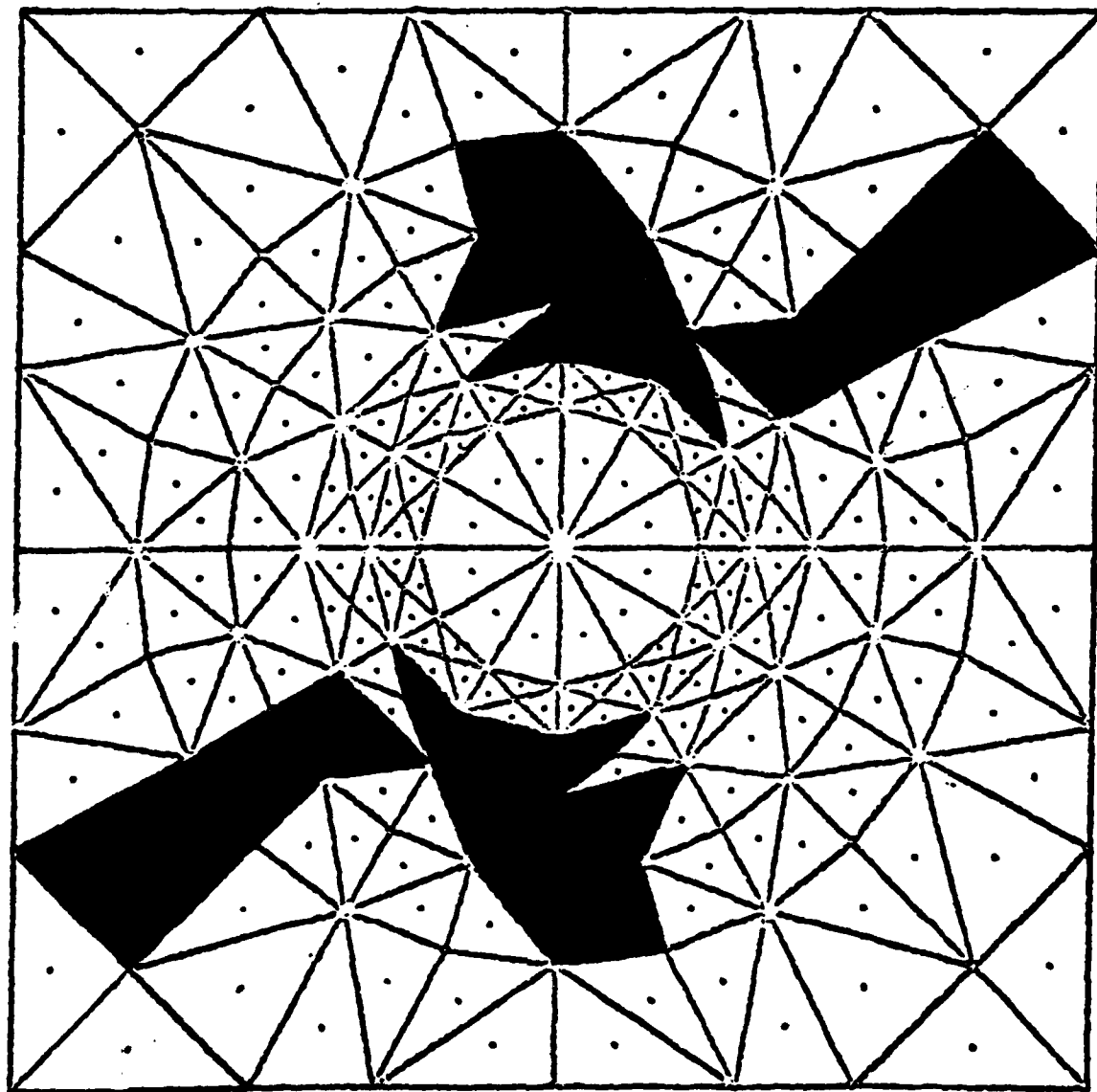
$$\frac{\gamma_{oct}}{\gamma_{lim}} > \left.\frac{\gamma_{oct}}{\gamma_{lim}}\right|_{far\ field} \qquad x1.05 \qquad \text{Multiple particles}$$
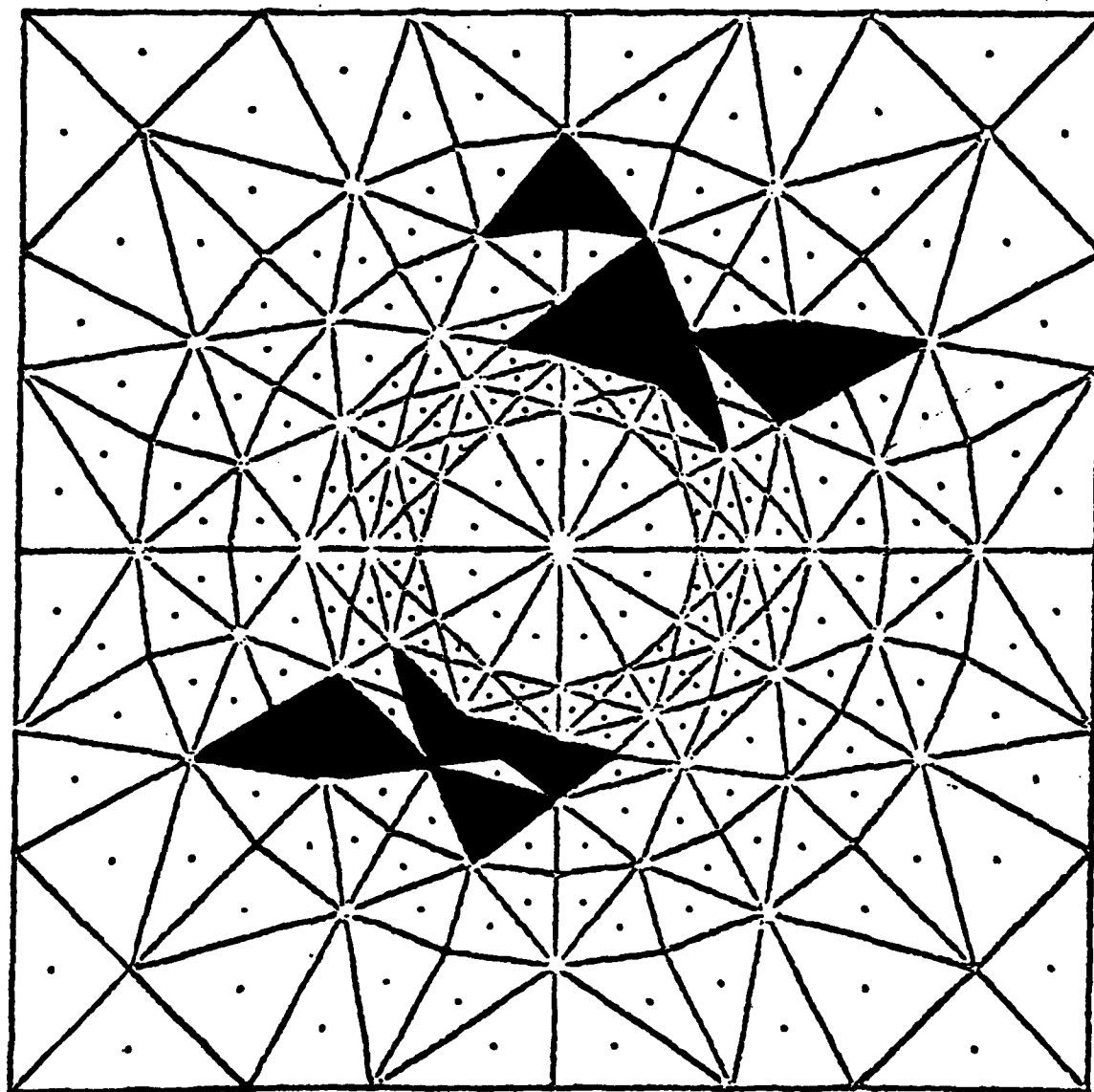
Figure 58

$$\left|\frac{\gamma_{oct}}{\gamma_{lim}} > \frac{\gamma_{oct}}{\gamma_{lim}}\right| \times 1.07$$

far field

Single particle

Figure 59
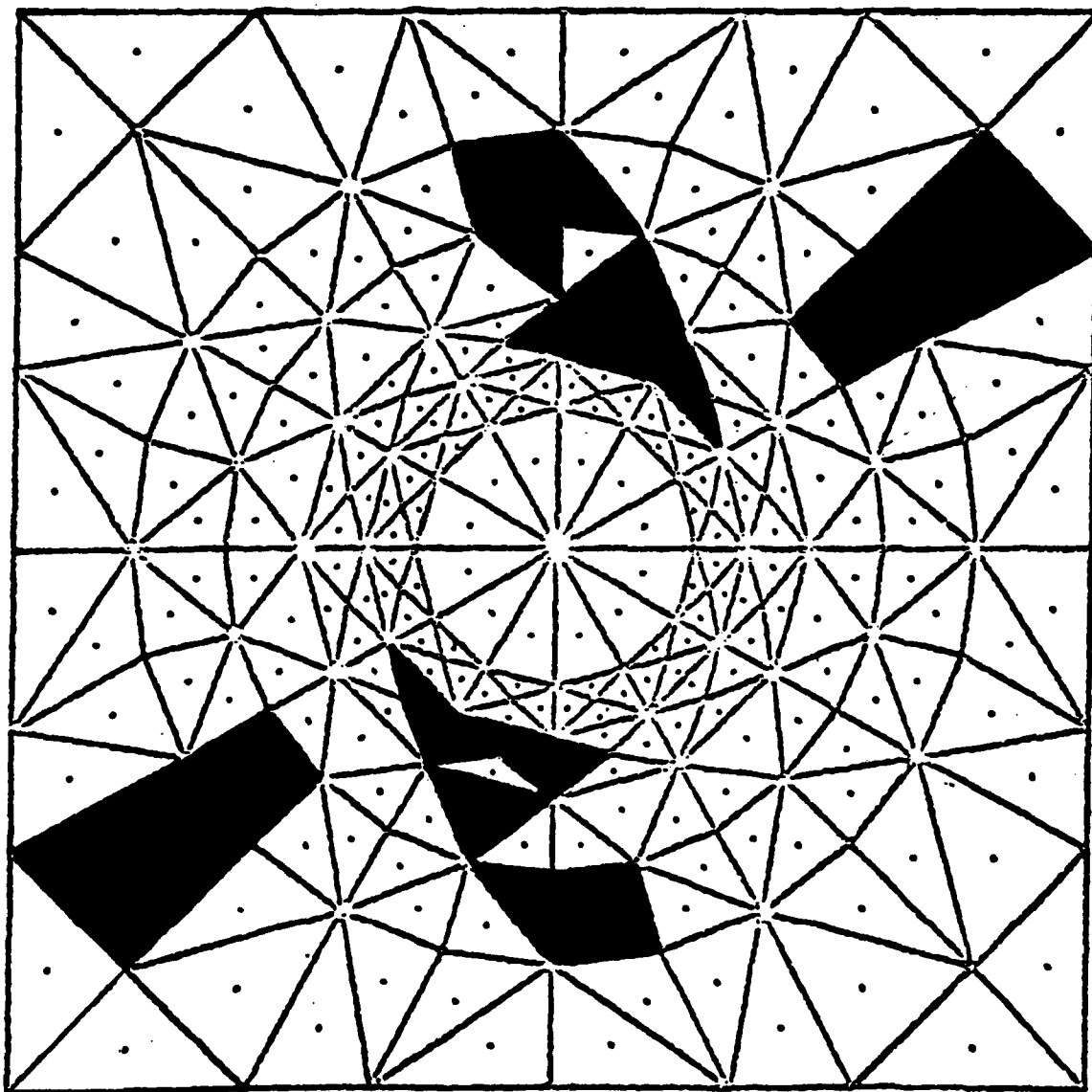
$$\frac{\gamma_{oct}}{\gamma_{lim}} > \left. \frac{\gamma_{oct}}{\gamma_{lim}} \right|_{far\ field} \quad x1.07 \qquad \text{Multiple particles}$$
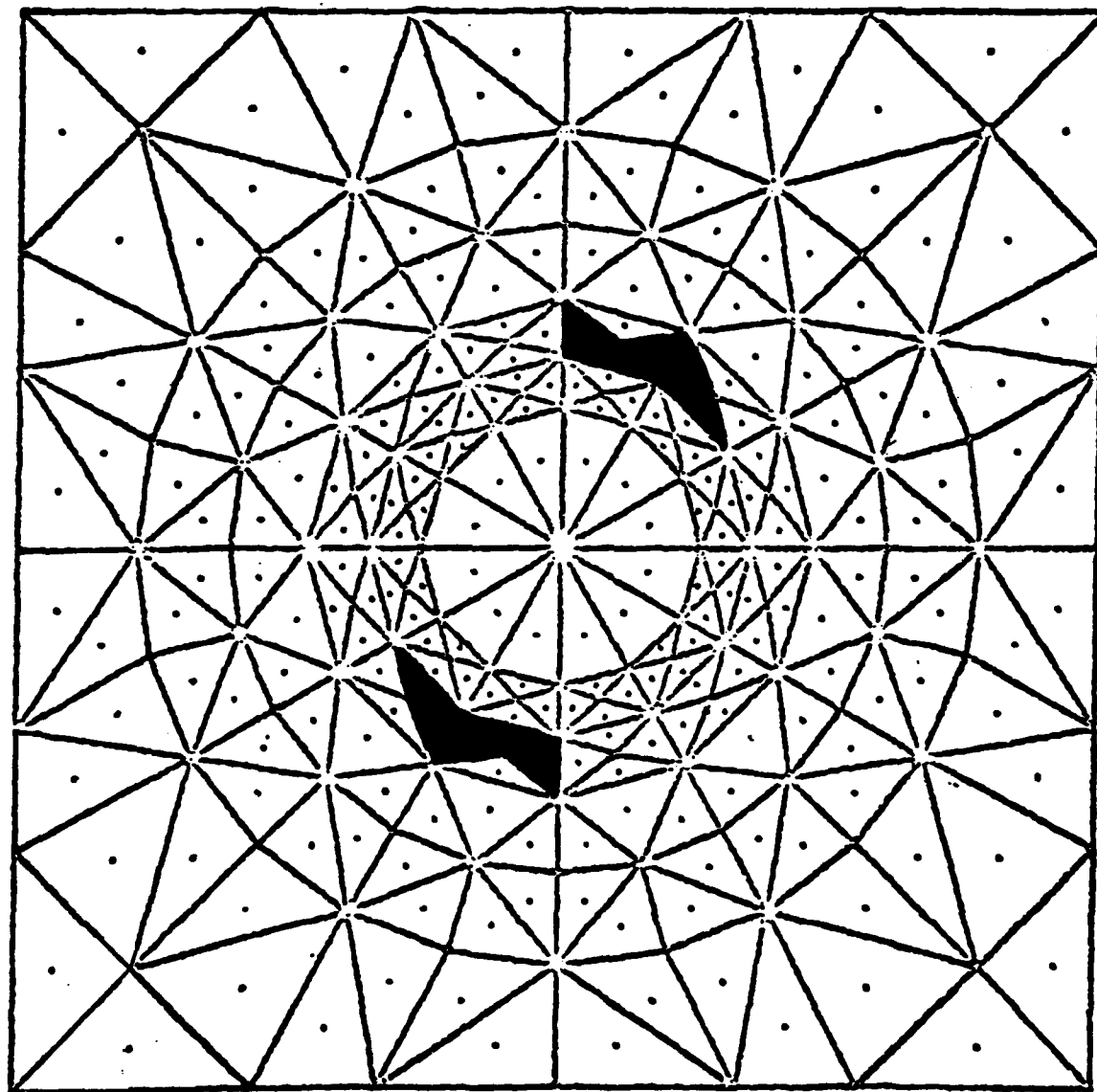
Figure 60

$$\left| \frac{\gamma_{oct}}{\gamma_{lim}} > \frac{\gamma_{oct}}{\gamma_{lim}} \right| \quad \text{x1.10} \qquad \text{Single particles}$$

far field

Figure 61
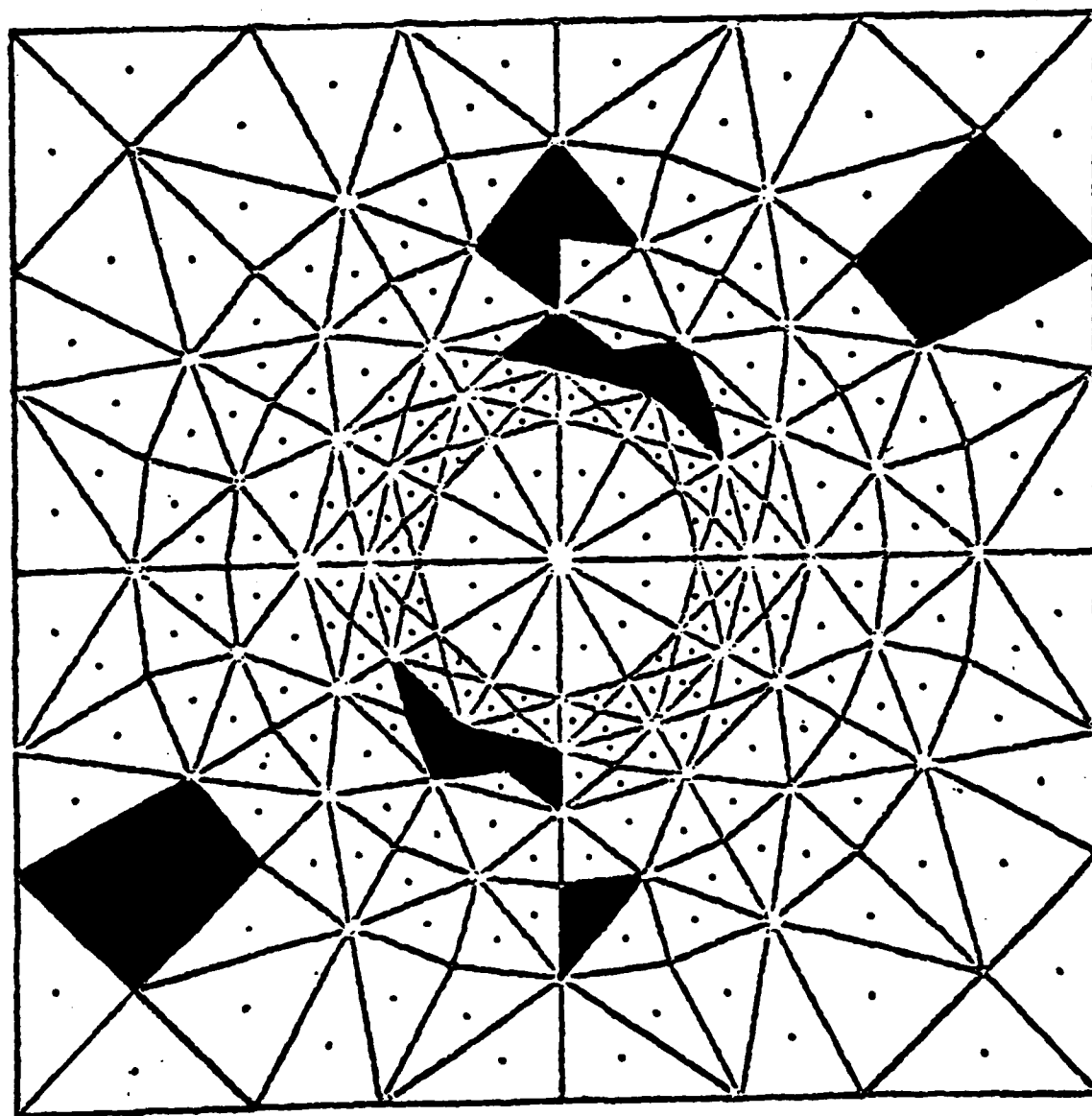
$$\frac{Y_{oct}}{Y_{lim}} > \frac{Y_{oct}}{Y_{lim}} \quad \times 1.10 \qquad \text{Multiple particles}$$

far field

Figure 62

A SIMPLE YET EFFECTIVE SUBSTRUCTURING PROCEDURE FOR

FINITE ELEMENT STRESS ANALYSIS

M. Kondo and G.B. Sinclair

Report SM81-1   February 1981

Department of Mechanical Engineering
Carnegie Institute of Technology
Carnegie-Mellon University
Pittsburgh, PA 15213

A SIMPLE YET EFFECTIVE SUBSTRUCTURING PROCEDURE FOR FINITE ELEMENT STRESS ANALYSIS
BY M. KONDO AND G.B. SINCLAIR

1. ABSTRACT

This report describes a simple substructuring technique for the finite element analysis of elastic bodies, one that can be implemented by an analyst without any internal modification to an existing code. In common with other substructuring approaches the technique offers greater resolution for less computational effort than would otherwise be required, and this is demonstrated by the analysis of a test problem involving a crack.

2. INTRODUCTION

In general, substructuring for static structural analysis using the finite element method (FEM) is based on subdividing a large structure into smaller parts which are analysed separately to obtain relationships between forces and displacements at the substructure interfaces. These interface variables are then determined and the results used to obtain the unknowns within each substructure. Essentially these approaches involve partitioning of the stiffness matrix in some sensible way (see Noor, Kamel and Fulton [1] for a fuller description).

Our approach to substructuring consists of analysing an entire body for stresses and displacements using FEM, then taking the displacements from this first analysis at a set of interior nodes as the boundary conditions for a second analysis which now occupies a smaller region. This smaller region is centered on the aspect of the original problem of greatest interest and has boundaries which are geometrically similar to those of the original problem so that the same finite element map can be used in the second analysis. This focusing process can then be repeated, with a third region within the second being analyzed and so on*.[1]

Both approaches offer, in effect, the opportunity for greater resolution for the same computational effort. This capability is particularly advantageous in analyses where there are some critical local regions such as a crack-tip. The main advantage of the approach presented here over those reported in, for example, Noor et.al. [1],

---

[1] In principle the approach is not confined to statics and could also be applied in elasto-plastic treatments

lies in its simplicity: it can be readily implemented by an analyst without modification to an existing code, i.e., externally to a standard finite element program.

In what follows we analyze a test problem for a crack geometry having an exact solution and show the level of resolution that can be achieved with a modest amount of effort when our substructuring technique is used.

3. TEST PROBLEM

In this section we describe an elastic test problem with an exact solution for a configuration containing a crack.

To construct a test problem, we seek some set of the field quantities- stresses σx, σy, τxy and displacements u, v - throughout a region R satisfying the field equations of two-dimensional elasticity. Moreover, to provide a stringent test of the substructuring procedure, we want these field quantities to include a singularity. One simple way, then, of constructing a suitable test problem is to take the first singular symmetric eigenfunction for the crack as identified by Westergaard [2], viz.

$$\sigma x = -\frac{K}{(2\pi r)^{1/2}} \cos \frac{\theta}{2} [1 - \sin \frac{\theta}{2} \sin \frac{3\theta}{2}],$$

$$\sigma y = \frac{K}{(2\pi r)^{1/2}} \cos \frac{\theta}{2} [1 + \sin \frac{\theta}{2} \sin \frac{3\theta}{2}],$$

$$\tau xy = \frac{K}{(2\pi r)^{1/2}} \sin \frac{\theta}{2} \cos \frac{\theta}{2} \cos \frac{3\theta}{2} , \qquad (1)$$

$$u = \frac{K}{G} [\frac{r}{2\pi}]^{1/2} \cos \frac{\theta}{2} [1 - 2\nu + \sin^2 \frac{\theta}{2}],$$

$$v = \frac{K}{G} [\frac{r}{2\pi}]^{1/2} \sin \frac{\theta}{2} [2 - 2\nu - \cos^2 \frac{\theta}{2}],$$

and then to pick R so as to include the crack-tip, and take as boundary conditions on R the values implied by (1). In (1), K is a constant, G the shear modulus, ν Poisson's ratio, and r and θ are cylindrical coordinates.
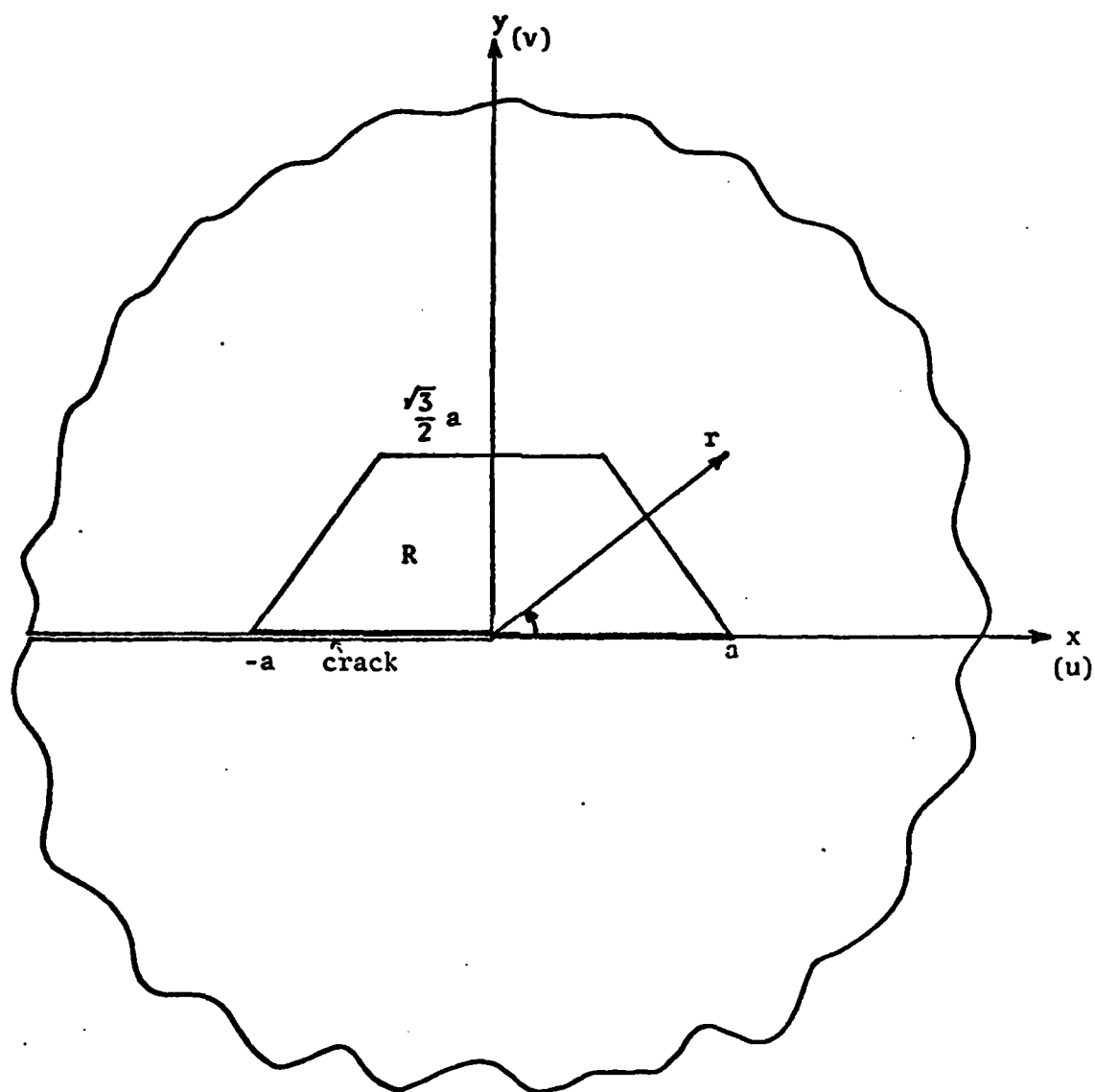
Fig. 1 Geometry and coordinates for the region R.

A suitable R for analysis is shown in Fig.1, and consists of a semi-hexagon within the upper half-plate, that is,

$$R = \{(x,y)\mid \; -a + \frac{y}{\sqrt{3}} < x < a - \frac{y}{\sqrt{3}}, \; 0 < y < \frac{\sqrt{3}a}{2}\}, \quad (2)$$

where a is the length of a side of the hexagon. The boundary conditions on R are taken to be the stress-free conditions on the crack-flank, the symmetry conditions ahead of the crack, and the displacements on the remainder of the boundary as prescribed in effect by (1), i.e.

$\sigma y = \tau xy = 0$ on $y = 0 (-a < x < 0)$,

$v = 0$, $\tau xy = 0$ on $y = 0$ $(0 < x < a)$,

$$u = \sqrt{\frac{K}{G}} \; \frac{a}{2\pi} \sin \frac{\pi}{3} \; \mathrm{cosec}\,(\theta + \frac{\pi}{3}) \; \cos \frac{\theta}{2} [1 - 2\nu + \sin^2 \frac{\theta}{2}] \text{ on } y = \sqrt{3}\,(a-x)$$

$$v = \sqrt{\frac{K}{G}} \; \frac{a}{2\pi} \sin \frac{\pi}{3} \; \mathrm{cosec}\,(\theta + \frac{\pi}{3}) \; \sin \frac{\theta}{2} [2 - 2\nu - \cos^2 \frac{\theta}{2}] \quad (0 < \theta \leq \pi/3),$$

$$u = \sqrt{\frac{K}{G}} \; \frac{a}{2\pi} \sin \frac{\pi}{3} \; \mathrm{cosec}\,\theta \; \cos \frac{\theta}{2} [1 - 2\nu + \sin^2 \frac{\theta}{2}] \qquad \text{on } y = \sqrt{3}a/2$$

$$(3)$$

$$v = \sqrt{\frac{K}{G}} \; \frac{a}{2\pi} \sin \frac{\pi}{3} \; \mathrm{cosec}\,\theta \; \sin \frac{\theta}{2} [2 - 2\nu - \cos^2 \frac{\theta}{2}] \quad (\pi/3 \leq \theta \leq 2\pi/3),$$

$$u = \sqrt{\frac{K}{G}} \; \frac{a}{2\pi} \sin \frac{\pi}{3} \; \mathrm{cosec}\,(\theta - \frac{\pi}{3}) \; \cos \frac{\theta}{2} [1 - 2\nu + \sin^2 \frac{\theta}{2}] \quad \text{on } y = \sqrt{3}\,(a + x)$$

$$v = \sqrt{\frac{K}{G}} \; \frac{a}{2\pi} \sin \frac{\pi}{3} \; \mathrm{cosec}\,(\theta - \frac{\pi}{3}) \; \sin \frac{\theta}{2} [2 - 2\nu - \cos^2 \frac{\theta}{2}] (\frac{2\pi}{3} \leq \theta \leq \pi).$$

It follows automatically that (1) is the exact solution to the elastic analysis of R with boundary condition as in (3) and thereby constitutes a suitable test problem.

4. ANALYSIS

Here we describe the analysis of the test problem using our substructuring technique and a constant-strain-triangle, finite element code.

Since the issue of interest is the effectiveness of our substructuring technique, we discretize R uniformly with a set of equivalent elements of equal area. To examine convergence we use a sequence of three maps - a coarse, a medium and a fine map - with the medium being constructed from the coarse by halving the element size and the fine being similarly derived from the medium. The coarse map has 48 elements (35 nodes), the medium 192 elements (117 nodes), the fine 768 elements (425 nodes), (Fig. 2).

The first step is to analyze the original problem using the sequence of maps. The particular sequence of maps chosen enables a straightforward but effective extrapolation technique to be used to improve the results. This extrapolation technique is based on the following argument. We define as our error measure in the displacement the difference e between the values obtained by the FEM analyses and the exact answer and model this error distribution with

$$e = e^o h^\alpha , \tag{4}$$

where e^o is the error with a mesh size h of unity and α is a parameter reflecting the convergence of the method ($\alpha > 0$ for convergence). For example, the errors in the displacements in the x-direction are

$$e^c = u^c - u^\infty = e^o h^\alpha ,$$
$$e^m = u^m - u^\infty = e^o (\frac{h}{2})^\alpha , \tag{5}$$
$$e^f = u^f - u^\infty = e^o (\frac{h}{4})^\alpha ,$$

where the superscripts c,m,f and ∞ denotes respectively the coarse, medium, fine, and "exact" (or infinite number of elements) results. Eliminating e^o and α from (5) then gives
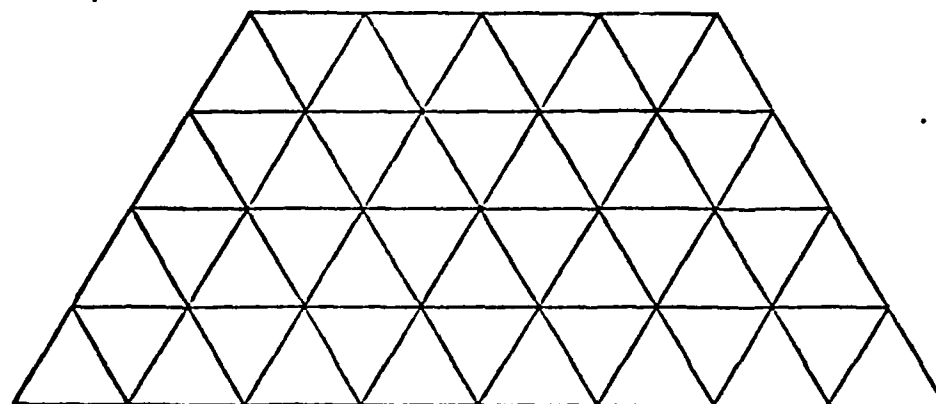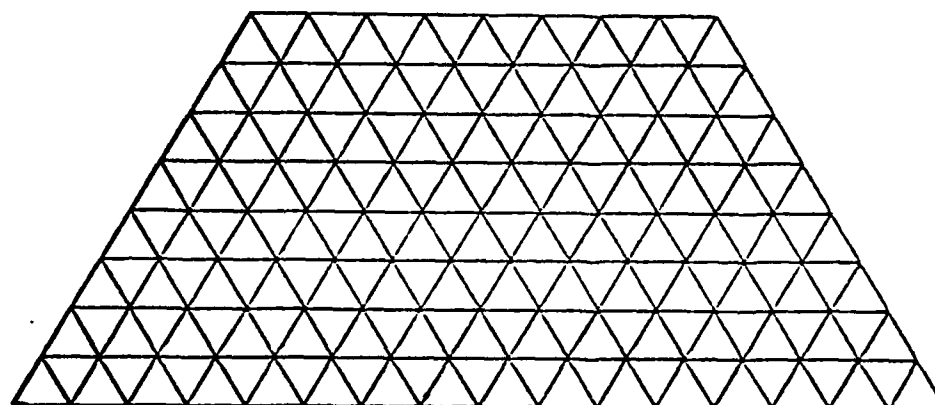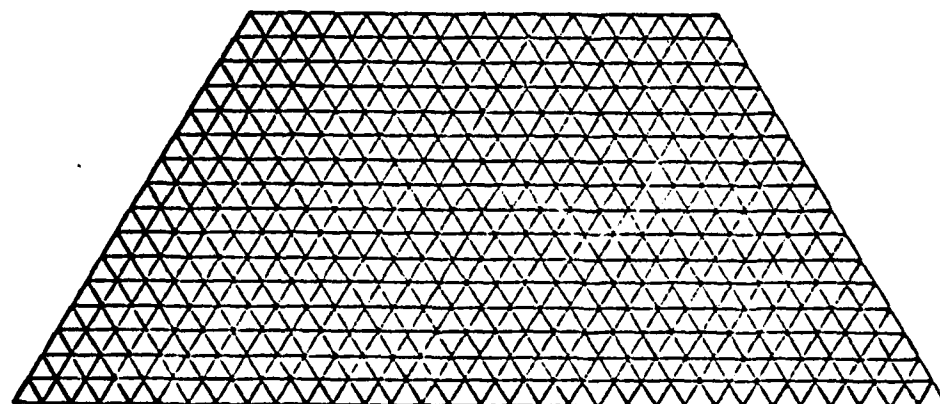
Fig. 2   Coarse, medium, and fine maps.

$$u^\infty = \frac{(u^m)^2 - u^c u^f}{2u^n - u^c - u^f} \quad ; \tag{6}$$

similarly,

$$v^\infty = \frac{(v^m)^2 - v^c v^f}{2v^m - v^c - v^f} . \tag{7}$$

Equations (6) and (7) are extrapolated estimates of u and v which realize improvements over the fine map values.

The next step is to perform a first substructure. We select as our subregion $\overline{R}$, a geometrically similar region to R centered on the crack-tip with sides equal to half those of R: thus

$$\overline{R} = \{(x,y)\,|\, -\frac{a}{2} + \frac{y}{\sqrt{3}} < x < \frac{a}{2} - \frac{y}{\sqrt{3}}, \quad 0 < y < \frac{\sqrt{3}a}{4}\}. \tag{8}$$

To obtain the boundary conditions on $\overline{R}$ from the analysis of R, we proceed as follows. We use the estimates u^∞, v^∞ obtained from (6) and (7) at nodes where there are u^c, u^m, u^f and v^c, v^m, v^f values. Where u^∞ and v^∞ can not be found in this manner because u^c and v^c are not available, we interpolate between the u^∞ and v^∞ determined from (6) and (7) using the fine map distribution. That is, let u_1^∞, and u_5^∞ be the extrapolated values of u at nodes 1 and 5 and suppose that the nodes of the intervening three fine map values are not supported by coarse map results. We estimate these intermediate node values -- u_2^∞, u_3^∞, u_4^β, by fitting the corresponding distribution of fine map values to the end points u_1^∞, u_5^∞ in accordance with[2].

---

2 Recall that the nine point uniform solution is a simple weights obtain over four intervals

END
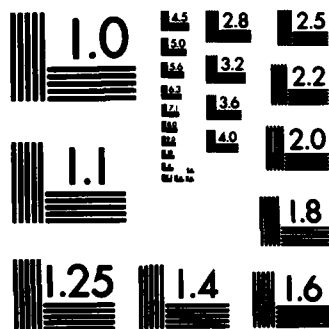
FILMED

$$u_2^\infty = u_2^f + \frac{3}{4} \Delta_1 + \frac{1}{4} \Delta_2,$$

$$u_3^\infty = u_3^f + \frac{2}{4} \Delta_1 + \frac{2}{4} \Delta_2, \qquad (9)$$

$$u_4^\infty = u_4^f + \frac{1}{4} \Delta_1 + \frac{3}{4} \Delta_2,$$

where Δ_1 and Δ_2 are defined as

$$\Delta_1 = u_1^\infty - u_1^f,$$

$$\Delta_2 = u_5^\infty - u_5^f. \qquad (10)$$

In instances where fine estimates are not even available - as at some ndoes in the fine map for $\overline{R}$ - we linearly interpolate over U_i^∞ and V_i^∞ determined as described above.

Using these extrapolated and interpolated values as boundary conditions and analyzing R constitutes our first substructure: applying the same procedure twice is the second and so on. In actuality, only two substructures were performed using the constant- strain-triangle, elastic, finite element code PLANDJ [3]. That is, we ran the coarse medium and fine maps for the pre-substructure, first substructure and second sub-structure geometries. In this manner we hoped to enjoy the resolution of "effective" coarse, medium and fine maps having 120 elements ($48 + \frac{3}{4} \cdot 48 + \frac{3}{4} \cdot 48$), 480 elements and 1920 elements, respectively (Fig.3 sketches the effective fine map). Our storage requirements using substructuring however are about 40% of those required for a direct analysis of these effective maps and the number of operations needed using substructuring is approximately 1/3 of the number required for a direct analysis even when the multiple analyses required for the substructuring are taken into account.[3]

---

[3] based on the assumption that the number of operations in FEM is proportional where N is the number of degrees of freedom and B is the band-width- see, for exa Zienkiewicz [4], p.463.
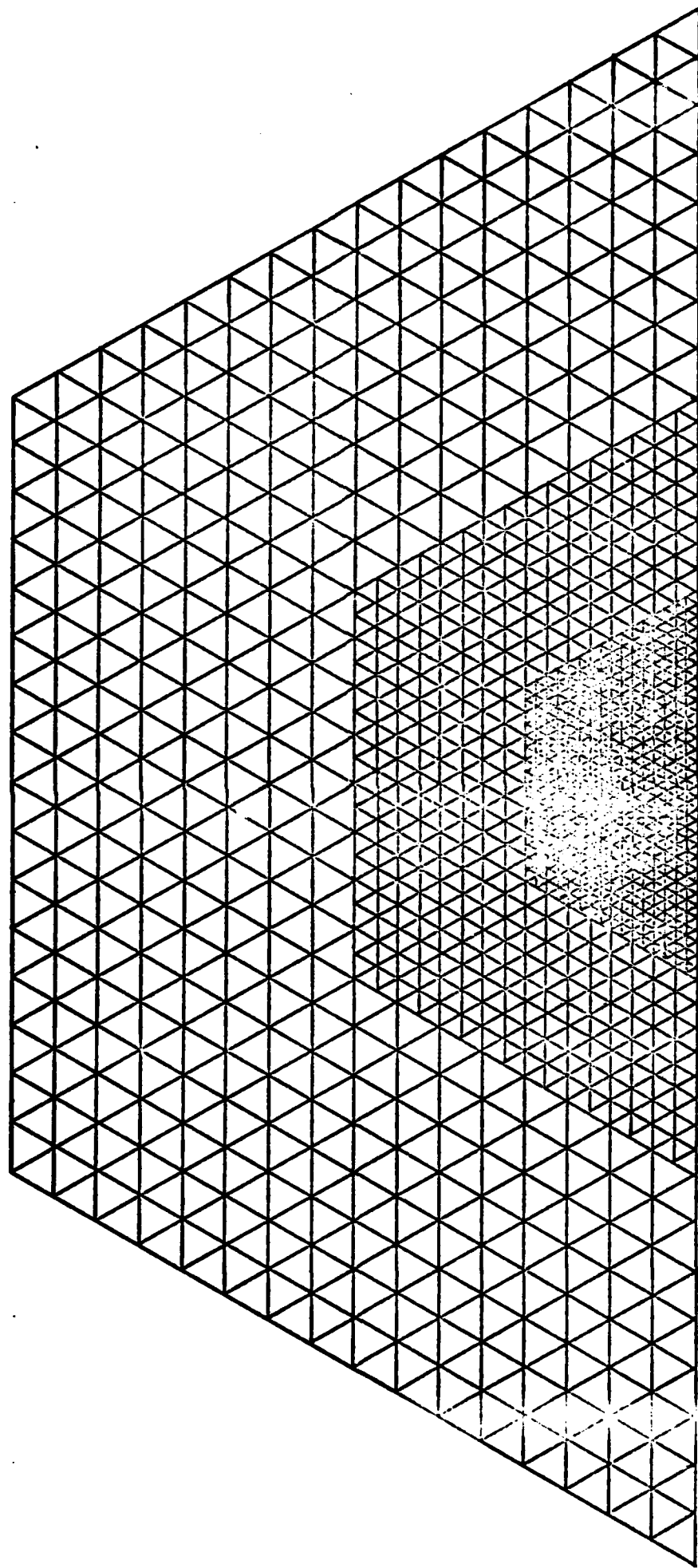
Fig. 3 Effective fine map.

5. RESULTS

In this section we show the results from the application of our substructuring technique, and in particular assess the increased resolution gained at the crack-tip using substructuring.

Figs. 4 through 6 show the convergence of the initial analysis by comparing the coarse, medium and fine results with the exact solution of (1). In Figs. 4 and 5 the dimensionless stresses, $\overline{\sigma}_x = \sqrt{a}\,\sigma_x/K$ and $\overline{\sigma}_y = \sqrt{a}\,\sigma_y/K$ formed from nodal averages, are plotted as a function of dimensionless distance $\overline{r} = r/a$ along a ray at $\theta = \pi/3$. The stresses converge except for the peak value at the innermost node, i.e. nearest the crack-tip $(\overline{r}=0)$. Fig. 6 shows the dimensionless, crack-opening, nodal displacement, $\overline{v}=Gv/K\sqrt{a}$ at $\theta = \pi$, as a function of $\overline{r}$. The displacements converge even at the crack-tip. This convergence allows us to use the extrapolation technique outlined earlier to form the boundary conditions in our first substructure.

Figs.7 through 10 show the displacement values used as the boundary conditions in the application of the substructuring technique, comparing the coarse, medium and fine map results with the exact solution of (1). In Figs. 7 and 8 the dimensionless nodal displacements, $\overline{u} = Gu/K\sqrt{a}$ and $\overline{v} = Gv/K\sqrt{a}$, around the upper boundary of $\overline{R}$ are shown i.e. as functions of the dimensionless distance $\overline{s} = s/a$ from the crack $\theta = \pi$ to $\theta = 0$, while the corresponding displacements obtained from the analysis of $\overline{R}$ for use in the second substructure are shown in Figs. 9 and 10. For both sets of curves the displacement values derived using the extrapolation interpolation technique described in the previous section are not distinquishable from the exact values on the size scale used in the figures. Accordingly no accumulation of error in the boundary values results from the present multiple application of our substructuring technique.

Lastly, we examine the error in the crack opening displacement near the crack-tip as the substructuring proceeds. Since v at $\theta = \pi$ goes to zero at $\overline{r}=0$ we normalize this error by dividing by a typical specific value of $v(\theta=\pi)$ rather than the exact crack-opening value at the corresponding $\overline{r}$ - position: the actual typical value taken is the crack-opening displacement at the crack mouth in R, that is at $\overline{r} = 1$. The error measure in extrapolated/interpolated values is then given by

$$e = (v^{\infty} - v^e)/v^t$$

where v^{∞} is the displacement found by extrapolating/interpolating the FEM results at $\theta=\pi$, as distinct from the exact solution v^e there, and v^t in the typical value of
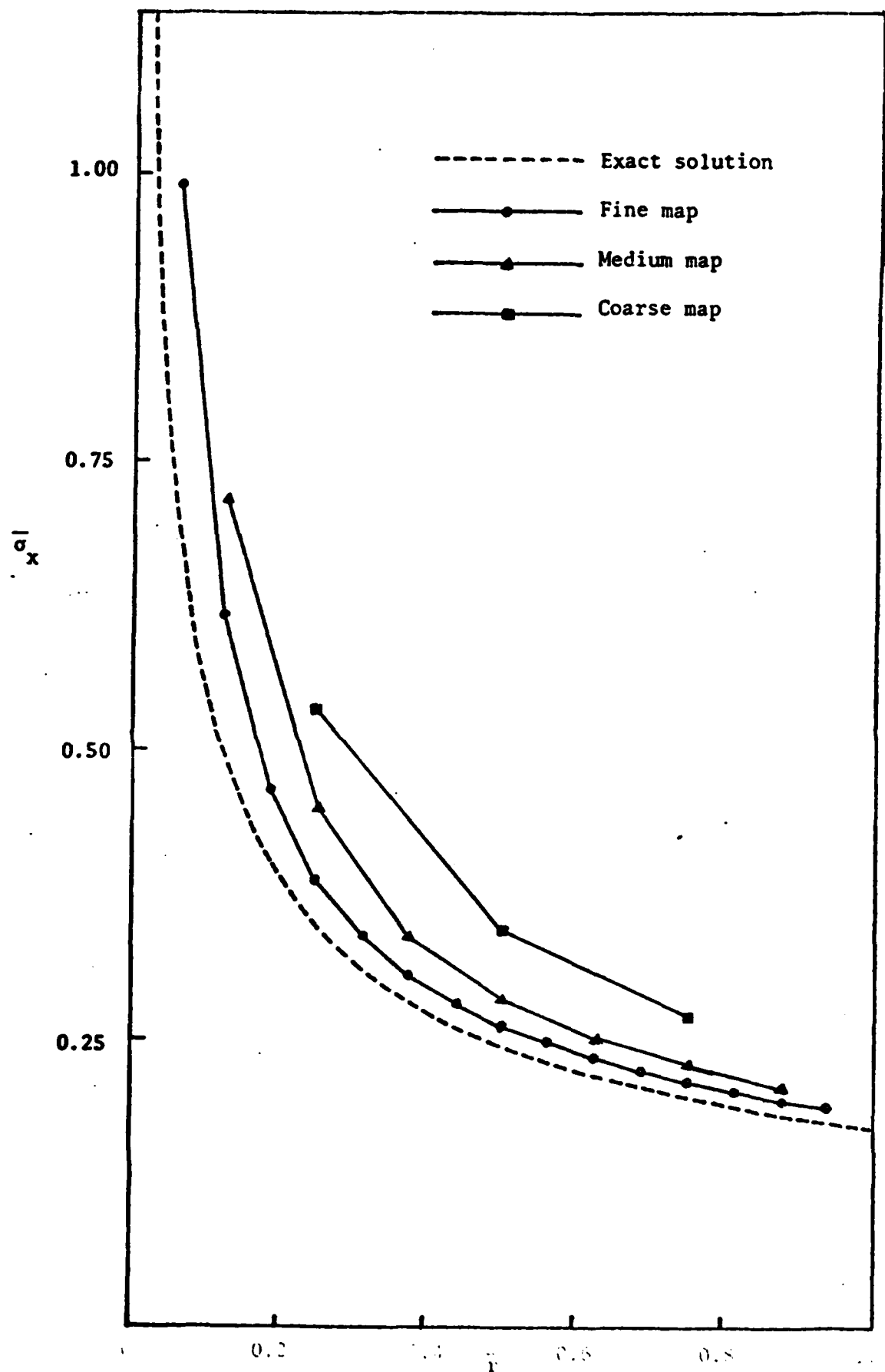
Fig. 4 Stress ($\overline{\sigma}_x$ at $\vartheta = \pi/3$) convergence approaching the crack-tip.
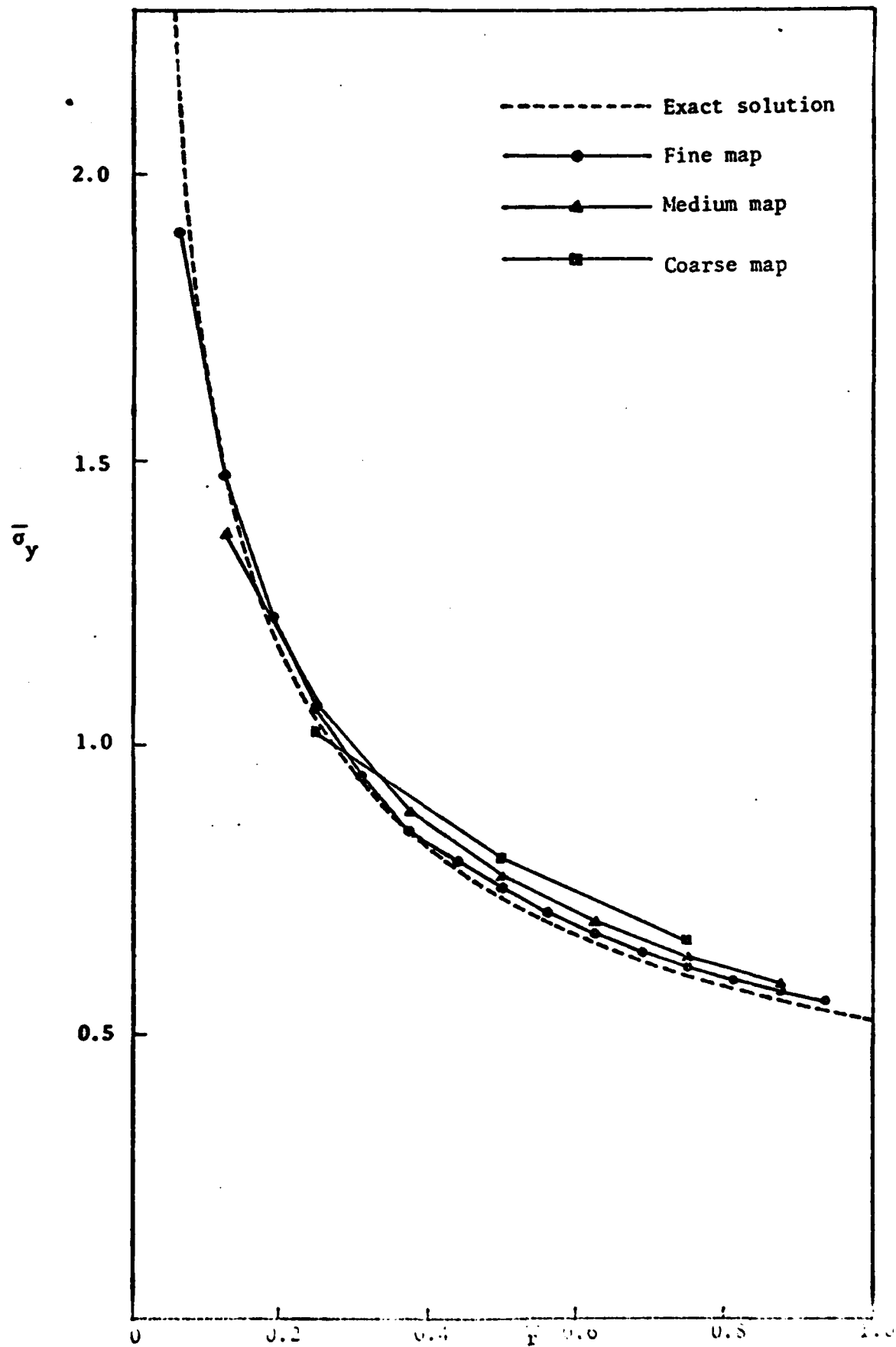
Fig. 5 Stress ($\overline{\sigma}_y$ at $0 = \pi/3$) convergence approaching the
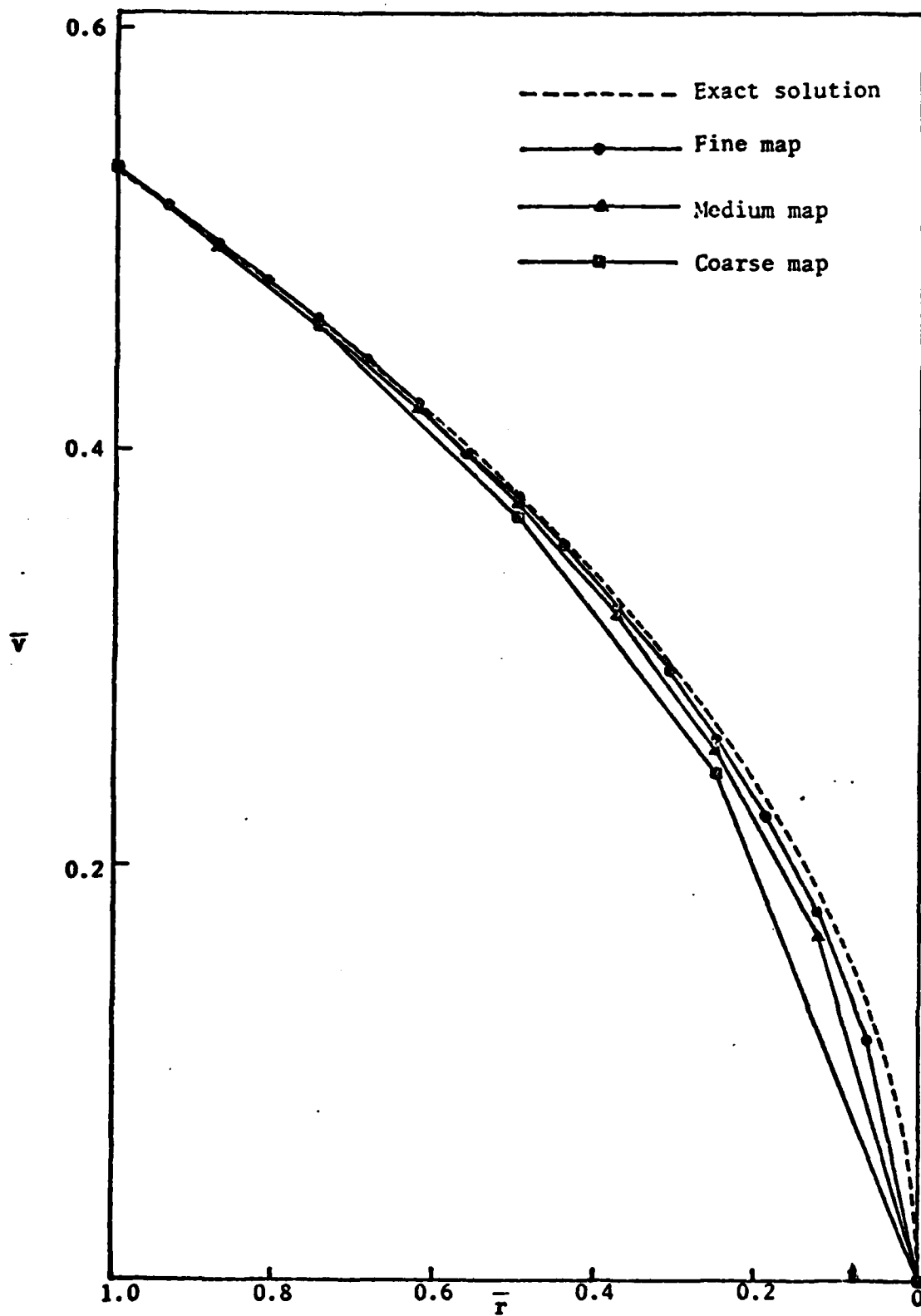
Fig. 6 Convergence of crack-opening displacement.
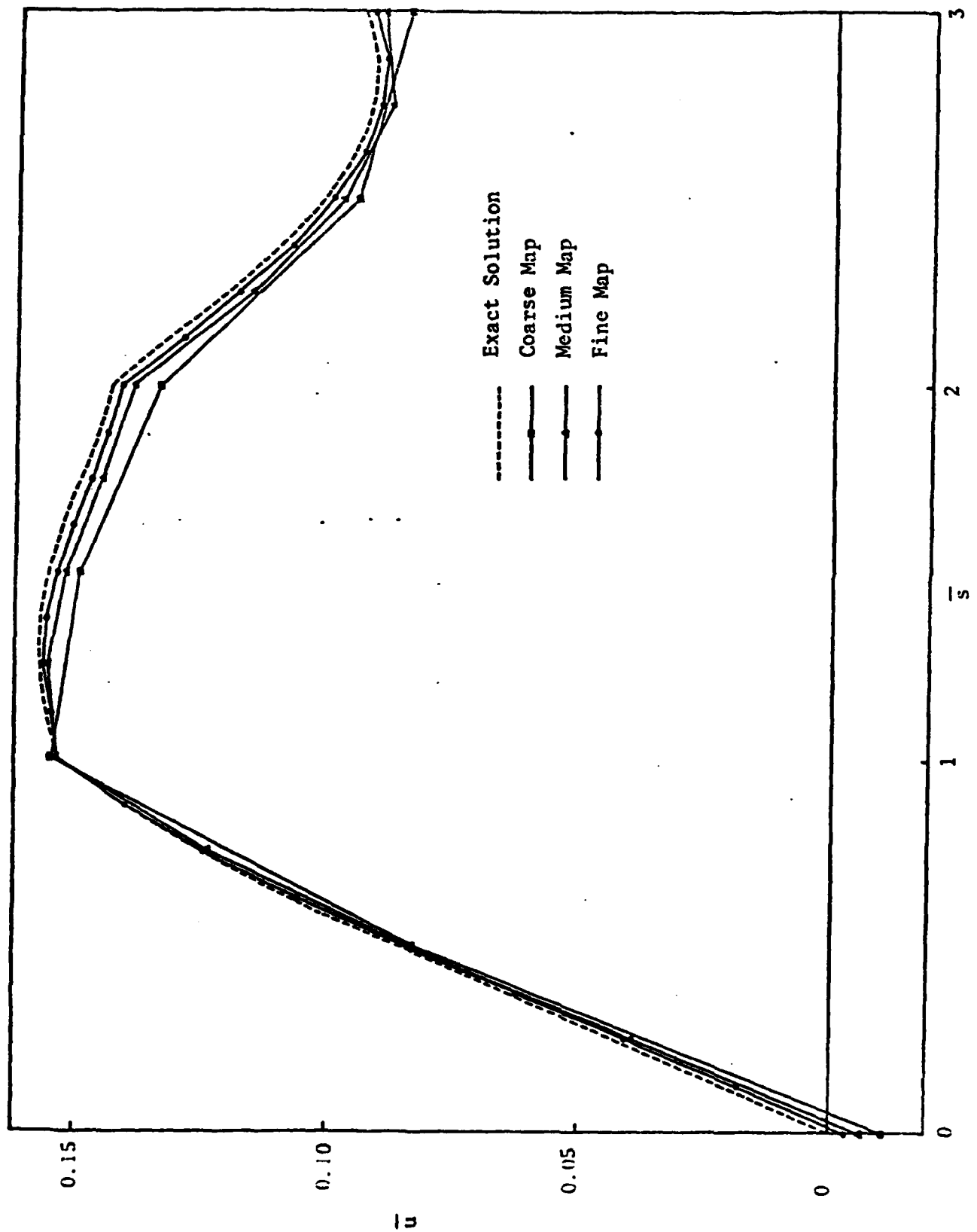
Fig. 7 Displacement $(\bar{u})$ along the boundary after pre-substructuring.
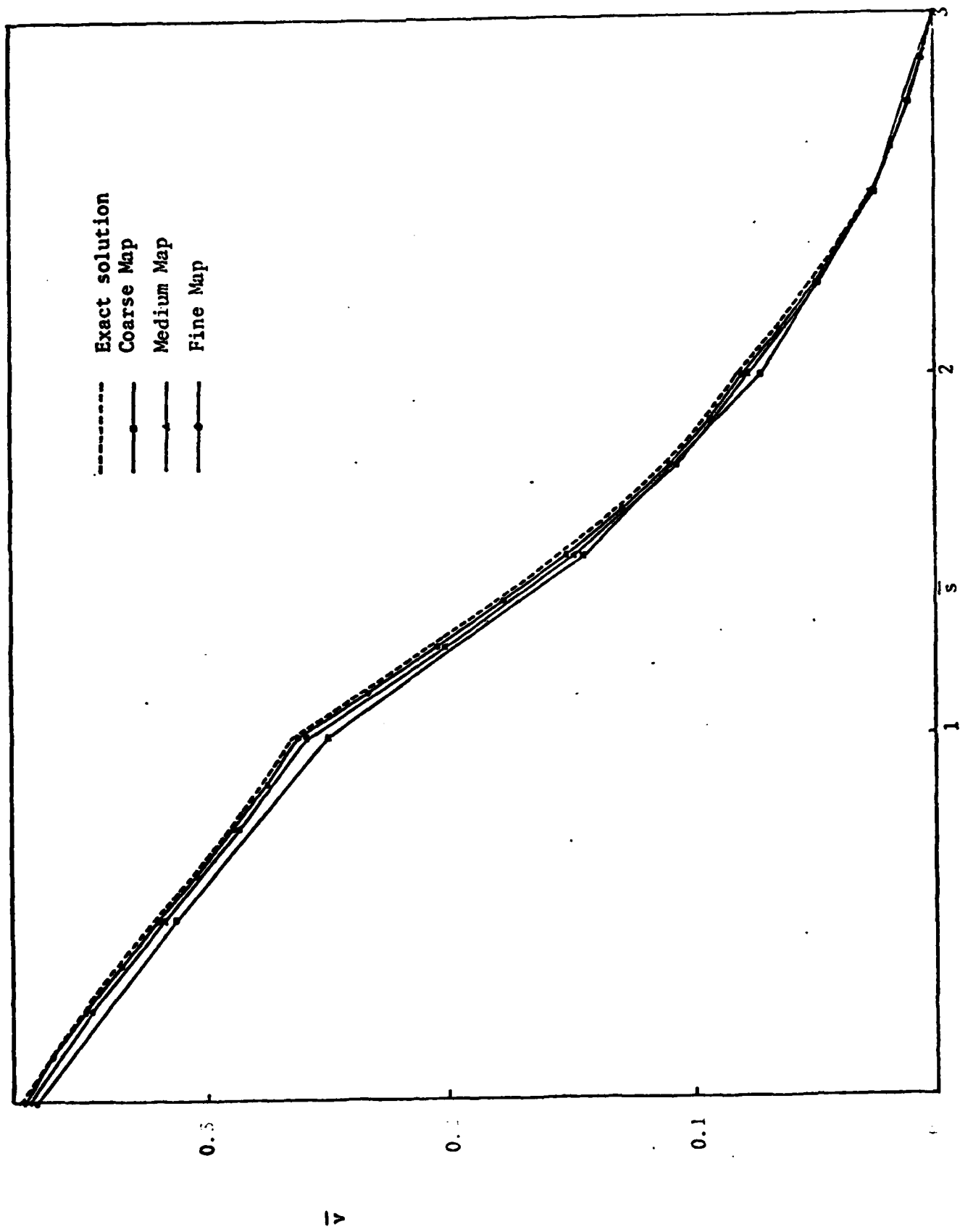
Fig. 8 Displacement ($\bar{v}$) along the boundary after pre-substructuring.
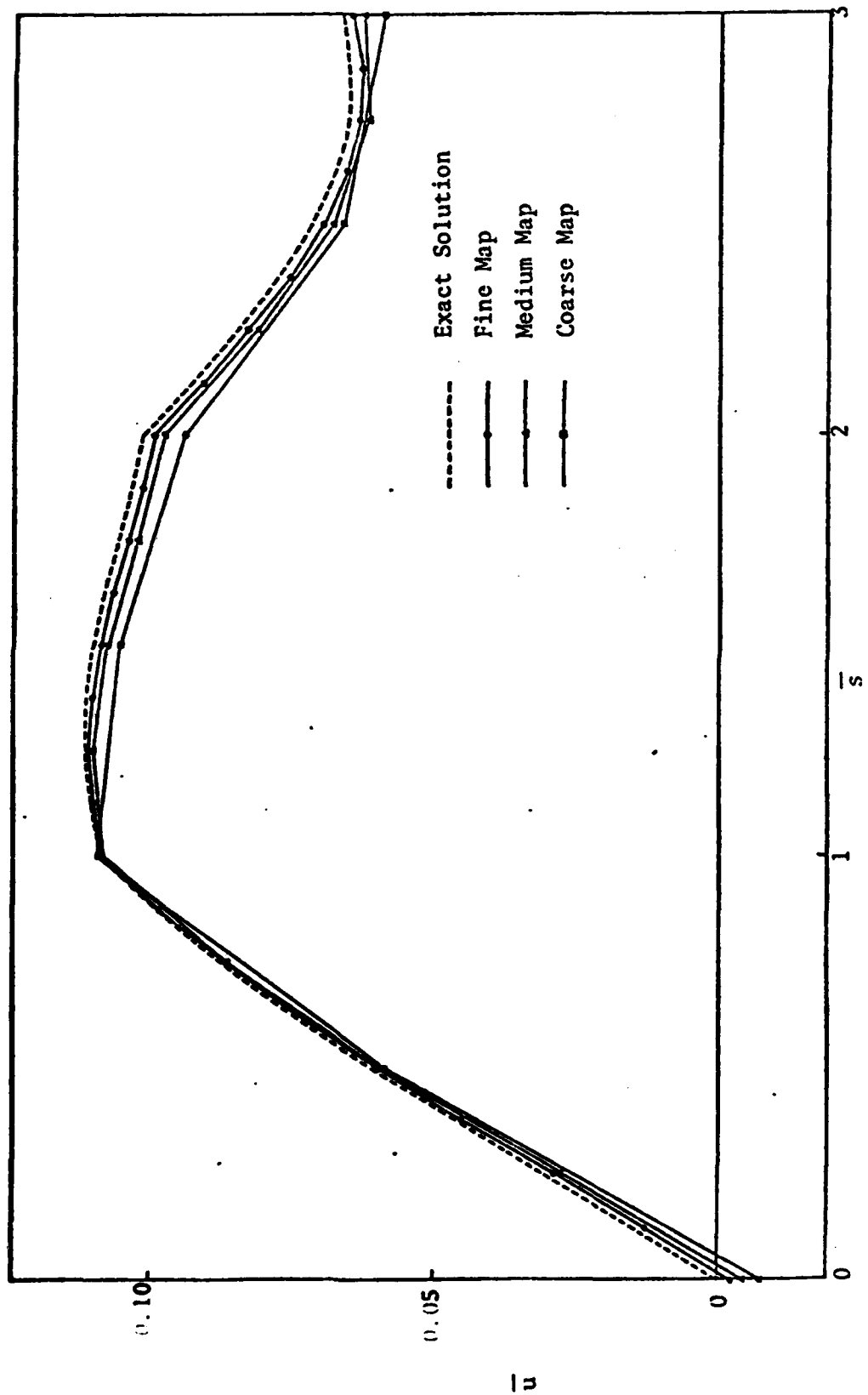
Fig. 9 Displacement ($\bar{u}$) along the boundary after first substructuring.
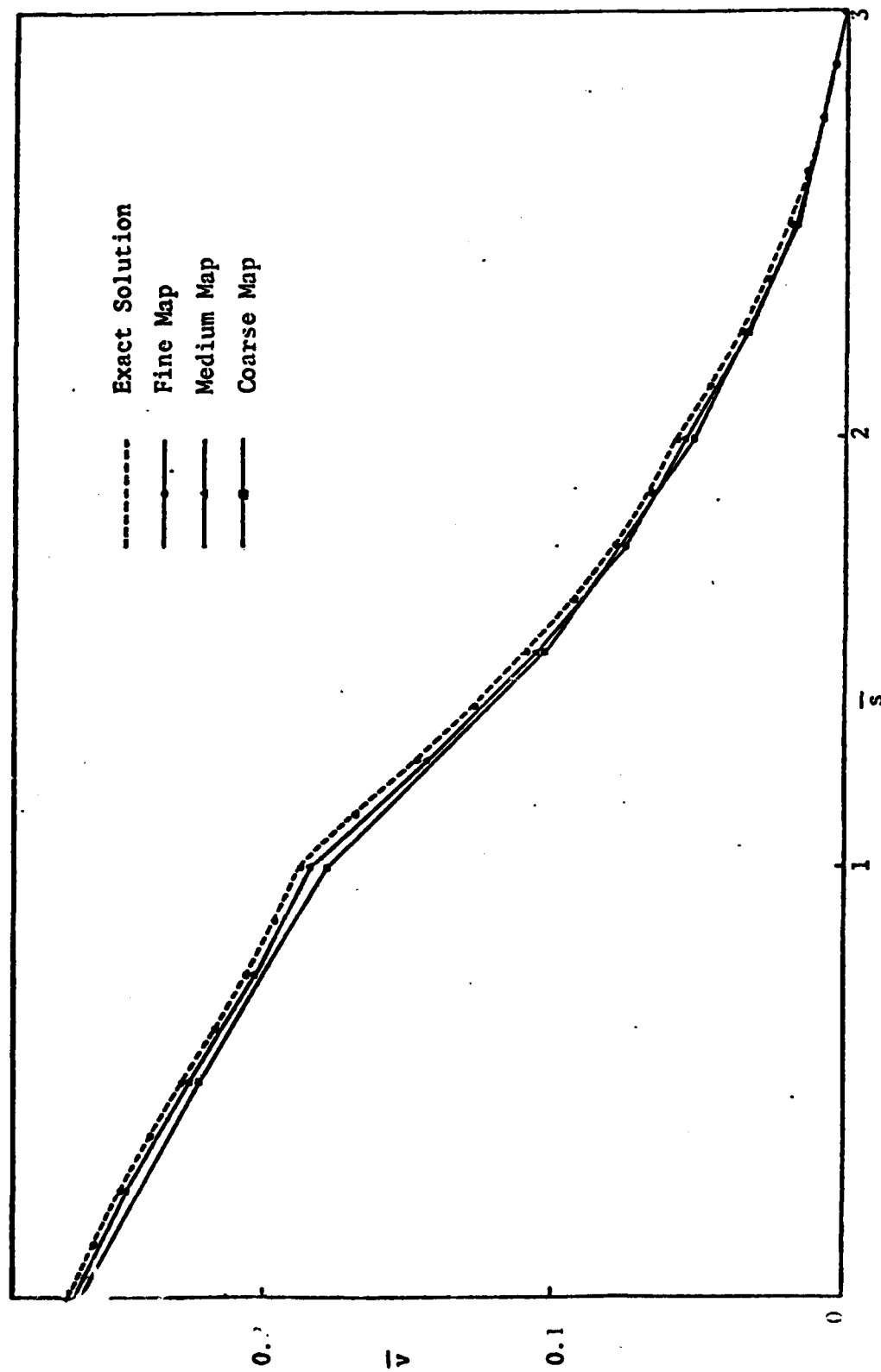
Fig. 10 Displacement $(\bar{v})$ along the boundary after first substructuring.

v. Fig. 11 shows e after the first analysis (pre-substructuring) and after the first and second substructure. The peak error occurs at the node adjacent to the crack tip in all three analyses and is uniformly reduced with substructuring. An alternative way of viewing this improvement is to track the reduction in extent of the region near the crack-tip in excess of some error. Taking, for example, the region in which e ≥ 0.01 then the associated radial dimensions are 0.282, 0.107 and 0.037 from the pre-, first, and second substructure analyses demonstrating the added resolution gained by the technique near the crack-tip. In practice, too, if it was necessary to drive this region to zero at this error level, further substructures could be performed: thus the technique can potentially be adjusted to achieve whatever level of resolution is desired.
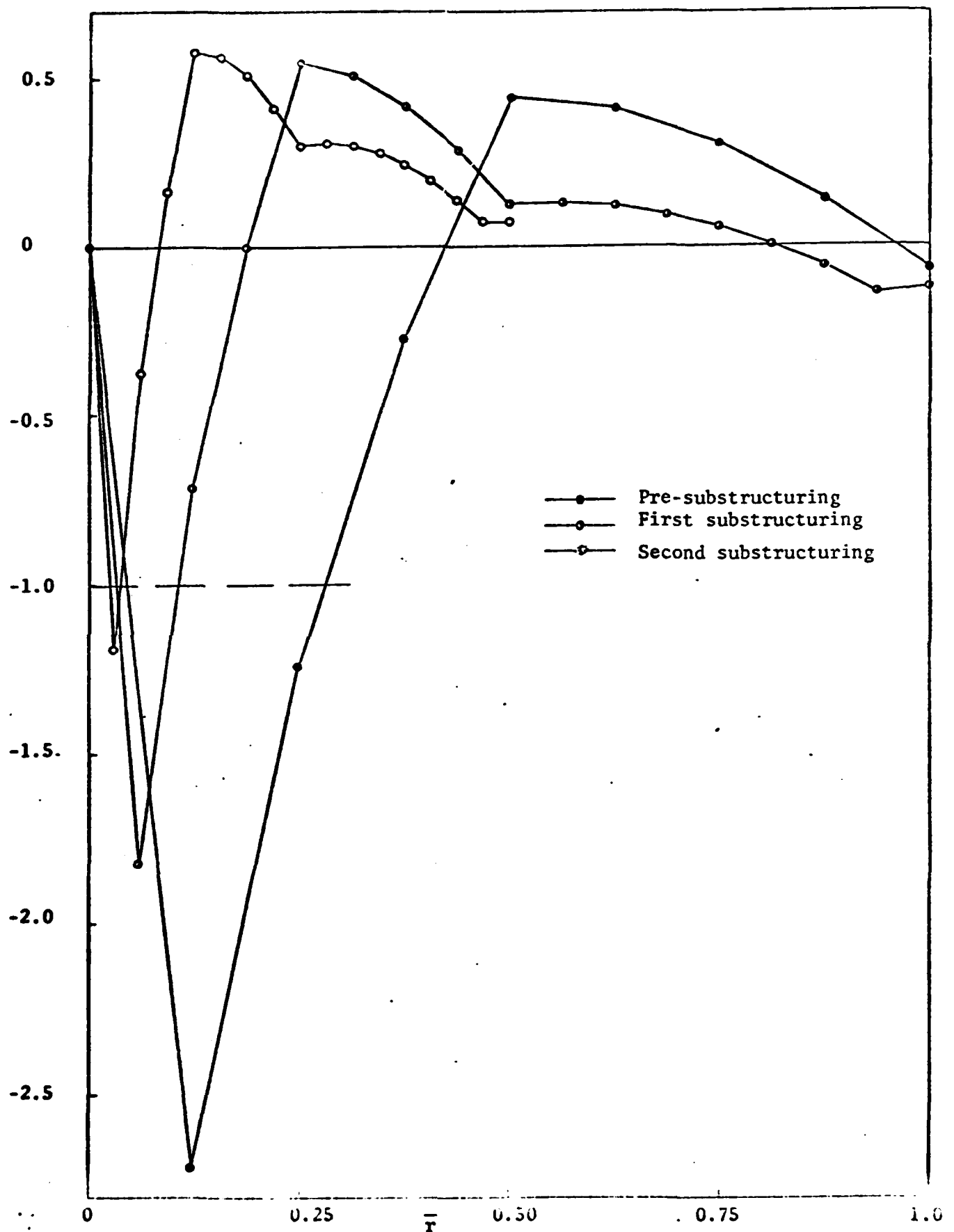
Fig. 11 Error in the crack opening displacement.

ACKNOWLEDGEMENTS

REFERENCES

1. Noor, A.K., Kamel, H.A. and Fulton, R.E., Substructuring Techniques - Status and Projections, Comput. Structures, 8, p. 621 (1978).

2. Westergaard, H.M., Bearing Pressures and Cracks, J. Applied Mechanics, 6, p. 49 (1939).

3. Ng, C.K. and Sinclair, G.B., Documentation of PLANDJ: A Constant-Strain-Triangle Finite Element Code for Elastic Problems, Report SM-78-2, Department of Mechanical Engineering, Carnegie-Mellon University (1978).

4. Zienkiewicz, O.C., The Finite Element Method in Egineering Science, McGraw-Hill, England (1971).

RESUME OF PROFESSIONAL ACTIVITIES

JEROLD L. SWEDLOW

Professor of Mechanical Engineering
Carnegie Institute of Technology
Carnegie-Mellon University
Pittsburgh, Pennsylvania

EDUCATION:

B.S., California Institute of Technology, 1957 (Mechanical Engineering)
M.S., Stanford University, 1960 (Mechanical Engineering)
Ph.D., California Institute of Technology, 1965 (Aeronautics)

MEMBERSHIPS:

American Academy of Mechanics (Member)
American Association for the Advancement of Science (Fellow)
American Institute of Aeronautics and Astronautics (Associate Fellow)
American Society of Mechanical Engineers (Member)
American Society for Testing and Materials (Member)
International Congress on Fracture (Founder Member)
Pi Tau Sigma (Honorary Member)
Sigma Xi (Member)

ACADEMIC EXPERIENCE:

Associate Dean, Carnegie Institute of Technology (1977-1979)
Professor of Mechanical Engineering, Carnegie-Mellon University (1973-)
Senior Visiting Fellow, Imperial College, London (1973-1974)
Associate Professor of Mechanical Engineering, Carnegie-Mellon University (1969-1973)
Assistant Professor of Mechanical Engineering, Carnegie-Mellon University (1966-1969)
Research Fellow in Aeronautics, California Institute of Technology (1965-1966)

INDUSTRIAL EXPERIENCE:

Consultant in fracture mechanics and structural integrity; elastic and elasto-plastic stress analysis; design of mechanisms and machinery.
Clients include agencies of the Department of Defense; consulting firms; and various manufacturing firms in the aerospace, power, and manufacturing industries. (1962 to present).
Engineer and designer for a variety of manufacturing firms, mainly in the instrumentation industry (1952-1959).

RESEARCH EXPERIENCE:

Development of a general theory of elasto-plastic flow, implementation for rapid, accurate problem-solving using finite elements, finite differences, boundaryintegral equations; applications to fracture of metallic materials and testing of materials; investigation of use of fracture mechanics with advanced fiber composites; and supervision of graduate work in the general area of solid mechanics (1965 to present).

PROFESSIONAL COMMITTEES:

American Society of Mechanical Engineers

> Faculty Advisor, CMU Student Section (1968-1970)
> Executive Board, Pittsburgh Section (1969-1972)
> Applied Mechanics Division
>> General Committee (1969-1975)
>> Committee for Computing in Applied Mechanics (1969-1975)
>> Publications Committee (1969-1971)
>> Sponsor for Computing Devices (1969-1971)

American Society for Testing and Materials

> Committee E-24 on Fracture Testing
>> Fracture Mechanics Test Methods Subcommittee (1965-1973)
>> Representative to International Congress on Fracture (1969-)
>> National Symposium Task Group (1972-), Chairman (1977-)
>> Executive Committee (1973-)
> Committee D-30 on High Modulus Fibers and Their Composites (1972-1975)

International Congress on Fracture

> Founder Executive Committee (1965-)
> Secretary (1965-1969)
> Nominating Committee (1969-1977)
> Scientific Steering Committee, 1977 Conference (1973-1977)

Society for Experimental Stress Analysis

> Papers Committee (1968-1971)

OTHER EXPERIENCE

Member, Organizing Committees for Fourth, Fifth, Sixth, and Tenth National Symposia on Fracture Mechanics (1970, 1971, 1972, 1976); Co-Chairman for Fourth Symposium (1970), Ninth Symposium (1975)

Member, Organizing Committee for National Symposium on Computerized Structural Analysis and Design (1972)

Organizer, ASME Symposium on the Surface Crack: Physical Problems and Computational Solutions (1972)

Co-Organizer, CMU Colloquium on Structural Reliability: The Impact of Advanced Materials on Design (1972)

Editor, Reports of Current Research, *International Journal of Fracture* (1969-)

Committee on Toughness Requirements for Materials in Weapon Systems, National Materials Advisory Board, Chairman (1977-80)

National Research Council Associateship Panel (Engineering) (1979-)

Reviewer for:

> *AIAA Journal*
>
> *Applied Mechanics Reviews*
>
> *Computers and Structures*
>
> *Engineering Fracture Mechanics*
>
> *Experimental Mechanics*
>
> *International Journal of Fracture*
>
> *International Journal of Solids and Structures*
>
> *Journal of Applied Mechanics*
>
> Midwestern Mechanics Conferences
>
> National Research Council (NAS, NAE)
>
> National Science Foundation
>
> Southeastern Conferences on Theoretical and Applied Mechanics

PERSONAL INFORMATION:

Born 31 August 1935 in Denver, Colorado

Married, three children

Good health, no physical defects

PUBLICATIONS:

1. Bibliography on Impact and Fracture Phenomena, J. L. Swedlow, published by Ingersoll-Rand Company and privately distributed throughout the United States, March 1959.

2. On the Effect of Thickness Near a Slender Perforation in a Flat Plate: Formulation of Approximate Problems, J. L. Swedlow, ARL 62-355, Aeronautical Research Laboratories, OAR, May 1962.

3. A Review of Recent Investigations into Fracture at GALCIT, J. L. Swedlow and M. L. Williams, ARL 64-175, Aerospace Research Laboratories, OAR, October 1964..

4. Plastic Strains and Energy Density in Cracked Plates, II. Comparison with Elastic Theory, J. L. Swedlow and W. W. Gerberich, *Experimental Mechanics*, 4 (1964) 345-351.

5. On Griffith's Theory of Fracture, J. L. Swedlow, *International Journal of Fracture Mechanics*, 1 (1965) 210-216.

6. The Thickness Effect and Plastic Flow in Cracked Plates, J. L. Swedlow, Ph.D. Thesis, California Institute of Technology, 1965.

7. The Thickness Effect and Plastic Flow in Cracked Plates, J. L. Swedlow, ARL 65-216, Aerospace Research Laboratories, OAR, October 1965.

8. Stiffness Analysis of Elasto-Plastic Plates, J. L. Swedlow and W. H. Yang, AFRPL-TR-66-5, Air Force Rocket Propulsion Laboratory, January 1966.

9. *Proceedings of the First International Conference on Fracture (1965)*, 3 vols, T. Yokobori, T. Kawasaki, and J. L. Swedlow (editors), The Japanese Society for Strength and Fracture of Materials, Sendai, Japan, 1966.

10. Elasto-Plastic Stresses and Strains in Cracked Plates, J. L. Swedlow, M. L. Williams, and W. H. Yang, *Proceedings of the First International Conference on Fracture (1965)*, 1 (1966) 259-282.

11. Three-Dimensional Stress Distribution Near a Sharp Crack in a Plate of Finite Thickness, G. C. Sih, M. L. Williams, and J. L. Swedlow, AFML-TR-66-242, Air Force Materials Laboratory, November 1966.

12. Analyses of Elasto-Plastic Plates with Cracks, J. L. Swedlow, M. L. Williams, and W. H. Yang, AFML-TR-66-248, Air Force Materials Laboratory, November 1966.

13. The Association Between Crack Opening Displacement and Fracture Toughness, M. L. Williams and J. L. Swedlow, *Transactions of the Metallurgical Society of AIME*, 239 (1967) 162-165.

14. Further Comment on the Association Between Crack Opening and G, J. L. Swedlow, *International Journal of Fracture Mechanics*, 3 (1967) 75-79.

15. Analysis of Cracks and Notches, J. L. Swedlow, *Transactions of the American Society for Metals Quarterly*, 60 (1967) 551.

16. Character of the Equations of Elasto-Plastic Flow in Three Independent Variables, J. L. Swedlow, *International Journal of Non-Lnear Mechanics*, 3 (1968) 325-336; 4 (1969) 77.

17. Initial Comparison Between Experiment and Theory of the Strain Fields in a Cracked Copper Plate, J. L. Swedlow, *International Journal of Fracture Mechanics*, 5 (1969) 25-31.

18. Elasto-Plastic Cracked Plates in Plane Strain, J. L. Swedlow, *International Journal of Fracture Mechanics*, 5 (1969) 33-44.

19. Solving Problems of Elasto-Plastic Flow, J. L. Swedlow, *AIAA Journal*, 5 (1969) 1214.

20. Computer Solution to Nonlinear Problems: The Example of Plasticity, J. L. Swedlow, *Computational Approaches in Applied Mechanics*, ASME, New York (1969) 191-199.

21. On the Sharpness of Cracks Compared with Well's COD, J. E. Srawley, J. L. Swedlow, and E. Roberts, Jr., *International Journal cf Fracture Mechanics*, 6, (1970) 441-444.

22. Experimental and Analytical Strains in an Edge-Cracked Sheet, J. H. Underwood, J. L. Swedlow, and D. P. Kendall, *Engineering Fracture Mechanics*, 2 (1971) 183-196.

23. Interactive Program for Analysis and Design Problems in Advanced Composites Technology, T. A. Cruse and J. L. Swedlow, AFML-TR-71-268, Air Force Materials Laboratory, December 1971.

24. Response: Discussions of "On the Sharpness of Cracks Compared with Wells's COD," by A. A. Wells and F. M. Burdekin, and L. P. Pook; J. E. Srawley, J. L. Swedlow, and E. Roberts, Jr., *International Journal of Fracture Mechanics*, 7 (1971) 242-246.

25. Formulation of Boundary-Integral Equations for Three-Dimensional Elasto-Plastic Flow, J. L. Swedlow and T. A. Cruse, *International Journal of Solids and Structures*, 7 (1971) 1673-1683.

26. Experimental Investigation of Fracture in an Advanced Fiber Composite, H. J. Konish, Jr., J. L. Swedlow, and T. A. Cruse, *Journal of Composite Materials*, 6 (1972) 114-124.

27. On Fracture Phenomena in Advanced Fiber Composite Materials, H. J. Konish, Jr., J. L. Swedlow, and T. A. Cruse, *AIAA Journal*, 11 (1973) 40-43.

28. Invited Discussion: Elastic Analysis of Cylindrical Configurations with Stress Singularities (by A. R. Zak), J. L. Swedlow, *Journal of Applied Mechanics*, 39 (1972) 1169.

29. Toward Assessing the Effects of Crack Front Curvature (CFC), J. L. Swedlow and M. A. Ritter, in *Stress Analysis and Growth of Cracks*, ASTM STP 513, American Society for Testing and Materials, Philadelphia (1972) 79-89.

30. *The Surface Crack: Physical Problems and Computational Solutions*, J. L. Swedlow, editor, American Society of Mechanical Engineers, New York (1972).

31. *Proceedings of the Colloquium on Structural Reliability: The Impact of Advanced Materials on Engineering Design*, J. L. Swedlow, T. A. Cruse, and J. C. Halpin (editors), Department of Mechanical Engineering, Carnegie-Mellon University, Pittsburgh, (1972).

32. Background of Fracture Mechanics, J. L. Swedlow, *Proceedings of the Colloquium on Structural Reliability: The Impact of Advanced Materials on Engineering Design*, (1972) 1-18.

33. *A Review of Developments in the Theory of Elasto-Plastic Flow*, J. L. Swedlow, CR-2321, National Aeronautics and Space Administration.

34. A Method for Estimating Fracture Strength of Specially Orthotropic Composite Laminates, H. J. Konish, Jr., T. A. Cruse, and J. L. Swedlow, in *Analysis of the Test Methods for High Modulus Fibers and Composites*, ASTM STP 521, AmericanSociety for Testing and Materials, Philadelphia (1973) 133-142.

35. Analysis of Transport in Crack-Like Regions - Part I, R. R. Shuck and J. L. Swedlow, *Localized Corrosion* NACE-3 (1974) 190-207.

36. One-Dimensional Analysis of Transport in Crack-Like Regions - Part II, R. R. Shuck and J. L. Swedlow, *Localized Corrosion* NACE-3 (1971) 208-220.

37. A Procedure for Solving Problems of Elasto-Plastic Flow, J. L. Swedlow, *Computers and Structures*, 3 (1973) 879-898.

38. Bending of an Elasto-Plastic Cracked Plate, Including the Effects of Crack Closure, D. P. Jones and J. L. Swedlow, *Proceedings, Third International Conference on Fracture II* (1973).

39. Finite Elasto-Plastic Deformation - I. Theory and Numerical Examples, J. R. Osias and J. L. Swedlow, *International Journal of Solids and Structures*, 10 (1974) 321-339.

40. A Combined Analytical-Experimental Fracture Study, P. C. Riccardella and J. L. Swedlow, in *Fracture Analysis*, ASTM STP 560, American Society for Testing and Materials, Philadelphia (1974) 134-154.

41. The Influence of Crack Closure and Elasto-Plastic Flow on the Bending of a Cracked Plate, D. P. Jones and J. L. Swedlow, *International Journal of Fracture*, 11 (1975) 897-914.

42. Further Results on the Angled Crack Problem, P. D. Ewing, J. L. Swedlow, and J G. Williams, *International Journal of Fracture*, 12 (1976), 85-93.

43. Criteria for Growth of the Angled Crack, J. L. Swedlow, in *Cracks and Fracture,* ASTM STP 601, American Society for Testing and Materials, Philadelphia (1976) 506-521.

44. A Case of Elasto-Plastic Flow Using a new Special Element, J. L. Swedlow and M. E. Karabin, Jr., in *Fracture 1977,* 1, University of Waterloo Press (1977) 117-131.

45. Crack-Tip Stress Analysis from Field Values of the Displacements Using Complementary Energy, J. L. Swedlow, M. E. Karabin, Jr., and G. E.. Maddux, in *Fracture 1977,* 3, University of Waterloo Press (1977) 103-109.

46. Analysis of Local Stresses and Strains in Ti-6A1-4V Widmanstatten $\alpha+\beta$ Microstructures, R. E. Smelser, J. L. Swedlow, and J. C. Williams, in *Toughness and Fracture Behavior of Titanium,* ASTM STP 651, American Society for Testing and Materials, (1978) 200-215.

47. Singularity Computations, J. L. Swedlow, *International Journal for Numerical Methods in Engineering,* 12 (1978) 1779-1798.

48. Path Dependence of J in Three Numerical Examples, M. E. Karabin, Jr., and J. L. Swedlow, in *Fracture Mechanics,* STP 677, American Society for Testing and Materials, Philadelphia (1979) 600-613.

49. Crack Closure in Bending of an Elasto-Plastic Plate, F. S. Heming, Jr., and J. L. Swedlow, *Nonlinear and Dynamic Fracture Mechanics,* AMD-35, American Society of Mechanical Engineers, New York (1979) 201-211.

50. Discussion of "Calculations of Stress-Strain Curve and Stress and Strain Distributions for an $\alpha-\beta$ Ti-8Mn Alloy," J. L. Swedlow and R. E. Smelser, *Materials Science and Engineering,* 40 (1979) 139-142.

51. Numerical Analysis of Elliptic-Hyperbolic Plastic Flow in Torsion, Y. K. Lee and J. L. Swedlow, *Journal of Applied Mechanics,* 47 (1980) 283-290.

52. Discussion on "On the Determination of Stresses, Displacements, and Stress-intensity Factors in Edge-cracked Sheets with Mixed Boundary Conditions," J. L. Swedlow, *Journal of Applied mechanics,* 47 (1980) 452.

53. A Direct Finite Element Approach to Elastoplastic Problems of the Mixed Type, J. L. Swedlow and Y. K. Lee, in *Innovative Numerical Analysis for the Applied Engineering Sciences,* University Press of Virginia, Charlottesville (1980) 381-393.

COMPUTATION OF SLOW, STABLE CRACK GROWTH

IN A FRACTURE TEST SPECIMEN

USING THE J-INTEGRAL

J.L. Swedlow, F.B. Prinz, Z.-C. Lai
Carnegie-Mellon University
Pittsburgh, Pennsylvania

and

C.W. Cho
ALCOA Laboratories
Pittsburgh, Pennsylvania

ABSTRACT

The title problem has been solved using a compact specimen of
7475-T6 aluminum. It is found that loading forces are accurately predicted.
Also, strain at the crack tip undergoes a modest rise during the course
of crack advance so that constant crack tip strain is inconsistent with
J-controlled crack growth. That these results are consistent with
experimental measurements leads to some discussion of a number of computational
sound round robins recently reported in the literature.

END

FILMED

11-83

DTIC